UNIVERSITY OF ALBERTA

LATE WISCONSINAN GLACIAL AND RELATIVE SEA LEVEL HISTORY OF AMUND AND ELLEF RINGNES ISLANDS, NUNAVUT, CANADA.

By

NIGEL ATKINSON

A thesis submitted to the Faculty of Graduate Studies and Research in partial fulfillment of the requirements for the degree of Doctor of Philosophy

Department of Earth and Atmospheric Sciences

Edmonton, Alberta

Spring 2004

Your file Votre référence
ISBN: 0-612-96234-2
Our file Notre référence
ISBN: 0-612-96234-2

ABSTRACT

Amund and Ellef Ringnes islands occupy the northwest Queen Elizabeth Islands, Arctic Canada. This thesis reconstructs the glacial and relative sea level history of the Ringnes Islands, and builds upon previous studies demonstrating that the Late Wisconsinan Innuitian Ice Sheet extended through the alpine and lowland sectors of the eastern and central Queen Elizabeth Islands.

Ice-flow indicators and granite dispersal along eastern Amund Ringnes Island record the inundation of Massey Sound by northwestward flowing trunk ice from Innuitian divides spanning the alpine and lowland sectors of the Queen Elizabeth Islands. Geochemically similar granite erratics occur within a dispersal train that extends from Ellesmere to Meighen islands, which documents a major flow trajectory of the Innuitian Ice Sheet. The interior of Amund Ringnes Island was overridden by granite-free Innuitian ice flowing north from a lowland divide spanning the central Queen Elizabeth Islands. Although Ellef Ringnes Island experienced widespread Late Wisconsinan glaciation, it remains uncertain whether this was due to Innuitian ice flowing north from this lowland divide, or a local ice cap.

Deglaciation of the Ringnes Islands commenced >10 ka BP. From 10 to 9.4 ka BP, trunk ice in Hassel and Massey sounds retreated to northeast Ellef Ringnes and northern Amund Ringnes islands, and from Prince Gustaf Adolf Sea onto western Ellef Ringnes Island. Local ice caps persisted along the coastlines of Ringnes Islands $\geq$1400 ^{14}C years after the initial evacuation of ice from the intervening marine channels. The

chronology of final deglaciation of residual ice caps on the Ringnes Islands remains unknown.

Provisional isobases drawn on deglacial shorelines record the diminishing thickness of the Innuitian Ice Sheet, northwestward across the Ringnes Islands. These support the proposal that an ice divide occupied the central Queen Elizabeth Islands. The continuity of the isobases across Amund and Ellef Ringnes islands is consistent with the glacial geologic evidence that suggests Massey and Hassel sounds were occupied by grounded ice during the last glaciation. Parallel isobases across Peary Channel suggest that this grounded ice extended beyond Massey Sound, although their northward deflection, parallel to western Axel Heiberg Island requires that ice thickness was greater on the eastern side of the channel.

ACKNOWLEDGEMEMTS

In the process of writing this thesis, there have been times when life seemed to echo the sentiments of Oscar Wilde, who quipped "I am in a duel to the death with this wallpaper, one of us has got to go!" Nevertheless, I count myself very fortunate to have had the opportunity to pursue this Ph.D. research, and it has provided me with a fantastic learning experience, both academically and personally. However, the lessons learned toward the completion of this thesis reflect the efforts and dedication of other people, as much as they do my own.

Firstly, I would like to thank my supervisor, John England. Throughout the course of my research, John has always allowed me the freedom to develop my own interests and ideas, and through his commitment to graduate student research in the Canadian Arctic, has provided me with the opportunity to experience a landscape that never ceases to inspire or humble. For this, as well as his discussions, meticulous reviews, advise, good humour and financial support, I am very grateful. On a personal note, I would like to acknowledge both John and Catherine for their friendship, generosity and kindness while I have been in Canada. I look back on many happy memories with you both, particularly on the pond, although I cannot help think that my inability to skate backwards spoiled what could have been a dazzling hockey career.

My committee members, Martin Sharp, Tom Chacko, George Ball and Julie Brigham-Grette (University of Massachusetts), who kindly served as my external examiner, made valuable comments on this thesis. I would particularly like to thank Martin Sharp, who has been an integral part of my development as a graduate student, especially during the last few months, when my thesis was in need of a firm push in the right direction. Thanks Martin for your friendship, sound advise, discussion and chapter reading. I would also like to thank Rod Smith (Geological Survey of Canada, Calgary), who has always been there to answer my questions or problems, and freely given his time to review my chapters, always providing encouraging and constructive comments, although using up large quantities of red ink in the process! Thanks also to Doug Hodgson (Geological Survey of Canada, Ottawa), who generously provided air photographs of Ellef Ringnes Island, as well as valuable discussion.

Financial support for this research was provided by the Natural Sciences and Engineering Research Council of Canada (Grant A6880 awarded to John England) and the Canadian Circumpolar Institute (BAR Grants). Further financial support through the Harington Paleoenvironmental Scholarship, and teaching and research assistantships provided by the Department of Earth and Atmospheric Sciences are gratefully acknowledged. My research on Amund and Ellef Ringnes islands would have been impossible without the generous and expert logistical support provided by the Polar Continental Shelf Project. Excellent field assistance was provided by Chelsea Hermus, Tanya Huynh and Lachlan MacLean. However, my recipe for granola surprise goes with me to the grave!

I have shared many happy memories with friends and fellow graduate students at the University of Alberta. I count myself very lucky to have been surrounded by such an excellent group of friends, who have always provided companionship, humour and understanding, particularly when my range of emotions have swung from frustration to jubilation. Thanks to you all; Joel, Sam, Melissa, Serge, Gabe, Jane, Maya, Doug, Colm, Thomas, Sarah, Alex, Patrick, Luke, Dave, Carolyn, Kathleen, Fiona, Libo, Chantel, Anna, Britta and Ingrid. Particular thanks to Trudy, my long-suffering office mate, who had to endure endless tirades whenever my computer crashed. I would also like to thank Rod and Sandra, who have, on numerous occasions, gone out of their way to provide friendship and generous hospitality. Thanks also to the Bzdel and Zaharia families, who welcomed me into their homes, and were sympathetic towards a brother-in-law who had many thesis-related distractions.

And finally to the three people who have made the biggest contribution to the successful completion of this thesis. Firstly, my parents (Alf and Diane), who have provided selfless love throughout my life, and always supported and encouraged my decisions, wherever they have taken me. Although I have not seen much of you over the last five years, you have always been in my thoughts, and through your continuous interest and concern, I truly never felt the distance between us. And finally, but by no means least, my wife Lana, who has been with me throughout the highs and lows of my graduate career. She deserves an enormous amount of recognition for her contribution to this thesis, and she really kept me going when things threatened to overwhelm me. Lana,

thanks so much for your unconditional love and support, for putting up with me when I came home late, dealing with my grumpy moods, and most importantly, for never letting me forget the true importance of life. I look forward to where it will take us next!

TABLE OF CONTENTS

CHAPTER FOUR

Postglacial emergence of Amund and Ellef Ringnes islands, Nunavut: implications for the northwest Innuitian Ice Sheet.

LIST OF TABLES

LIST OF FIGURES

CHAPTER THREE

CHAPTER FOUR

CHAPTER FIVE

CHAPTER ONE

Introduction

1.1 Background

Increasing attention is being given to the reconstruction of high latitude palaeoenvironmental change, particularly due to the issue of global change (cf. CLIMAP Members 1981). This thesis builds on systematic regional studies of past glaciation and sea-level change in the Queen Elizabeth Islands (QEI), Canadian Arctic Archipelago (Figure 1.1). These studies have recently reconciled the pattern of postglacial emergence throughout the eastern and central QEI with geological evidence of extensive glaciation (Ó Cofaigh 1999; Ó Cofaigh et al. 2000; Bednarski 1998; Dyke 1998, 1999; England 1998, 1999; Bischof and Darby 1999; Lamoureux and England 2000). Such evidence demonstrates that the Innuitian Ice Sheet (IIS; Blake 1970, 1972; Walcott 1972) extended through the alpine sector of the eastern QEI and the lowland sector of the central QEI during the Late Wisconsinan, and coalesced with the Greenland Ice Sheet to the east and the Laurentide Ice Sheet to the south. However, the glacial history of the lowland sector of the western QEI, where fieldwork has only been conducted at a reconnaissance level (St-Onge 1965, Stott 1969; Balkwill et al. 1974; Hodgson 1982; Balkwill 1983), remains unaddressed by the most recent reconstruction of Northern Hemisphere ice sheets presented at the EPILOG (Environmental Processes of the Ice Age: Land, Oceans, Glaciers) Project workshop (Clark and Mix 2002). Establishing the history and dynamics of these ice sheets will provide improved input to geophysical, glaciological and climate modelling, which offer insight into the sensitivity of Earth systems to change, the

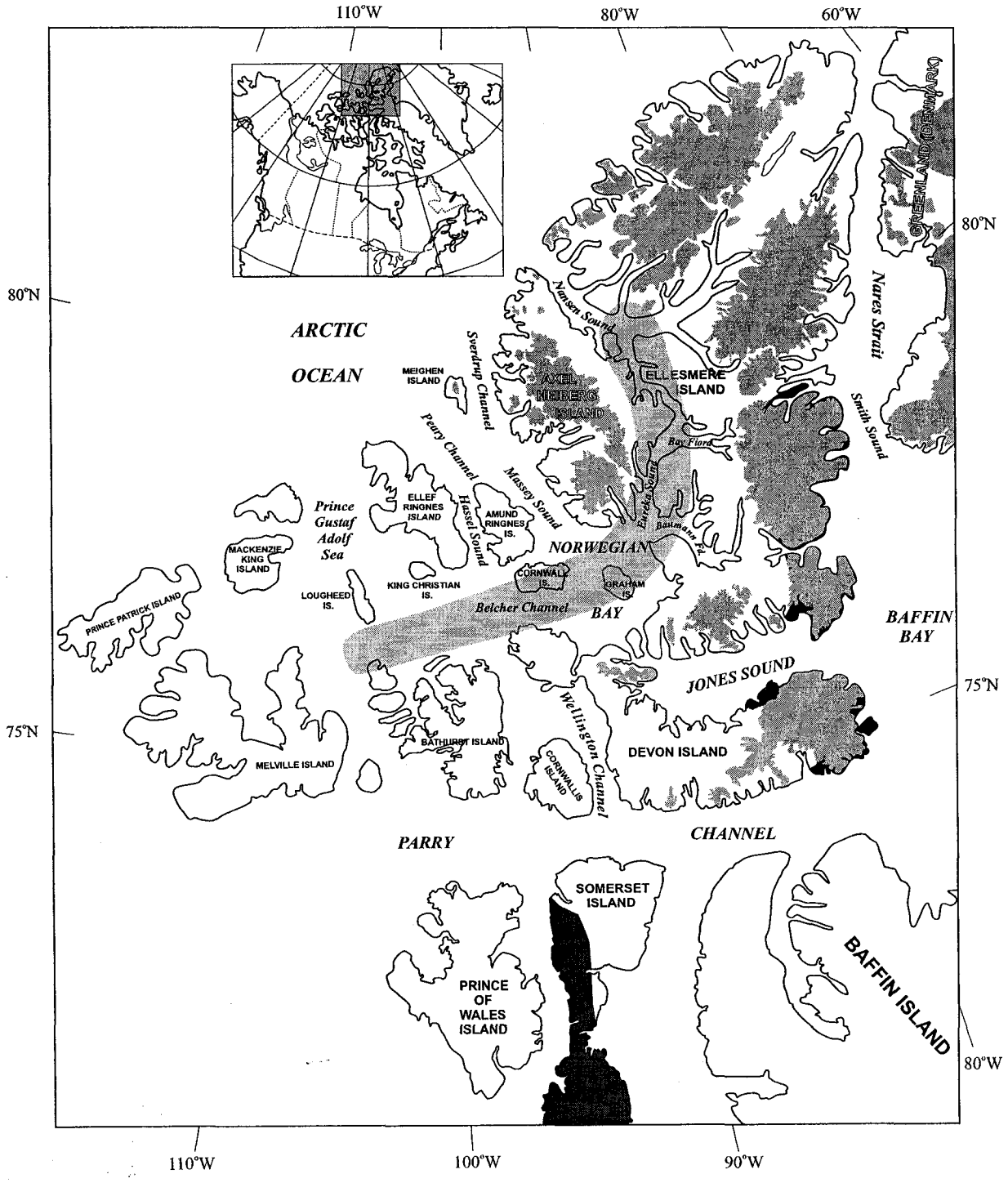

Figure 1.1. Location map of the Queen Elizabeth and central Arctic islands, and the adjacent coast of Greenland. Axis of the Innuitian uplift is shaded in transparent gray. Contemporary ice caps are shaded light gray. Precambrian Sheild is shaded dark gray.

role of external forcing relative to internal feedback in driving change and the linkages between the various climate subsystems (Clark and Mix 2002). Although estimates of the magnitude of ice-equivalent sea-level lowering resulting from the growth of the IIS are small (<7% of the total contribution from North American ice sheets during the Last Glacial Maximum; Clark and Mix 2002), clarifying the extent, dynamics and chronology of the IIS will provide further understanding of the characteristics of high latitude palaeoenvironmental change. Such change includes the linkages between the IIS and other circumarctic ice sheets, the linkage between ocean/atmosphere boundary conditions and the behaviour of large scale atmospheric circulation patterns above 70°N that favoured glacial initiation over the QEI (Rogers et al. 2001; Bromwich et al. 2002), as well as the potential impact of the IIS's retreat on the climate of the polar North Atlantic (Darby et al. 2002). Moreover, refining reconstructions of the IIS will provide an improved understanding of landscape evolution of the Canadian Arctic Archipelago, as well as the sedimentary history of the polar continental shelf and the adjacent Arctic Ocean Basin, where extensive glaciation of unknown origin has recently been proposed (Polyak et al. 2002; Dyke et al. 2002).

This thesis addresses the glacial and relative sea-level history of Amund and Ellef Ringnes islands, northwest QEI (Figures 1.1 and 1.2). The lack of systematic fieldwork on the Ringnes Islands constitutes a gap in the reconstruction of Quaternary glaciation and postglacial emergence across the QEI. Reconnaissance surveys during the 1960's and 1970's identified at least one extensive glaciation of the Ringnes Islands, but it is uncertain whether this was the product of the IIS from the east (Blake 1970, 1972), the

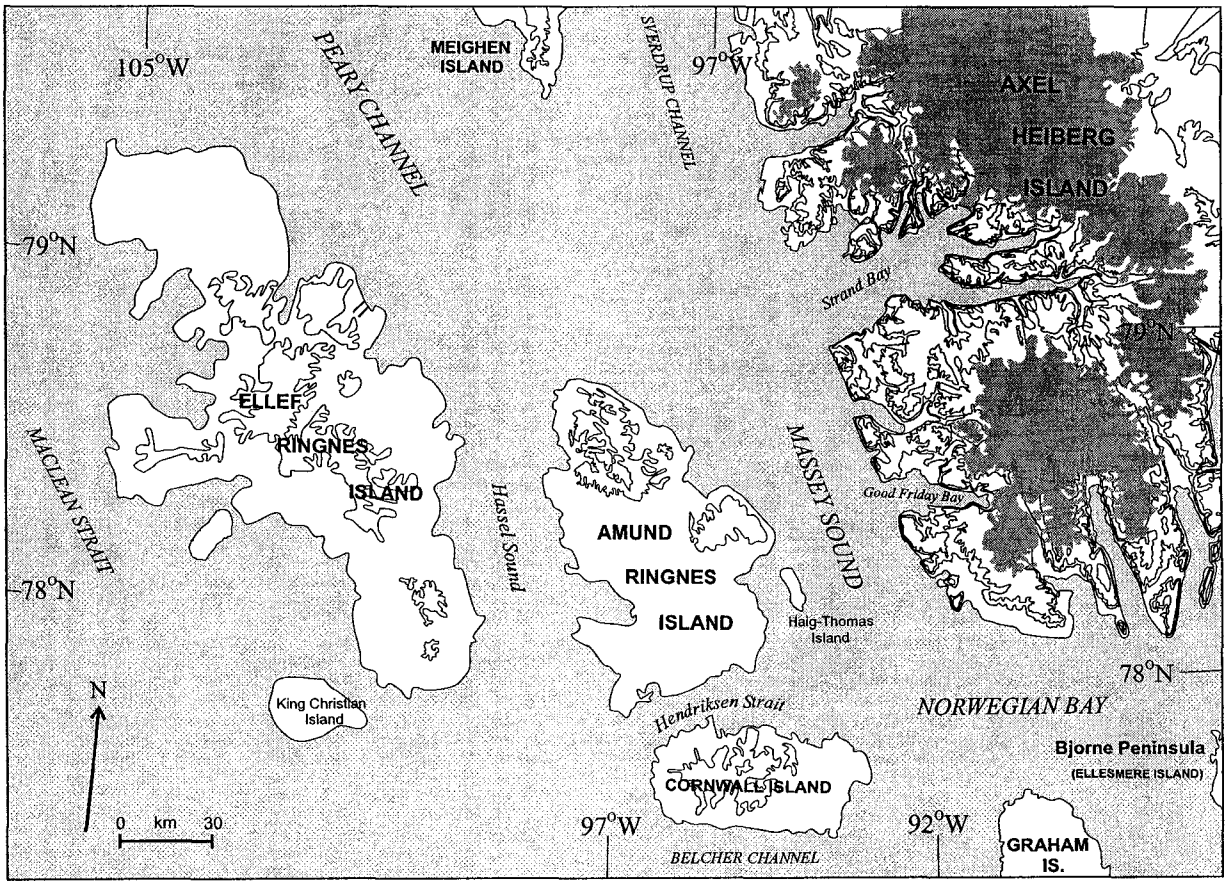

Figure 1.2. Location map of the central and northwest Queen Elizabeth Islands. Contour interval 100 m. Contemporary ice caps are shaded.

Laurentide Ice Sheet from the south, the expansion of island-based ice caps, or a combination of the three (cf. Hodgson 1982).

Research in the eastern QEI has demonstrated that alpine divides supplied ice that converged in the intervening lowland occupied by Nansen and Eureka sounds and Norwegian Bay (Hodgson 1985; Bell 1996; Bednarski 1998; Ó Cofaigh et al. 2000; England et al. in press; Figure 1.1). In the central QEI, a NE-SW trending lowland divide supplied ice that flowed into Norwegian Bay to the north, and Wellington Channel to the south (Dyke 1999; Lamoureux and England 2000; Figure 1.1). An axis of maximum postglacial emergence, referred to as the Innuitian uplift (Walcott 1972), is attributed to the axis of maximum former thickness of the IIS. In the eastern QEI, the Innuitian uplift trends north-south, coinciding with the central basin of convergent ice flow into Eureka Sound, while in the central QEI, it trends NE-SW, marking the position of the former lowland ice divide. Collectively, these reconstructions demonstrate that convergent outflow from Innuitian ice divides spanning both the eastern and central QEI filled Norwegian Bay (Dyke 1998, 1999; Ó Cofaigh et al. 1999; Ó Cofaigh et al. 2000; England et al. in press; Figure 1.1). The Ringnes Islands constitute low lying terrain surrounded by marine channels immediately northwest of Norwegian Bay and provide the opportunity to examine the extent to which the IIS expanded across the northwest QEI and on to the polar continental shelf.

1.2 Objectives

This thesis is designed to build upon the systematic mapping and surveying of both glacial and raised marine deposits across the QEI (Bell 1996; Bednarski 1998; Dyke 1998, 1999; England 1976a and b, 1992, 1996, 1998, 1999; Ó Cofaigh et al. 1999; Ó

Cofaigh et al. 2000; Lamoureux and England 2000; England et al. 2000, in press). This research has only recently been completed for the alpine sector to the east and is now focussed on the westernmost islands. The objectives of this thesis are:

1) to examine the glacial geomorphology and date raised marine sediments on Amund and Ellef Ringnes islands in order to reconstruct former ice sheet extent (configuration), dynamics and subsequent deglacial chronology. Particular emphasis will be placed on determining whether previously reported glacial geological evidence records former advances of the Innuitian or Laurentide ice sheets, and/or the expansion of local ice caps.
2) to investigate the distribution and geochemistry of glacially transported granite erratics across the northwest QEI to determine whether there are spatial and compositional trends reflecting source areas of the Precambrian Shield that were overridden by either the Innuitian or Laurentide ice sheets.
3) to determine the magnitude, form and spatial pattern of postglacial relative sea-level (RSL) change on Amund and Ellef Ringnes islands, and integrate these data with published work for areas to the south and northeast (Walcott 1972; England 1976b; Dyke 1999; Ó Cofaigh 1999; England et al. in press). These data can be used to reconstruct postglacial isobases that record the pattern of shoreline delevelling across the northwest QEI. The isobases help clarify the signature of glacioisostatic recovery on Amund and Ellef Ringnes islands, and can be used to infer the distribution of ice loading across the northwest QEI, which provides an independent measure of maximum former ice thickness that can be compared to the ice sheet configuration investigated under objectives 1 and 2. Determining the form and response times of

postglacial RSL curves from the Ringnes Islands also provides the opportunity to assess whether the region has been emerging continuously since deglaciation. Recent studies have proposed that postglacial relaxation of the crust occurs exponentially, with the response times of RSL curves reflecting a systematic relationship dependant on proximity to the former loading centre (Dyke and Peltier 2000). The position of the Ringnes Islands relative to an axis of maximum former ice thickness, investigated under objectives 1 and 2, may help test this hypothesis, or determine whether other factors, such as neotectonics are involved.

1.3 Structure

This thesis is written in paper format, and is presented as a group of three independent, yet complementary chapters, in addition to the introduction and conclusions. Details relating to previous research, study sites, methodology and techniques are contained in each paper.

Chapter 2, *Late Wisconsinan glaciation of Amund and Ellef Ringnes islands, Nunavut: evidence for the configuration, dynamics and deglacial chronology of the northwest Innuitian Ice Sheet* (a version of this paper has been published in the Canadian Journal of Earth Sciences, 40: 351-363) presents the glacial geomorphology, as well as the distribution, elevation, age and stratigraphic context of radiocarbon-dated raised marine sediments on the Ringnes Islands. These data record the inundation of the Ringnes Islands by northwestward-flowing ice from divides spanning the alpine and lowland sectors of the Innuitian Ice Sheet. Ice-flow indicators and granite dispersal along eastern Amund Ringnes Island suggest that Massey Sound was filled by actively flowing trunk ice, possibly forming an ice stream, fed by convergent alpine and lowland ice

entering Norwegian Bay (Figure 1.2). In contrast, the interior of Amund Ringnes Island was overridden by predominantly non-erosive, granite-free ice from a divide in the lowland sector of the ice sheet (Figure 1.1). Glacial landforms on Ellef Ringnes Island suggest coverage by largely non-erosive ice, but it remains uncertain whether these features relate to northward-flowing lowland ice, or a local, island-based ice cap. Deglaciation of the Ringnes Islands commenced ~10 000 ^{14}C years ago. Deglacial dates between 9.7 and 9.2 ka BP record the sequential entry of marine fauna along Massey and Hassel sounds, concomitant with the southward retreat of trunk ice towards Norwegian Bay (Figure 1.2). These data suggest that the marine-based trunk glaciers were especially vulnerable to thinning and calving, as the early Holocene insolation maximum (Berger 1988) enhanced the impact of ongoing eustatic sea-level rise on ice retreat. In contrast, deglacial dates from inner embayments indicate that residual ice caps persisted on Amund and Ellef Ringnes islands for 800 to 1400 ^{14}C years after retreat of trunk ice from the adjacent marine channels. Lateral meltwater channels record the retreat of these ice caps, which became increasingly confined within upland valleys after 8.6 ka BP.

Chapter 3, *A statistical technique for source area determination of glacially transported granite erratics in the Queen Elizabeth Islands* develops a methodology that utilizes spatial and compositional trends in granite erratics distributed across the study area to discriminate between glacial dispersal trains originating from the Precambrian Shield of Ellesmere Island and the Canadian mainland (Figure 1.2). The distribution of glacially transported granite erratics in the eastern and northwest QEI defines a coherent pattern of regional dispersal from the Precambrian Shield of eastern Ellesmere Island (Figure 1.2). Principal components and cluster analyses demonstrate that most of the

granite erratics within this dispersal train cluster within the same compositional group. Other members of this group consist of granite outcrops in the Precambrian Shield of southeast Ellesmere Island and Somerset Island, which define the locations of possible erratic source areas. However, other compositional clusters which are unique to outcrops on Somerset Island are absent from the erratic population of the QEI. Collectively, these spatial and compositional trends suggest that granite erratics on southwest Ellesmere, Amund Ringnes and Meighen islands derive from the same glacial dispersal train and are most likely attributable to the westward expansion of the IIS from the Precambrian Shield of southeast Ellesmere Island. This technique may determine what differences, if any, exist between the compositional trends of granite erratics deposited by the expansion of the IIS across the northwest QEI, and those deposited by the well-documented northward expansion of the Laurentide Ice Sheet on to Melville Island (Figure 1.1; cf. Hodgson 1989). Any such trends may be useful in determining whether granite erratics of presently unknown provenance on Lougheed and Prince Patrick islands (Figure 1.1) are of Laurentide or Innuitian origin.

Chapter 4, *Postglacial emergence of Amund and Ellef Ringnes islands, Nunavut: implications for the northwest Innuitian Ice Sheet* (accepted for publication in the Canadian Journal of Earth Sciences) presents relative sea-level curves and postglacial isobases from Amund and Ellef Ringnes islands. These relative sea-level curves are of exponential form, and record continuous, ongoing emergence from Holocene marine limit (up to 106 m asl), except on northwest Ellef Ringnes Island, where submergence appears to be occurring after establishment of a late Holocene sea-level lowstand. This is recorded by the accumulation of older wood (>600 years) along a micro-cliff being

eroded by high tide. Isobases drawn on Holocene shorelines rise southeastwards, towards an uplift centre in Norwegian Bay. This isobase pattern suggests that the Ringnes Islands occupied the northwest radius of the Innuitian uplift (Figure 1.1), which is consistent with glacial geological evidence suggesting that parts of the Ringnes Islands were overridden by the Late Wisconsinan IIS. The isobases help to better clarify the signature of glacioisostatic recovery, and by inverting these Holocene RSL data, enable inferences to be made concerning the distribution of ice loading within the northwest Innuitian uplift. The isobases support earlier reconstructions showing that maximum Late Wisconsinan ice thickness in the central QEI occurred across Norwegian Bay, which in this location, marks a former ice divide (Dyke 1998). This ice divide configuration is also consistent with ice-flow features on Amund Ringnes Island. The isobases record the diminishing thickness of the IIS from Norwegian Bay to the Arctic Ocean. The absence of an isobase embayment across the Ringnes Islands suggests a relatively uniform ice load across both islands, as well as across Hassel and Massey sounds, although data confirming this inferred pattern is unavailable from the intervening channels. Parallel isobases across Peary Channel indicate that this ice load likely extended beyond Massey Sound, although their northward deflection suggests the increasing influence of the former Axel Heiberg Island ice load to the north. Evidence of recent transgression of northwest Ellef Ringnes Island is similar to observations on eastern Melville Island (Hansen 2003; Figure 1.1). These studies provide new data to map the position of the zero isobase, which describes the boundary between coasts that are still undergoing isostatic recovery, and those that are submerging. To date, this is poorly constrained in the western QEI (Andrews and Peltier 1989).

1.5 References

Andrews, J.T. 1970. A geomorphic study of postglacial uplift with particular reference to Arctic Canada. Institute of British Geographers, London, England, Special Publication 2.

Andrews, J.T., and Peltier, W.R. 1989. Quaternary geodynamics in Canada. *In* Quaternary Geology of Canada and Greenland. *Edited by* R.J. Fulton. Geological Survey of Canada, Geology of Canada, **1**.

Balkwill, H.R., Roy, K.J., and Hopkins, W.S., Jr. 1974. Glacial features and pingos, Amund Ringnes Island, Arctic Archipelago. Canadian Journal of Earth Sciences, **11**: 1319-1325.

Balkwill, H.R. 1983. Geology of Amund Ringnes, Cornwall, and Haig Thomas islands, District of Franklin. Geological Survey of Canada, Memoir **390**.

Bednarski, J.M. 1998. Quaternary history of Axel Heiberg Island, bordering Nansen Sound, Northwest Territories, emphasizing the last glacial maximum. Canadian Journal of Earth Sciences, **35**: 520-533.

Berger A. 1988. Milankovitch theory and climate. Reviews of Geophysics, **26**: 624-657.

Bischof, J., and Darby, D. 1999. Quaternary ice transport in the Canadian Arctic and extent of Late Wisconsinan glaciation in the Queen Elizabeth Islands. Canadian Journal of Earth Sciences, **36**: 2007-2022.

Blake, W., Jr. 1970. Studies of glacial history in Arctic Canada. Canadian Journal of Earth Sciences, **7**: 634-664.

Blake, W., Jr. 1972. Climatic implications of radiocarbon-dated driftwood in the Queen Elizabeth Islands, Arctic Canada. *In* Climatic change in the arctic areas during the last ten thousand years. *Edited by* Y. Vasari, H. Hyvarinen, and S. Hicks.

Bromwich, D.H., Toracinta, E.R., and Wang, S-.H. 2002. Meteorological perspective on the initiation of the Laurentide Ice Sheet. Quaternary International, **95-96**: 113-124.

Clark, P.U., and Mix, A.C. 2002. Ice sheets and sea level of the Last Glacial Maximum. Quaternary Science Reviews, **21**: 1-7.

CLIMAP. 1981. Seasonal reconstruction of the Earth's surface at the last glacial maximum. Geological Society of America, Map and Chart Series, C36.

Darby, D.A., Bischof. J.F., Spielhagen, R.F., Marshall, S.A., and Herman, S.W. 2002. Arctic ice export events and their potential impact on global climate during the late Pleistocene. Paleoceanography, **17**: 1-17.

Dyke, A.S. 1998. Holocene delevelling of Devon Island, Arctic Canada: implications for ice sheet geometry and crustal response. Canadian Journal of Earth Sciences, **35**: 885-904.

Dyke, A.S. 1999. The last glacial maximum and the deglaciation of Devon Island: support for an Innuitian Ice Sheet. Quaternary Science Reviews, **18**: 393-420.

Dyke, A.S., and Peltier, W.R. 2000. Forms, response times and variability of relative sea-level curves, glaciated North America. Geomorphology, **32**: 315-333.

Dyke, A.S., Andrews, J.T., Clark, P.U., England, J.H., Miller, G.H., Shaw, J., and Veillette, J.J. 2002. The Laurentide and Innuitian ice sheets during the Last Glacial Maximum. Quaternary Science Reviews, **21**: 9-31.

England, J. 1976a. Late Quaternary glaciation of the Queen Elizabeth Islands, Northwest Territories, Canada: alternative models. Quaternary Research, 6: 185-202.

England, J. 1976b. Postglacial isobases and uplift curves from the Canadian and Greenland High Arctic. Arctic and Alpine Research, **8**: 61-78.

England, J. 1992. Postglacial emergence in the Canadian High Arctic: integrating glacioisostasy, eustasy, and late deglaciation. Canadian Journal of Earth Sciences, **29**: 984-999.

England, J. 1996. Glacier dynamics and paleoclimatic change during the last glaciation of eastern Ellesmere Island, Canada. Canadian Journal of Earth Sciences, **33**: 779-799.

England, J. 1998. Support for the Innuitian Ice Sheet in the Canadian High Arctic during the Last Glacial Maximum. Journal of Quaternary Science, **13**: 275-280.

England, J. 1999. Coalescent Greenland and Innuitian ice during the Last Glacial Maximum: revising the Quaternary of the Canadian High Arctic. Quaternary Science Reviews, **18**: 421-556.

England, J., Smith, I.R., and Evans, D.J.A. 2000. The last glaciation of east-central Ellesmere Island, Nunavut: ice dynamics, deglacial chronology, and sea level change. Canadian Journal of Earth Sciences, **37**: 1355-1371.

England, J., Atkinson, N., Dyke, A.S., Evans, D.J.A., and Zreda, M. in press. Late Wisconsinan buildup and wastage of the Innuitian Ice Sheet across southern Ellesmere Island, Nunavut. Canadian Journal of Earth Sciences.

Hansen, M.A. 2003. Late Quaternary glaciation, relative sea level history and coastal submergence of northeast Melville Island, Nunavut. Unpublished M.Sc. Thesis, University of Alberta, Edmonton.

Hodgson, D.A. 1982. Surficial materials and geomorphological processes, western Sverdrup and adjacent islands, District of Franklin. Geological Survey of Canada, Paper **81-9**.

Hodgson, D.A. 1989. Quaternary stratigraphy and chronology (Queen Elizabeth Islands). *In* Quaternary Geology of Canada and Greenland, Fulton, R.J. (ed), Geological Survey of Canada, Geology of Canada, No 1, pp. 452-459.

Lamoureux, S.F., and England, J. 2000. Late Wisconsinan of the central sector of the Canadian High Arctic. Quaternary Research, **54**: 182-188.

Ó Cofaigh, C., Lemmen, D.S., Evans, D.J.A., and Bednarski, J. 1999. Glacial sediment/landform assemblages in the Canadian High Arctic and their implications for Late Quaternary glaciation. Annals of Glaciology, **28**: 195-207.

Ó Cofaigh, C., England, J., and Zreda, M. 2000. Late Wisconsinan glaciation of southern Eureka Sound: evidence for extensive Innuitian ice in the Canadian High Arctic during the Last Glacial Maximum. Quaternary Science Reviews, **19**: 1319-1341.

Polyak, L., Edwards, M.H., Coakley, B.J., and Jokobsson, M. 2001. Ice shelves in the Pleistocene Arctic Ocean inferred from glaciogenic deep-sea bedforms. Nature, **401**: 453-457.

Rogers, A. N., Bromwich, D. H., Sinclair, E. N., and Cullather, R. I. 2001. The atmospheric hydrologic cycle over the Arctic Basin from reanalyses. Part 2: Interannual variability. Journal of Climate, **14**: 2414-2429.

Stott, D.F. 1969. Ellef Ringnes Island, Canadian Arctic Archipelago. Geological Survey of Canada, Paper **68-16**.

St-Onge, D.A 1965. La géomorphologie de I'lle Ellef Ringnes, Territoires du Nord-Ouest, Canada. Geographical Branch, Paper **38**.

Walcott, R.I. 1972. Late Quaternary vertical movements in eastern North America: quantitative evidence of glacio-isostatic rebound. Reviews of Geophysics and Space Physics, **10**: 849-884.

CHAPTER TWO

Late Wisconsinan glaciation of Amund and Ellef Ringnes islands, Nunavut: evidence for the configuration, dynamics and deglacial chronology of the northwest sector of the Innuitian Ice Sheet[1].

2.1 Introduction

Previous studies of the Quaternary geology of the Queen Elizabeth Islands (QEI) have indicated that the Innuitian Ice Sheet (IIS) extended through the central and eastern sectors of the archipelago during the Late Wisconsinan and coalesced with the Greenland Ice Sheet to the east and the Laurentide Ice Sheet to the south (England 1998, 1999; Dyke 1998). The IIS was originally proposed by Blake (1970, 1972), who suggested that a broad zone of greater Holocene emergence between Bathurst Island and Eureka Sound recorded glacioisostatic rebound following the removal of a pan-archipelago ice sheet (Figure 2.1). This glacioisostatic signature, termed the Innuitian uplift (Walcott 1972), was inferred to coincide with the former axis of maximum ice sheet thickness. Recent investigations have unified the glacial and relative sea-level history of islands bordering the Innuitian uplift and demonstrate that the IIS consisted of an alpine sector in the eastern QEI and a lowland sector in the central QEI (Ó Cofaigh 1997, 1999; Bednarski 1998; Dyke 1998, 1999; England 1998, 1999; England and Ó Cofaigh 1998; Ó Cofaigh et al. 2000; Lamoureux and England 2000). The glacial and emergence history of islands along the western margin of the Innuitian uplift, however, remains uncertain, and requires clarification so that the terrestrial record of the western QEI can be better integrated with

[1] An earlier version of this chapter has been published in Can. J. Earth Sci. **40**: 351-363 (2003).

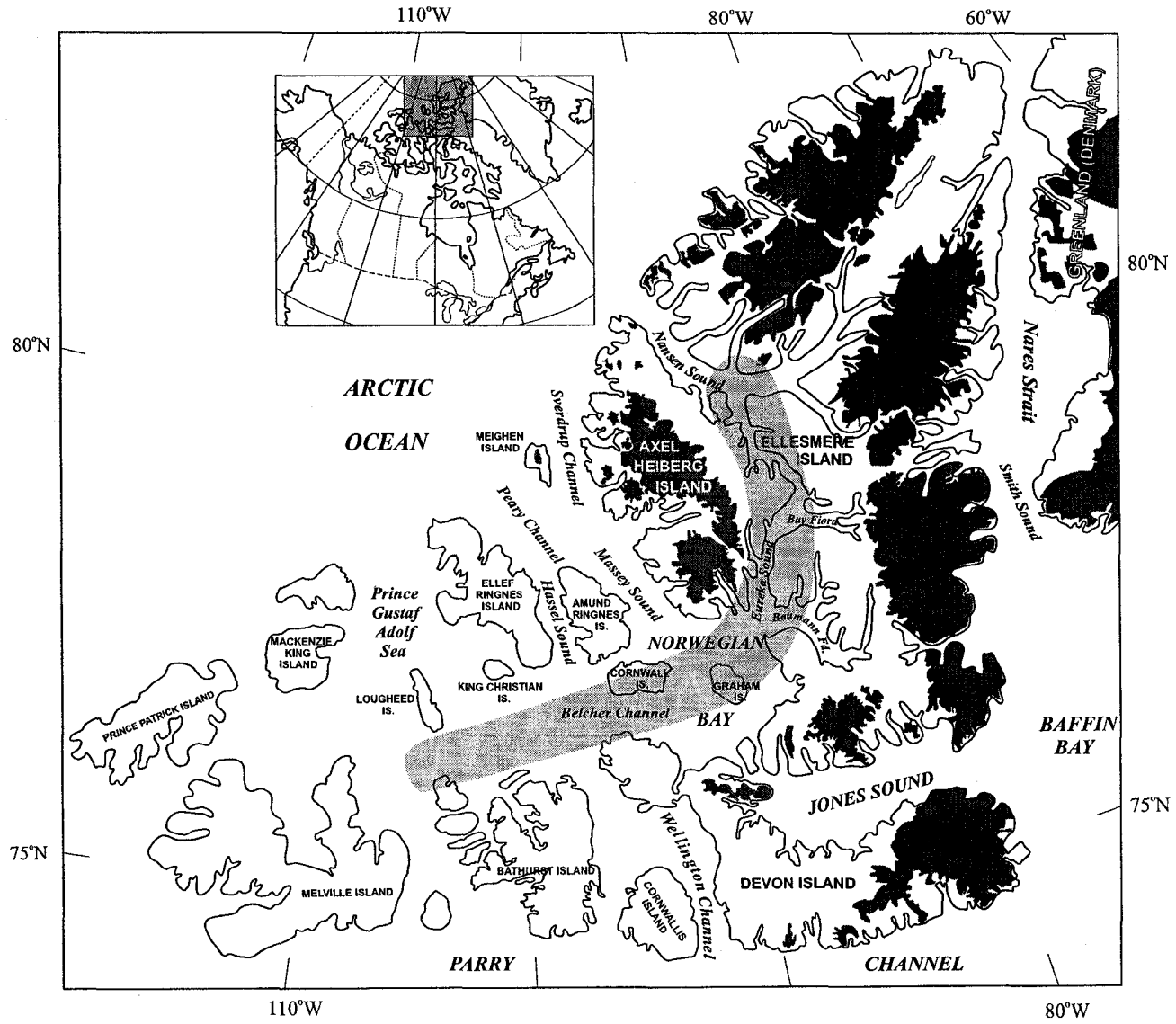

Figure 2.1. Regional map of the Queen Elizabeth Islands and the adjacent coast of Grenland. Axis of the Innuitian uplift is shaded light gray. Contemporary ice caps are shaded in dark gray.

ice sheet reconstructions for the eastern and central QEI. Amund and Ellef Ringnes islands occupy the northwest margin of the Innuitian uplift (Figures 2.1 and 2.2). This chapter presents new data concerning the glacial history of the Ringnes Islands that further clarify the extent, configuration and dynamics of the IIS and contribute to our understanding of its role in the ocean-atmosphere system (cf. Rogers et al. 2001; Darby et al. 2002).

2.2 Previous Research

Striae, esker-like ridges, diamict and glacial erratics record at least one extensive glaciation of Amund and Ellef Ringnes islands (St-Onge 1965, Stott 1969; Balkwill et al. 1974; Hodgson 1982; Balkwill 1983). However, it has not been determined whether these features record coverage of the islands by the IIS, or if they relate to former advances of the LIS, the expansion of local ice caps (cf. Hodgson 1982) or a combination of the three. Evidence of glaciation elsewhere in the western QEI includes northwest-oriented ice-flow indicators on Lougheed Island (Hodgson 1981), and granite erratics of unknown provenance on King Christian, Lougheed and Prince Patrick islands (Hodgson 1977, 1982, 1990; Figure 2.1).

East of the Ringnes Islands, in the alpine sector of the QEI, striae, granite dispersal trains and lateral meltwater channels are attributed to ice-flow from Late Wisconsinan divides on Ellesmere and Axel Heiberg islands. These supplied ice that converged in the intervening lowlands surrounding Nansen and Eureka sounds and Norwegian Bay (Hodgson 1985; Bell 1996; Bednarski 1998; Atkinson 1999; England 1999; Ó Cofaigh et al. 2000; England et al. in press; Figure 2.1). South of the Ringnes Islands, glacial landforms on Cornwall Island are also of Late Wisconsinan age

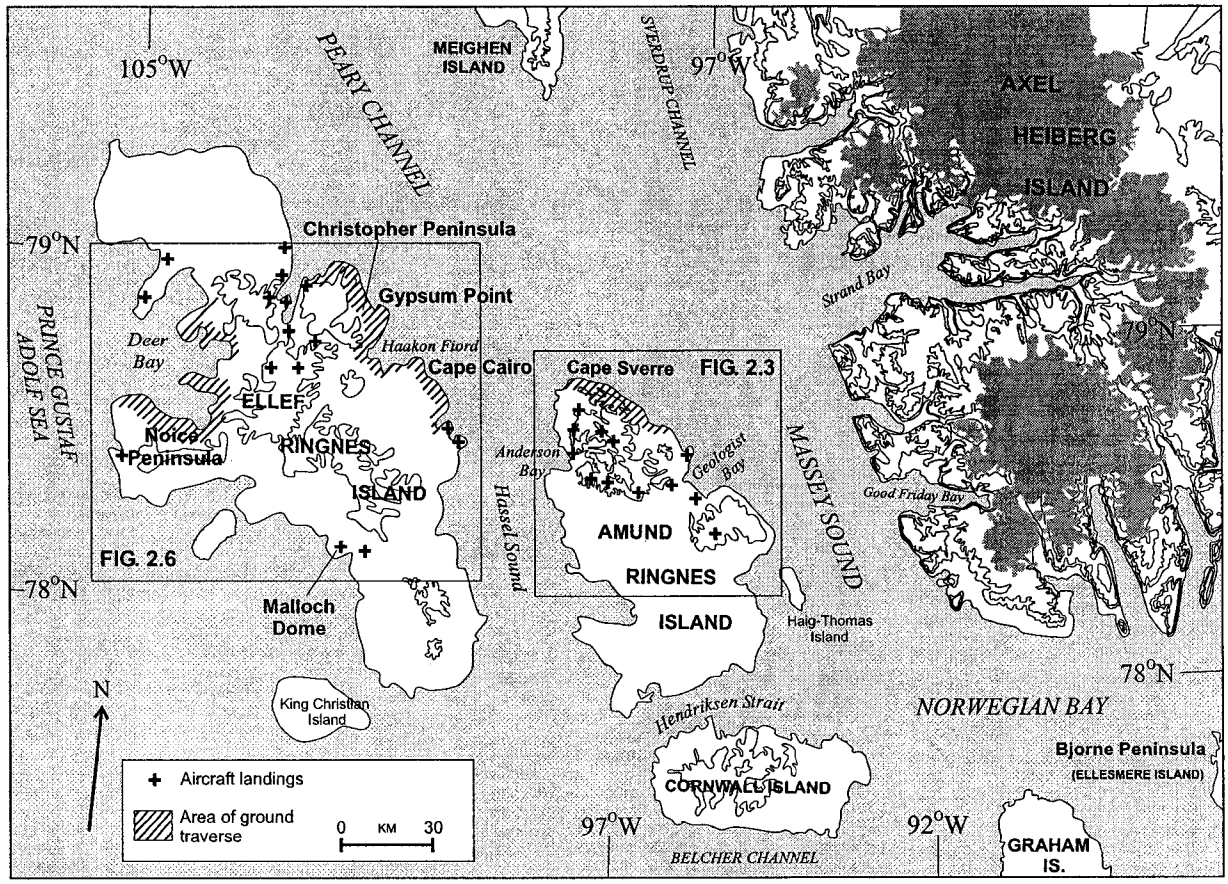

Figure 2.2. Northwest Queen Elizabeth Islands, showing Amund and Ellef Ringnes islands, and place names referred to in the text. Countour interval 100 m. Contemporary ice caps are shaded.

and are attributed to the northward flow of lowland ice from a NE-SW trending divide that is recorded by the extension of the Innuitian uplift through Belcher Channel (Lamoureux and England 2000). Southward flow from this divide supplied a proposed ice stream in Wellington Channel (Dyke 1999; Figure 2.1). England (1998) hypothesized that Norwegian Bay was an important conduit within the IIS because it was the focus of convergent ice-flow from encircling alpine divides of the eastern QEI as well as the lowland divide north of Wellington Channel. This paper tests the hypothesis that the convergence of alpine and lowland ice in Norwegian Bay resulted in the dispersal of Innuitian ice across the Ringnes Islands and through Massey and Hassel sounds during the Late Wisconsinan (Blake 1970, 1972; Figure 2.2).

2.3 Study area

2.3.1 Physiography and climate

Amund and Ellef Ringnes islands (5, 255 and 11, 295 km^2 respectively) occupy the eastern part of the Sverdrup Lowland, a shallow topographic depression within the Sverdrup Basin (Dawes and Christie 1991). The lowland is bounded to the south and east by the Parry Uplands and Axel Heiberg mountains and opens to the northwest towards the Arctic Coastal Plain and Arctic Ocean (Dawes and Christie 1991). The region is characterized by gently dipping Mesozoic bedrock that is poorly to moderately consolidated (Dawes and Christie 1991; Balkwill 1983). The dominant surficial material is residual weathered bedrock and unconsolidated, clay to sand-sized marine-reworked rock (Hodgson 1982). The surface morphology comprises lowland plains (<60 m asl), scarped lowlands containing castellated, basic igneous intrusions (≤150 m asl) and dissected, evaporite piercement domes that commonly contain basic igneous dykes and

sills (150 to 265 m asl; Roots 1963). Plateau gravels of quartzose sandstone with minor siltstone, gabbro, carbonate, quartzite and occasional granite clasts occur as scattered remnants, particularly on primary watersheds, on both islands, and indicate that the bedrock morphology developed through Late Tertiary and Quaternary fluvial planation and dissection (Hodgson 1982). In contrast to Ellesmere and Axel Heiberg islands, this region, to paraphrase Sugden (1978, p. 373), would not be in much demand for the making of Canadian whisky commercials or Secret Service movies! Shallow shelves, less than 200 m deep, surround both islands (Horn 1963), but these are incised by broad, northwest-oriented channels, 200-500 m deep. Within Peary Channel, Massey and Hassel sounds and Prince Gustaf Adolf Sea (Figure 2.1), locally elongate, northwest-oriented troughs have water depths between 500 and 700 m (Horn 1963).

The Ringnes Islands are currently ice-free, and lie below the regional equilibrium line altitude (300-400 m asl; Miller et al. 1975), as they receive only small amounts of precipitation (≤125 mm; Maxwell 1981). Nevertheless, the islands experience the lowest mean summer temperatures in Arctic Canada (3°C) due to the reduction of insolation by persistent low-lying stratus and stratocumulus clouds from the Arctic Ocean (Maxwell 1981). Hence, the Ringnes Islands could have supported local ice caps in the past, as neighbouring Meighen Island, ~100 km to the north, does today.

2.4 Research methods

Reconstruction of the glacial history of Amund and Ellef Ringnes islands involved mapping glacigenic sediments, landforms and glacially transported erratics as well as surveying raised marine shorelines and sediments, and radiocarbon dating associated molluscs and driftwood. Mapping was based on aerial photo interpretation of

both islands, ground traverses across coastal areas located above and below marine limit, and helicopter surveys of inland sites (Figure 2.2). Wherever possible, stratigraphic exposures were examined. Raised marine sediment was surveyed by altimetry and wherever possible, related to former ice margins, recorded by lateral meltwater channels or moraines. Altimeter readings were corrected for changes in temperature and pressure and measured relative to high tide (tidal range in the area is ~1 m). Chronologic control was provided by Accelerator Mass Spectrometry (AMS) radiocarbon dating of organic materials recovered from glacigenic and raised marine sediments.

2.5 Field Observations

The distribution of glacial landforms in the study area is discussed for northern Amund Ringnes Island (ARI), followed by eastern and western Ellef Ringnes Island (ERI).

2.5.1 Glacial Geomorphology

Amund Ringnes Island

Large grooves, ~5 km inland and parallel to the coast of Massey Sound occur on east-central ARI (Balkwill et al. 1974; Figure 2.3). Well-preserved wedge and nailhead striae (cf. Drewry 1986; Benn and Evans 1998), record a similar flow direction across sandstone and ice-moulded basalt on the northeast coast of ARI (Figure 2.3). East of Cape Sverre, ice-moulded basalt is overlain by a blanket of diamict, termed the Amund Ringnes diamicton (Hodgson 1982). The blanket is up to 10 m thick, extends 14 km alongshore and 2.5 km onshore, forming a generally horizontal, coast-parallel margin to 100 m asl (Figures 2.3 and 2.4). It has a largely featureless surface, although

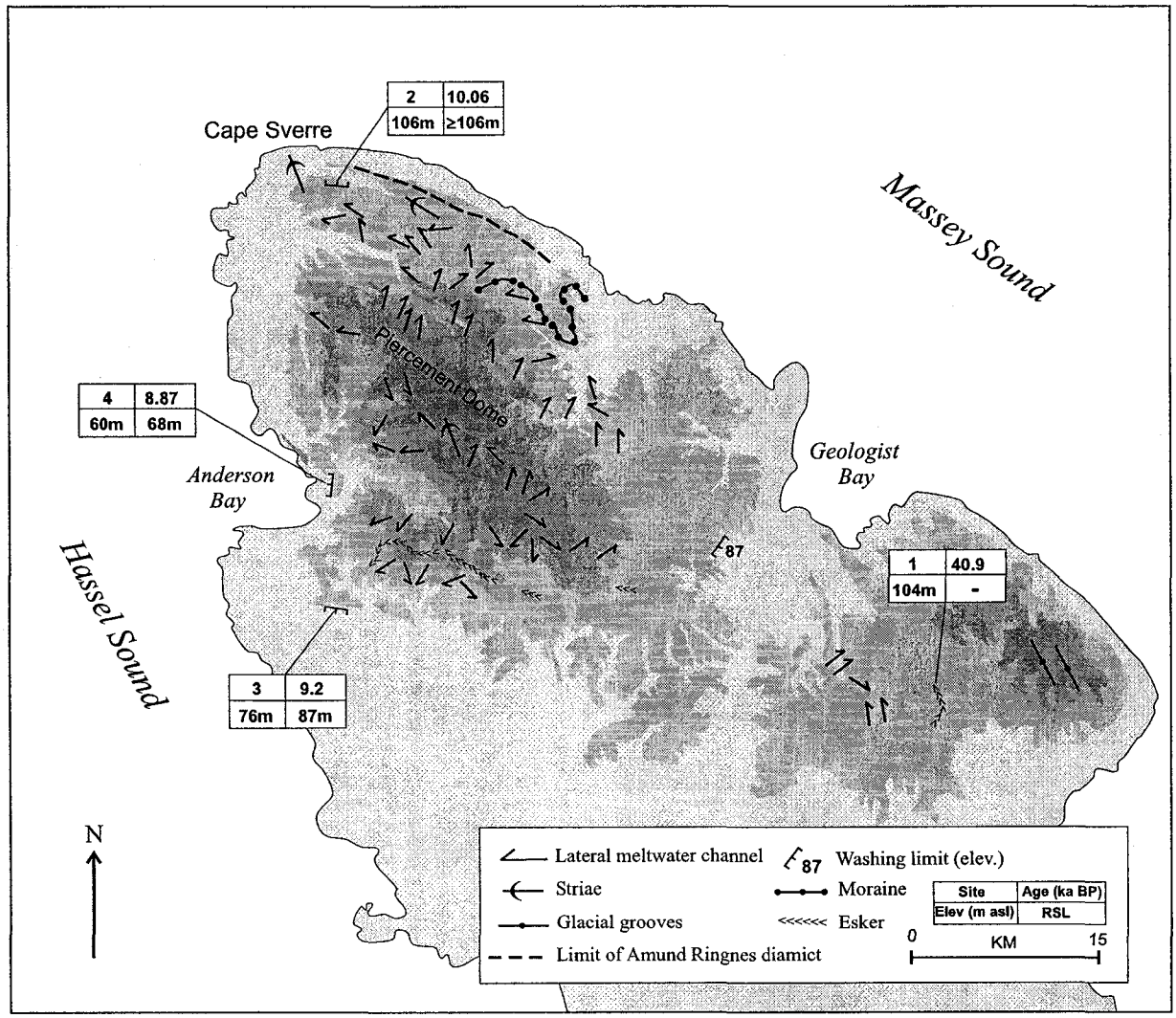

Figure 2.3. Glacial geomorphology, northern Amund Ringnes island. Hypsometric tint interval 100. Elev (m asl), elevation (metres above sea level); RSL, relative sea level.

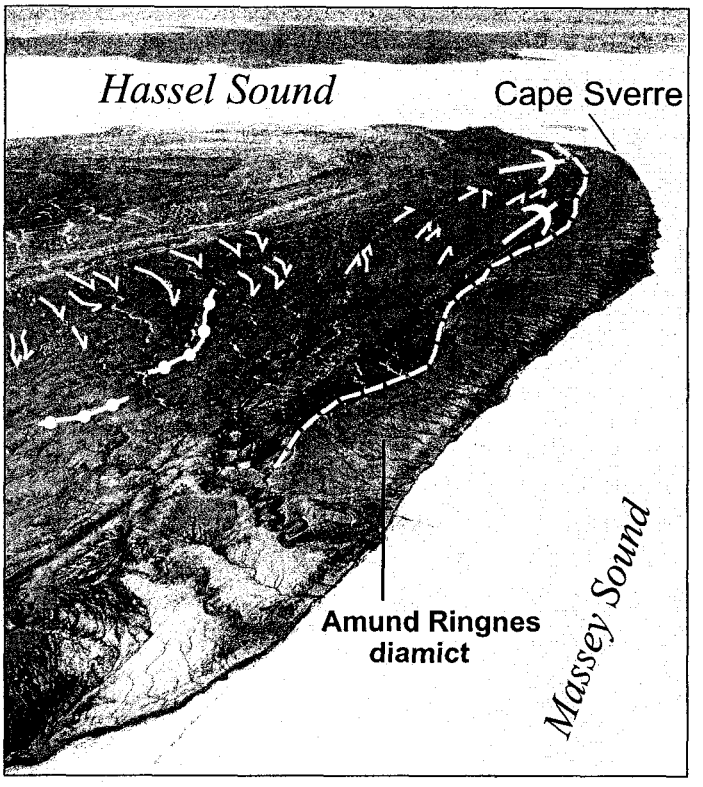

Figure 2.4. Oblique photograph showing glacial geomorphology of northern Amund Ringnes Island. Symbols used are the same as in Figure 2.3.

occasional gravelly sand kames occur towards the inland margin. The diamict is structureless, moderately plastic, containing abundant striated clasts, including granite, within a massive silty matrix, and is off-lapped by Holocene raised marine sediment (Hodgson 1982). Striated and faceted granite erratics (Figure 2.5) are widespread between Cape Sverre and Geologist Bay and cover all terrain, including upland ridges (up to 140 m asl), although their abundance decreases inland, and none were observed >7 km west of the coast (Figure 2.3). Balkwill (1983) reported a granite block (~1 m^3) at 245 m asl on Piercement Dome (Figure 2.3). However, despite additional searches during the course of this study, granite erratics were not observed elsewhere on the dome, which is largely mantled by gypsum residuum, and to a lesser extent, calcareous and intrusive igneous felsenmeer and fine-grained colluvium. Northerly oriented striae described on Piercement Dome (Balkwill et al. 1974) parallel striae at Cape Sverre and record ice-flow across the interior of the island into Peary Channel (Figures 2.2 and 2.3).

Northwest-trending, linear to slightly sinuous eskers of variable width (30-200 m) and thickness (≤6 m) extend oblique to bedrock strike across ARI, from Massey Sound to Anderson Bay (Figure 2.3). One esker on east-central ARI is 3.4 km long and is composed of local granule to boulder gravel with occasional granite pebbles. A maximum estimate of its age is provided by a surface fragment of *Hiatella arctica* dating 40 890 ± 580 years BP (Site 1, Figure 2.3; Table 2.1). South of Piercement Dome, a sinuous, sharp-crested esker extends for 15 km towards Anderson Bay (Balkwill et al. 1974; Hodgson 1982; Balkwill 1983). It is comprised of well-rounded cobble to boulder gravel of local origin, but also contains significant quantities of granite.

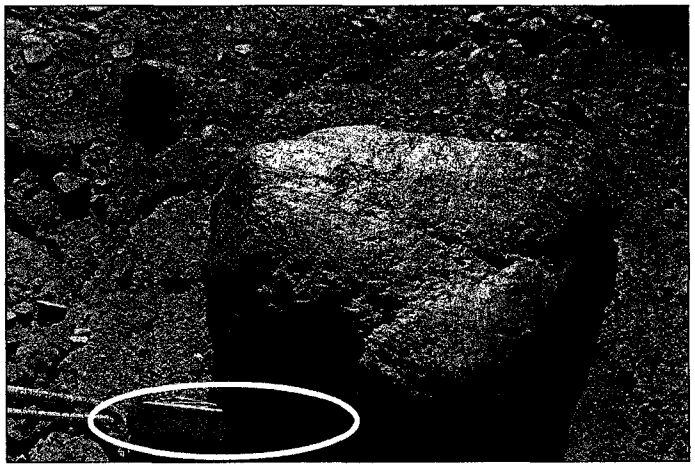

Figure 2.5. Striated granite erratic on the surface of the Amund Ringnes diamict. Penknife is circled for scale.

Table 2.1. Pre-Holocene radiocarbon dates (see Figures 2.2 and 2.3 for sample locations).

Sample	Location	Laboratory dating No.[a]	Material	Age (14C years BP)	Enclosing material	Sample elevation (m asl)	Relative sea level (m asl)	Lat. °N	Long. °W	Reference
1	Geologist Bay	CAMS-66145	*H. arctica*	40 890 ± 580	Gravel	104	unknown	78° 46'	97° 40'	Atkinson (2003)
	Cornwall Island	AA-23577	*M. truncata*	37 280 ± 1000	Diamict	119	unknown	78° 33'	97° 58'	Lamoureux & England (2000)
	Cornwall Island	TO-5616	*A. Borealis*	30 710 ± 350	Diamict	149	unknown	78° 28'	97° 48'	Lamoureux & England (2000)
	Cornwall Island	AA-23580	shell fragment	43 110 ± 1870	Diamict	128	unknown	78° 34'	97° 58'	Lamoureux & England (2000)
	Cornwall Island	Beta-111708	*A. Borealis*	35 820 ± 540	Diamict	120	unknown	78° 35'	98° 04'	Lamoureux & England (2000)
	Cornwall Island	Beta-111710	*A. Borealis*	35 750 ± 490	Diamict	121	unknown	78° 02'	95° 14'	Lamoureux & England (2000)
	Graham Island	GSC-1590	*H. arctica*	>22 000	unknown	130	unknown	78° 19'	97° 45'	Blake (1987)
	SW Ellesmere Island	TO-5602	*M. truncata*	35 310 ± 400	Till	191	unknown	78° 10'	87° 24'	O'Cofaigh et al. (2000)
	SW Ellesmere Island	GSC-6469	*H. arctica*	>33 000	Marine silt	67	>90	77° 48'	87° 46'	England et al. (in press)
	SW Ellesmere Island	TO-9486	shell fragment	33 460 ± 380	Till	175	unknown	77° 50'	86° 47'	England et al. (in press)
	SW Ellesmere Island	TO-9485	shell fragment	32 670 ± 310	Till	175	unknown	77° 50'	86° 47'	England et al. (in press)
	SW Ellesmere Island	TO-9498	shell fragment	32 070 ± 290	Till	209	unknown	77° 15'	85° 30'	England et al. (in press)
	SW Ellesmere Island	GSC-2700	*H. arctica*	30 100 ± 750	Gravelly silt	103-108	unknown	77° 29'	85° 45'	Hodgson (1985)

Notes: m asl, metres above sea level.

[a] *Laboratory designations*: CAMS, Lawrence Livermore; Beta, Beta Analytic; GSC, Geological Survey of Canada; TO, IsoTrace Laboratory; AA, University of Arizona. Samples of marine shells were corrected for isotopic fractionation to a base of ^{13}C=-25°/$_{oo}$ and corrected for a marine reservoir effect of 410 years. Quoted errors represent 68% confidence limits.

Lateral meltwater channels are the most prominent erosional landform and flank a number of the valleys in the scarped lowlands (Figure 2.3). They descend towards the coast, but were not observed to terminate at ice-contact deltas. Lateral meltwater channels are particularly well developed on Piercement Dome and elsewhere extend across all terrain, including local summits (~230 m asl). An arcuate moraine is nested between a series of lateral meltwater channels in the scarped lowlands of northeast ARI (Figures 2.3 and 2.4).

East-central Ellef Ringnes Island

The surficial geology of Christopher Peninsula and Cape Cairo has a non-glacial character and is dominated by weathered bedrock ranging from blockfields to blankets of stony to fine-grained residuum, and patchy diamict. The major outcrops in the area consist of basalt escarpments along Peary Channel and sandstone hoodoos in central Christopher Peninsula. The coastal lowlands of east-central ERI are characterized by seaward-dipping, well-sorted, fine to medium grained, cemented to nonindurated sandstone, with occasional silt interbeds. The sandstone does not contain erratics, ice-rafted debris (IRD) or shells, and is therefore considered to be part of the Isachsen and Eureka Sound formations (cf. Balkwill 1983). However, the bedrock is off-lapped by a veneer of marine sand and mud, containing clasts of IRD and early Holocene valves of *Mya truncata* and *H. arctica* (Sites 5, 6, 7 and 10, Figure 2.6; Table 2.2).

Two east-west trending, linear to slightly sinuous eskers extend for 5 and 20 km across central ERI, to the east and south of Louise Fiord (St-Onge 1965; Figures 2.6 and 2.7). Both eskers are broad-crested, 1-5 m thick and consists of a well-rounded cobble

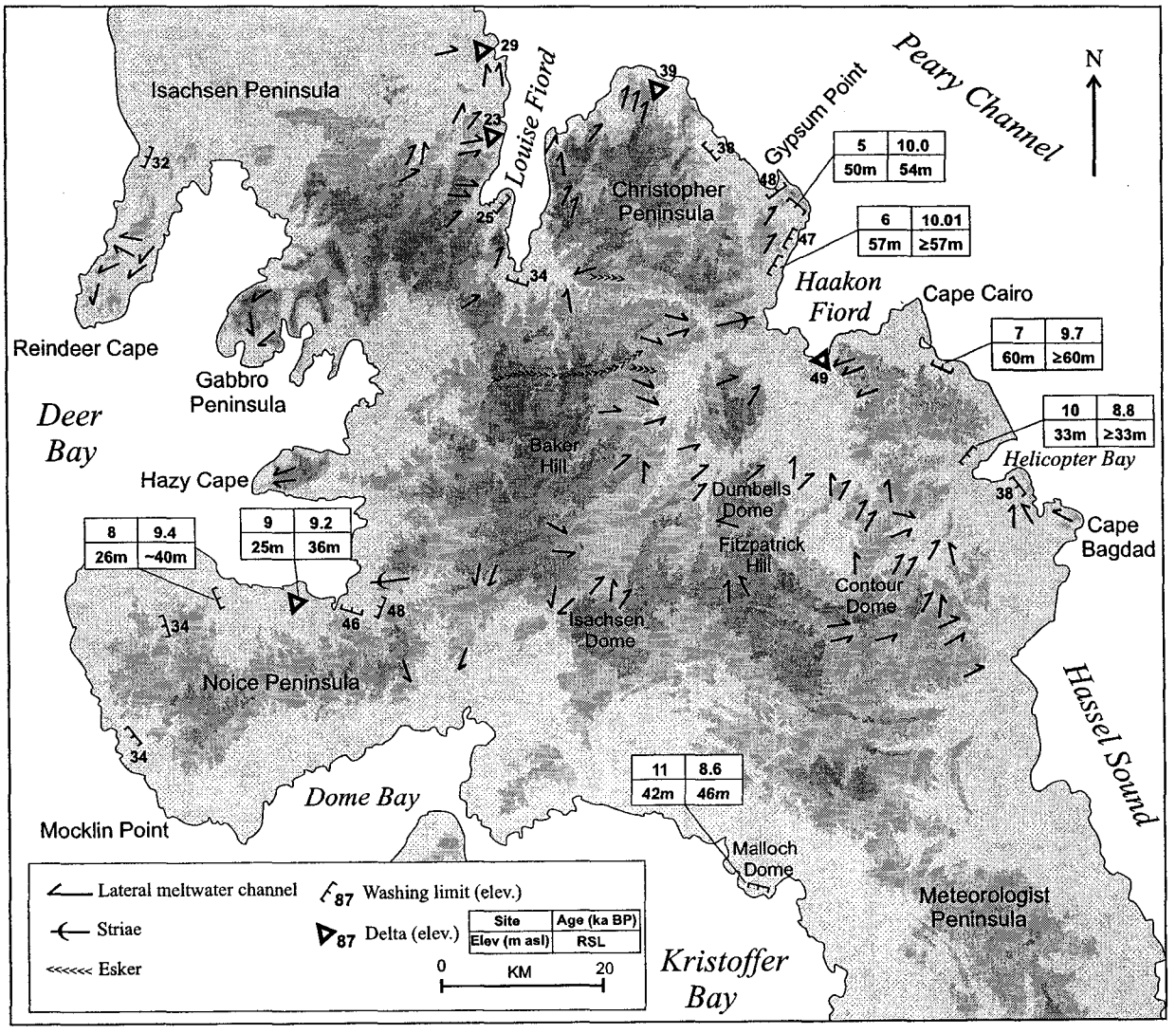

Figure 2.6. Glacial geomorphology of Ellef Ringnes Island. Hypsometric tint interval 100 m. Abreviations as in Figure 2.3.

Table 2.2. Holocene Radiocarbon Dates (see Figures 2.3 and 2.6 for sample locations)

Sample	Location	Laboratory dating No.[a]	Material	Age (14C years BP)	Calibrated age[b] (cal. years BP)	Enclosing material	Sample elevation (m asl)	Relative sea level (m asl)	Lat. N	Long. W	References
Amund Ringnes Island											
2	Cape Sverre	CAMS-66145	*H. arctica*	10 060 ± 60	11 200	fine-grained residuum	106	≥106	78° 46'	97° 40'	Atkinson (2003)
3	Anderson Bay	Beta 141599	*M. truncata*	9230 ± 60	10 300	fine-grained *residuum*	76	≥76- ≤87	78° 28'	97° 48'	Atkinson (2003)
4	Anderson Bay	Beta-141600	*M. truncata*	8870 ± 60	9660	marine silt	60	≥60- ≤68	78° 33'	97° 58'	Atkinson (2003)
Ellef Ringnes Island											
5	Haakon Fiord	TO-9501	*M. truncata*	10 000 ± 70	11 140	marine sand	50	54	78° 56'	101° 01'	Atkinson (2003)
6	Haakon Fiord	TO-9503	*M.truncata*	10 010 ± 70	11 140	gravelly residuum	56	≥56	78° 52'	101° 10'	Atkinson (2003)
7	Cape Cairo	TO-9750	*H. arctica*	9690 ± 90	10 680	fine-grained residuum	60	≥60	78° 45'	100° 15'	Atkinson (2003)
8	N. Noice Peninsula	TO-9748	*H. arctica*	9400 ± 70	10 260	marine-reworked sand	26	≥26- ≤40	78° 58'	101° 06'	Atkinson (2003)
9	N. Noice Peninsula	TO-9747	*H. arctica*	9190 ± 90	10 080	marine-reworked sand	25	≥25- ≤36	78° 58'	101° 07'	Atkinson (2003)
10	Helicopter Bay	TO-9749	*H. arctica*	8770 ± 160	9530	fine-grained residuum	33	≥33			Atkinson (2003)
11	Malloch Dome	TO-9751	*H. arctica*	8560 ± 110	9410	beach gravel	42	≥42- ≤46	78° 44'	100° 10'	Atkinson (2003)
	Dome Bay	GSC-2472	Plant material	11 800 ± 380	14 300	unknown	26	unknown	78° 44'	100° 10'	McNeely (1989)

Notes: m asl, metres above sea level.

[a] Laboratory designations: CAMS, Lawrence Livermore; Beta, Beta Analytic; GSC, Geological Survey of Canada; TO, IsoTrace Laboratory; L, Lamont-Doherty. Samples of marine shells were corrected for isotopic fractionation to a base of ^{13}C=-25‰ and corrected for a marine reservoir effect of 410 years. Quoted errors represent 68% confidence limits.

[b] All ages calibrated using CALIB4.4 (Stuvier and Reimer 1986-2002).

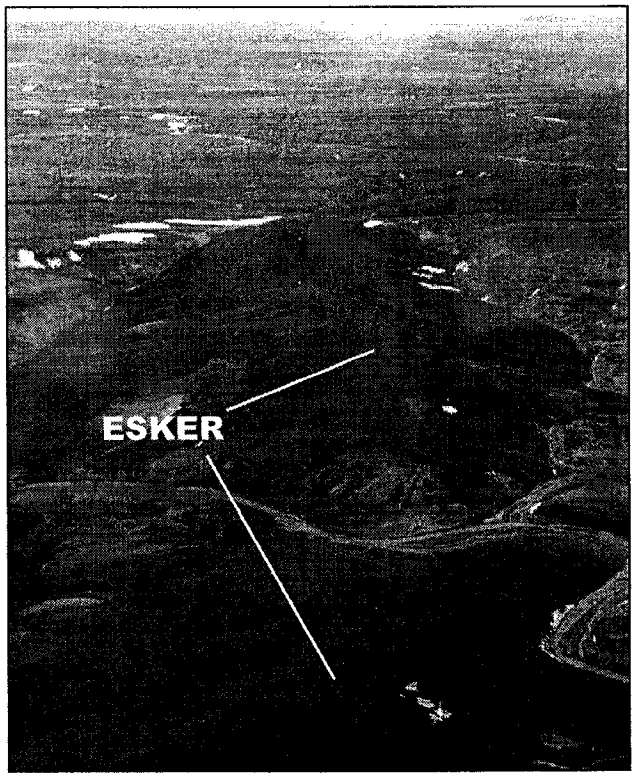

Figure 2.7. Oblique photograph of esker south of Louise Fiord. Image faces east.

to boulder gravel of local lithologies, draped over weathered bedrock. Imbrication records an easterly palaeoflow. On southeast Christopher Peninsula, ice-moulding of limestone at 67 m asl also has an east-west orientation (Figure 2.6). Locally derived, well-rounded and occasionally facetted quartzite boulders and striated basalt blocks record ice-flow across Christopher Peninsula and Cape Cairo. However, the direction of their transport is unknown. Granite erratics are only observed on the north coast of Helicopter Bay, where they mantle wave-washed rock up to 29 m asl.

Lateral meltwater channels eroded in diamict and bedrock occur throughout the uplands flanking Louise and Haakon fiords (Figure 2.6). The uppermost channels extend along these fiords and terminate at the outermost coast of central ERI. In the uplands of east-central ERI, lower lateral meltwater channels terminate at ice-contact, marine limit deltas. Elsewhere, lateral meltwater channels are nested in the direction of ice retreat into Baker and Fitzpatrick hills and Dumbells and Contour domes (Figure 2.6).

West-central Ellef Ringnes Island

Wedge striae on quartzose sandstone record westerly ice-flow from the interior of ERI into Deer Bay (Figures 2.6 and 2.8). Along the south coast of Deer Bay, polished quartzite and ironstone erratics are scattered from marine limit to upland summits (up to 100 m asl) and provide the only indicators of ice cover on Noice Peninsula. Striae or erratics of unequivocally glacial origin were not observed on the uplands along northern Deer Bay, from Hazy to Reindeer capes, where outcrops are mantled by blockfields, stony residuum and scattered veneers of well-rounded gravel containing local and erratic pebbles, including granite. Along much of the coastal plain of Deer Bay, outcrops of cemented to nonindurated Isachsen Formation sandstone are mantled by marine reworked

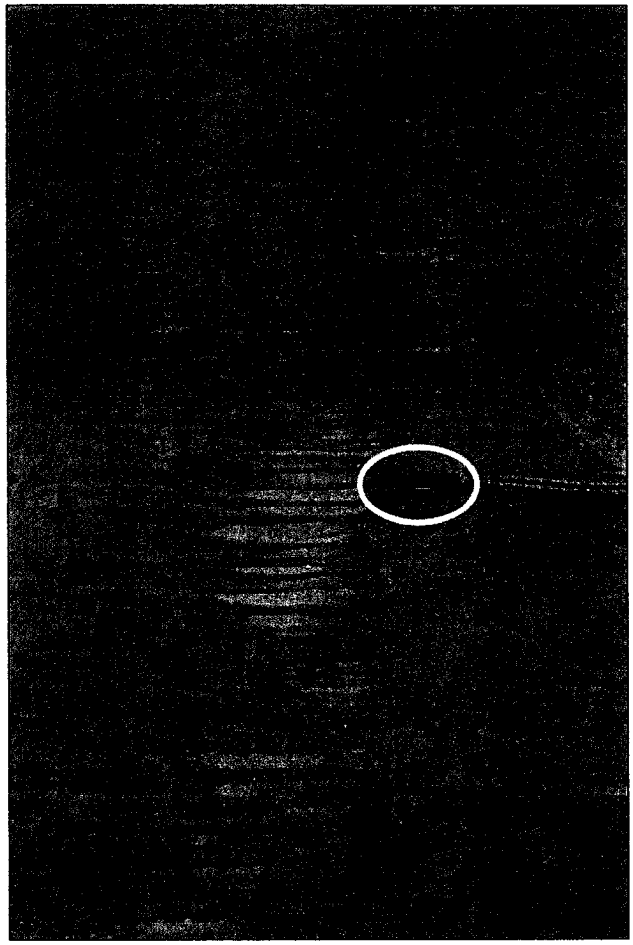

Figure 2.8. Striated sandstone recording ice-flow into Deer Bay, west-central Ellef Ringnes Island. Ice-flow is from left to right. Penknife is circled for scale.

veneers of sand containing IRD and early Holocene shells of *H. arctica*. (Sites 8 and 9, Figure 2.6; Table 2.2).

Lateral meltwater channels are poorly developed in west-central ERI. Where lateral meltwater channels do occur, they are nested towards the interior of the island (Figure 2.6). Channels are better developed to the north, and flank a number of the valleys on Reindeer Cape and Gabbro Peninsula, extending towards the coast across local summits (≤150 m asl; Figure 2.6). These channels were not observed to terminate at ice-contact landforms, and lower lateral meltwater channels were not observed elsewhere on these peninsulas, restricting further delineation of this ice margin.

2.5.2 Marine limit

Marine limit on Amund and Ellef Ringnes islands often has no geomorphic expression, and in several locations, a minimum estimate can only be inferred from the highest elevation of marine shells. Radiocarbon dating of such shells provides a minimum estimate of the age of marine limit. To reduce the possibility of inferring marine limit from glacially re-deposited shells, the survey and collection of intact, thin-walled valves was favoured over shell fragments. Where marine limit was observable, it was recorded either by the highest raised marine delta and beach, or the lowest elevation to which undisturbed residuum extended, marking a former washing limit. The locations of radiocarbon-dated shell samples are presented in Figures 2.3 and 2.6, corresponding to site numbers in Table 2.2. A full presentation of marine limit is reserved for Chapter Four, in which glacioisostatic recovery and inferences concerning the distribution of ice loading along the northwest margin of Innuitian uplift are discussed.

Although Holocene marine limit in the Ringnes Islands is diachronous, it does exhibit a NW-SE slope, which rises southeastward, from Deer Bay and outer Louise Fiord (~30 m asl) across Hassel Sound to northern ARI (≥100 m asl; Figure 2.9). This slope is also demonstrated by isobases drawn across the Ringnes Islands (Chapter 4). Collectively, these data are consistent with regional marine limit elevations, which rise towards Norwegian Bay (~140 m asl) and the centre of the Innuitian uplift (Blake 1970; Walcott 1972; England and Ó Cofaigh 1998; Dyke 1998; England 1999; Ó Cofaigh 1999; Lamoureux and England 2000).

The oldest reported Holocene shells on Amund and Ellef Ringnes islands occur between Cape Sverre (Figure 2.3, Site 2; Table 2.2) and Haakon Fiord (Figure 2.6, Sites 5 and 6; Table 2.2). AMS dates on single valves from these sites record the establishment of marine limit 10 ka BP. Radiocarbon-dated marine fauna between eastern ERI and western ARI document a successive decrease in the age of marine limit along northern Hassel Sound, from 9.7 to 9.2 ka BP (Figure 2.6, Site 7 and Figure 2.3, Site 3, respectively). Similarly, radiocarbon-dated shells from northern Noice Peninsula record a decrease in the age of marine limit towards the head of Deer Bay, from 9.4 to 9.2 ka BP (Figure 2.6, Sites 8 and 9, respectively). The youngest radiocarbon-dated shells (8.9 to 8.6 ka) occur at the heads of Anderson Bay (Figure 2.3, Site 4; Table 2.2), Helicopter Bay (Figure 2.6, Site 10; Table 2.2) and Malloch Dome (Figure 2.6, Site 11; Table 2.2). These dates are all related to marine limit, hence record local deglaciation as ice retreated into the interior.

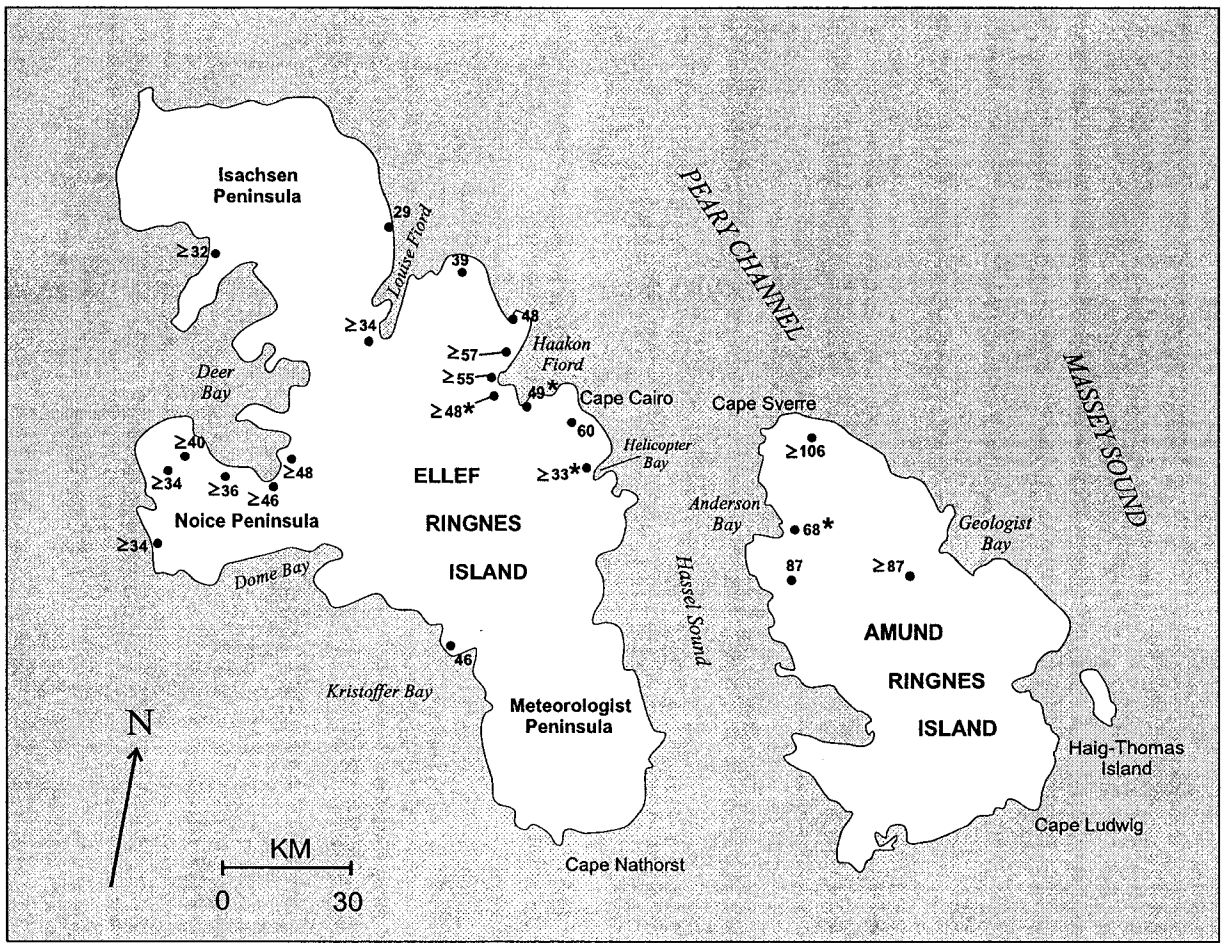

Figure 2.9. Elevation of Holocene marine limit on the Ringnes Islands. Sites where later retreat of residual ice occurred are shown (*).

2.6 Discussion

2.6.1 Ice configuration and dynamics

Striae and granite dispersal along eastern ARI suggest that Massey Sound was a major conduit for ice flowing from the alpine sector of the IIS on eastern Ellesmere Island (Figure 2.10). The uppermost striae and erratics provide a minimum estimate of the extent and thickness of granite-carrying trunk ice in Massey Sound, and indicate that it was at least 440 m thick, assuming a mean water depth of 300 m (Horn 1963; Canadian Hydrographic Service 1976). The origin of the single granite erratic reported on Piercement Dome by Balkwill et al. (1983) remains enigmatic, since there is no other glacial geomorphic evidence on northeast ARI that indicates granite-carrying trunk ice in Massey Sound extended >7 km inland. Instead, striae on Piercement Dome and at Cape Sverre indicate that the interior of ARI was overridden by predominantly granite-free ice flowing into Peary Channel. It is proposed that this flowline originated from an Innuitian divide occupying Belcher Channel, hence represents the northward extension of lowland ice that first crossed Cornwall Island (Figure 2.10; Dyke 1998; Lamoureux and England 2000). This flowline may have overtopped Piercement Dome (up to 245 m asl), and converged with granite-carrying trunk ice along the east coast of ARI, thereby keeping granite-carrying ice largely offshore, in Massey Sound.

The limited evidence of basal sliding, coupled with the preservation of pre-Quaternary surfaces in the interior of ARI, suggests northward-flowing lowland ice was generally non-erosive, possibly reflecting a cold-based thermal regime. In contrast, evidence of basal sliding along eastern ARI indicates that trunk ice flowing through Massey Sound was warm-based. This is attributed in part to internal deformation and

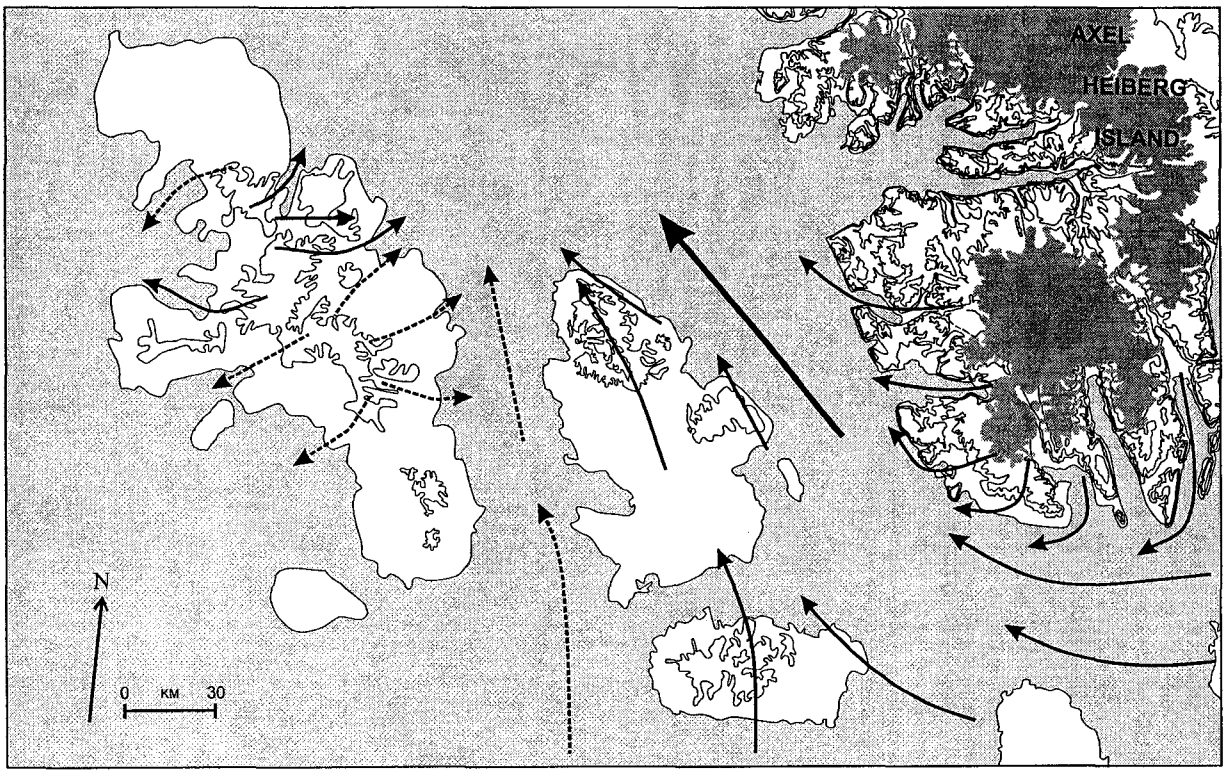

Figure 2.10. Proposed (solid arrows) and provisional (dashed arrows) ice-flow directions in the northwest Innuitian Ice Sheet across the Ringnes Islands (modified from Lamoureux and England 2000). Place names as in Figure 2.2.

strain heating downstream of Norwegian Bay (~22, 000 km^2), which, based on the inferred configuration of encircling divides, was the focus of convergent ice-flow from a catchment basin of ~78, 000 km^2 (Figures 2.1 and 2.10). The resulting acceleration of trunk ice could have been further enhanced by subglacial deformation over marine sediment within Norwegian Bay and Massey Sound (cf. Fisher et al. 1985; Hart and Boulton 1991; Lamoureux and England 2000). Consequently, it is proposed that during full-glacial conditions, flow along Massey Sound developed an ice stream (cf. Paterson 1994; Dyke 1999). This proposal is consistent with glaciological modelling of Late Wisconsinan ice sheet dynamics in the Canadian Arctic islands, which predicted an ice stream in Massey Sound, assuming that the former ice margin extended to the polar continental shelf (Reeh 1984). The probable ice-surface gradient associated with this full-glacial configuration can explain the orientation and composition of the eskers on ARI, since glaciofluvial transport of granite erratics is consistent with a north to northwest-oriented drainage system originating from alpine ice entering Massey Sound from Norwegian Bay. Such a drainage system would be favoured if the boundary between the ice stream and cold-based lowland ice was characterized by a crevassed shear zone, as displayed by contemporary ice streams in Greenland and Antarctica (Paterson 1994), which could capture supraglacial meltwater. Granite in the eskers may have originated from the Massey Sound ice stream, or been reworked from local Tertiary plateau gravel.

If granite-carrying ice extended beyond Massey Sound, there is no evidence to suggest it impinged on northeast ERI. All of the granite erratics described on ERI in this chapter are either below marine limit, and could therefore have been transported by ice rafting, or are confined to scattered gravel veneers that may be the remnants of a sheet of

Late Tertiary gravel, possibly the Beaufort Formation (cf. Hodgson 1982). Moreover, although St-Onge (1965) described well-rounded granite erratics (up to 20 cm diameter) on ERI which he considered too large to have been fluvially transported, subsequent research identified erratic *boulders* of similar lithology in the remnants of Late Tertiary fluvial gravels on this, and other islands in the region (Hodgson 1982; Fyles 1990). Nevertheless, eskers and lateral meltwater channels on ERI record widespread glaciation that covered uplands up to 210 m asl and extended at least as far as Peary Channel and Prince Gustaf Adolf Sea (Figure 2.2). Imbrication in the eskers indicates that the ice-surface gradient at the time of deposition descended from the interior towards Haakon Fiord. Ice-moulded bedrock at the head of Haakon Fiord similarly records eastward flow from the interior of ERI. However, it remains unknown whether ERI was covered by a full-glacial, local ice cap, or Innuitian ice flowing north through Hassel Sound from the lowland divide which extended through western Belcher Channel, north of Bathurst Island (Figures 2.1 and 2.10). Although there is no first-order glacial geologic evidence recording ice advance through Hassel Sound, one explanation for the absence of pre-Holocene marine fauna from the surrounding coasts of Amund and Ellef Ringnes islands is that the sea was unable to enter the channel due to trunk ice occupation prior to 10 ka BP.

2.6.2. Chronology of ice buildup

AMS dates on individual shell fragments in till on east-central Ellesmere Island provide the youngest estimates on the buildup of the alpine sector of the IIS, and indicate that Ellesmere trunk glaciers advanced east after 19 ka BP (England et al. 2000; Figure 2.1). AMS dated subtill organic deposits on southeast Ellesmere Island suggest that the

westward flow of granite-carrying ice from an alpine divide over part of the Canadian Shield that supports the modern Prince of Wales Icefield occurred after 19.8 ka BP (Blake 1992; Figure 2.1). Currently, the only pre-Holocene radiocarbon dates that constrain the advance of the IIS towards the Ringnes Islands occur on southwest Ellesmere, Graham and Cornwall islands, where 12 mid-Wisconsinan AMS dates from individual shell fragments from diamicts deposited above marine limit date between >22 and 43 ka BP (Figures 2.1 and 2.2; Table 2.1; Hodgson 1985; Blake 1987; Lamoureux and England 2000; Ó Cofaigh et al. 2000; England et al. in press). The youngest finite date (30.1 ka BP) provides a maximum estimate for ice buildup in the central QEI. Although these dates are superceded by the 19.8 ka BP date adjacent to the Prince of Wales Icefield, they do suggest that mid Wisconsinan shells were redeposited on southwest Ellesmere, Graham and Cornwall islands by ice advancing through Baumann Fiord and Norwegian Bay during the Late Wisconsinan (Figure 2.2; Lamoureux and England 2000; Ó Cofaigh et al. 2000; England et al. in press). Although a 40.9 ka BP shell fragment is incorporated within an esker on east-central ARI (Figure 2.3, Site 1; Table 2.1), this date may be older (cf. Bradley 1985), so it remains unknown whether this and other glacigenic sediments on the Ringnes Islands were also deposited during Late Wisconsinan glaciation. Nevertheless, if these sediments were deposited during a pre-mid Wisconsinan glaciation, there is no evidence in the stratigraphic record of the Ringnes Islands for a glaciation of that age. McNeely (1989) reported a date of 11.8 ka BP on allochthonous plant material (mainly moss and lichen) enclosed in silt and fine sand at 26 m asl at Dome Bay, west-central ERI (Table 2.2). However, the significance of this date is equivocal, since it was based on a mixed sample of uncertain stratigraphic context,

therefore may have included material of different ages (pre and post-glacial) and origin (local or ice transported). Therefore, aside from mid Wisconsinan aged erratic shells, all of the chronologically constrained raised marine sediments and landforms surveyed on the Ringnes Islands and presented in this paper relate to deglaciation and postglacial emergence during the early Holocene.

2.6.3 Deglaciation and Holocene ice dynamics

Prior to 10 ka BP, parts of the Ringnes Islands were subsumed beneath the northwest sector of the IIS, which consisted of coalescent ice-flow originating from an alpine divide on southeast Ellesmere Island and lowland divide centered on Belcher Channel (Figure 2.2). However, by 10 ka BP, trunk ice in Hassel and Massey sounds had retreated to Gypsum Point and Cape Sverre (Figure 2.11). Deglacial dates from Lougheed Island indicate that Prince Gustaf Adolf Sea was also ice-free by 10 ka BP (Lowdon et al. 1967; Figure 2.1). The distribution of radiocarbon-dated marine fauna along eastern ERI and western ARI records the sequential re-entry of the sea into Hassel Sound, accompanying the retreat of trunk ice between 9.7 and 9.2 ka BP (Figure 2.11). Radiocarbon dates from northern Noice Peninsula suggest deglaciation of western ERI commenced prior to 9.4 ka BP, and that by 9.2 ka BP, Deer Bay was ice-free (Figure 2.11). Up-ice, towards the lowland divide, deglaciation of Cornwall Island commenced by 9 ka BP (Lamoureux and England 2000), suggesting that trunk ice had retreated from Massey Sound and into Norwegian Bay within ~1000 ^{14}C years. These data are complemented by the deglacial history of the outer coast of west-central Axel Heiberg Island, which became ice-free from ~8.8 ka BP (Morrison 2000). Collectively, these data document the breakup of the northwest IIS and suggest that its marine-based trunk

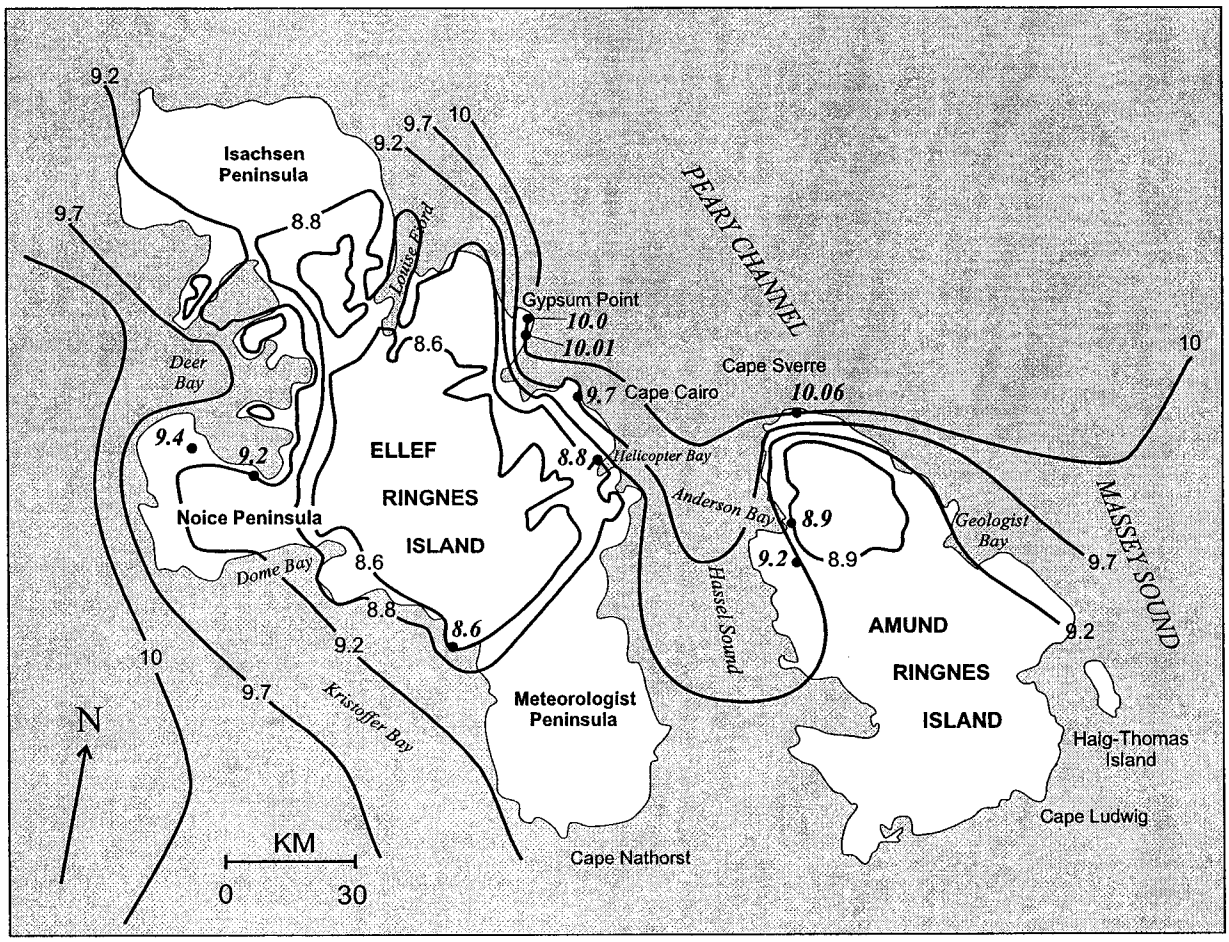

Figure 2.11. Provisional deglacial isochrones based on geomorphology and available radiocarbon dates from the Ringnes Islands.

glaciers became vulnerable to calving, likely due to the combined effects of ongoing global eustatic sea-level rise (Fairbanks 1989; Bard et al. 1990), changes in mass balance and basal ice conditions in response to the early Holocene insolation maximum (Berger 1988; Koerner and Fisher 1990; Van der Veen 1996), as well as warmer sea surface temperatures (Dyke et al. 1996; Briffa et al. 2001).

Geomorphic evidence along northeast ARI provides further indication of the style of deglaciation, and suggests that eustatic sea-level rise was responsible for decoupling trunk ice in Massey Sound from its bed. This is demonstrated by the morphology of the Amund Ringnes diamict, which forms a generally featureless coastal sheet that extends 2.5 km inland and has a low gradient margin (Figure 2.4). The horizontality and elevation of this sheet in relation to marine limit is attributed to deposition by ice with a low driving stress, and is similar to till sheets deposited by former ice shelves on southern Melville and Victoria islands (Hodgson and Vincent 1984; Hodgson, Vincent and Fyles 1984; Hodgson 1994). The Amund Ringnes diamict is thus considered to be a till sheet deposited by an ice shelf that flowed onshore by creep spreading (cf. Paterson 1994) prior to 9 ka BP. This explanation is favoured over a full-glacial origin, since the Amund Ringnes diamict lacks features characteristic of moraines at ice stream shear margins, such as are found along the M'Clintock Channel ice stream, which drained the northwest margin of the Laurentide Ice Sheet (cf. Stokes and Clark 2002)

Deglaciation of Anderson and Helicopter bays at 8.9 and 8.8 ka BP, respectively, indicates that local ice caps maintained tidewater margins along the coasts of northern ARI and east-central ERI up to 1200 ^{14}C years *after* the initial evacuation of ice from Massey and Hassel sounds (Figure 2.11). Similarly, the persistence of local ice on west-

central ERI is reflected by a deglacial date of 8.6 ka BP on Malloch Dome, suggesting inner Kristoffer Bay remained glaciated at least 1400 ^{14}C years after ice had vacated Prince Gustaf Adolf Sea (Figure 2.11). This style of regional deglaciation is consistent with the Ringnes Islands landform assemblage, which display radial retreat towards their interiors.

Deglacial landforms and radiocarbon-dated shells on ERI suggest that local trunk glaciers were retreating from the outer fiords by at least 9.2 ka BP. However, higher lateral meltwater channels that extend along the coasts of Christopher and Gabbro peninsulas and Reindeer Cape are not associated with early Holocene ice-contact landforms. This suggests that local trunk glaciers in Louise Fiord and northern Deer Bay extended offshore prior to the thinning and landward retreat of ice lobes towards the interior of ERI, concomitant with the establishment of Holocene marine limit. It is possible that diminished buttressing in the adjacent marine channels following the retreat of Innuitian trunk glaciers enhanced outflow from residual dispersal centres on ERI. Therefore, the striae and eskers on ERI *may* record areas of late-glacial extensional flow and supraglacial meltwater drainage in a local ice cap, rather than landscape zonation reflecting basal thermal conditions during full-glacial conditions (cf. Dyke 1993).

The chronology of final deglaciation of residual ice caps on the Ringnes Islands remains unknown. Nevertheless, the distribution of ice-marginal landforms, particularly lateral meltwater channels, indicates that residual ice caps on ARI and ERI became increasingly confined within upland valleys after the establishment of Holocene marine limit (Figures 2.3 and 2.6). The abundance of nested lateral meltwater channels on a

landscape otherwise appearing unaltered by glacial erosion records retreat of cold-based, topographically constrained ice lobes towards uplands in the interior of each island.

2.7 Regional implications

Recent studies have noted that the initial buildup of the IIS after 19 ka BP is significantly out-of-phase with the buildup of the LIS, which attained its *maximum* extent between 24 and 20 ka BP (Dyke et al. 2002a; England et al. in press). Further increases in the volume of the LIS culminated at the LGM (~18 ka BP), which is defined as occurring during a period of low global sea-level and relative climate stability (Clark and Mix 2000; Mix et al. 2001; Dyke et al. 2002). However, the IIS likely did not culminate until well after the LGM, suggesting that the history of the LIS and IIS was influenced by additional controls (cf. Dyke et al. 2002a). This asynchrony likely reflects in part, a positive feedback between falling eustatic sea levels at the LGM, and the subsequent expansion of the IIS, particularly of its lowland sector, through the more exposed inter-montane basins that now form the interisland channels and fiord systems of QEI. England et al. (in press) proposed that such expansion was augmented by the Greenland Ice Sheet, which impinged on eastern Ellesmere Island after 20 ka BP and blocked the eastward outflow of Innuitian trunk glaciers into Nares Strait (Figure 2.1.). This buttressing caused the primary alpine divide covering eastern Ellesmere Island to thicken, and strengthen its westward flow towards Norwegian Bay, and ultimately the polar continental shelf.

The deglacial chronology of the Ringnes Islands demonstrates that the retreat of the IIS from the polar continental shelf at ~10 ka BP lags both the initial rise of global eustatic sea-level at 16.5 ka BP (Yokoyama et al. 2000; Hanebuth et al. 2000), and the Last Termination (~14.5 ka BP), which prompted the recession of the LIS (Dyke et al.

2002a). Hence, the deglacial history of the IIS also appears to be influenced by additional controls.

Significant retreat of the IIS also postdates the Younger Dryas, which defines a return to full glacial temperatures between 11 to 10 ka BP (Mangerud et al. 1974). During this interval, retreat of the Laurentide and Scandinavian ice sheets following the Last Termination was either delayed, or punctuated by readvances that produced sequences of large end moraines along their margins (Mangerud 1980; Dyke and Prest 1987; Dyke and Savelle 2000). Dyke and Savelle (2000) remarked that it remained unclear whether the rate of ice retreat in the western Arctic was less during the Younger Dryas than during preceding or succeeding intervals. However, although the rate of initial retreat of the IIS remains unknown, the absence of deglacial landforms on the Ringnes Islands prior to 10 ka BP suggests that ice margins remained on the polar continental shelf throughout the Last Termination, and persisted there until the end of the Younger Dryas. This asynchrony may reflect in part, a positive feedback between mass balance of the IIS, climatic conditions in the Innuitian region prior to 10 ka BP, and changes in the atmosphere-ocean circulation resulting from large meltwater discharges into the North Atlantic from the retreating LIS (cf. Broecker et al. 1988). Such discharges may have temporarily shut down North Atlantic Deep Water production, causing the North Atlantic polar front to shift south (to ~45°N) and initiate cooling in the circum-subpolar North Atlantic (Broecker et al. 1988). Such cooling also occurred elsewhere in the circumpolar region, including western North America, due to atmospheric teleconnections between the North Atlantic and North Pacific (Mikolajewicz et al. 1997).

The deglacial chronology of the Ringnes Islands indicates that local ice caps persisted along the coasts of northern ARI and east-central ERI for at least 1400 ^{14}C years after the initial evacuation of ice from the surrounding marine channels (Figure 2.11). The maintenance of tidewater margins throughout an interval of continued Holocene warming (Bradley 1990; Koerner and Fisher 1990) may reflect a delayed response of these island-based ice caps to Younger Dryas cooling, or possibly Preboreal cooling (~9.6 ka BP) triggered by the diversion of Lake Agassiz outflow from the Atlantic to the Arctic Ocean at 9.9 ka BP (Fisher et al. 2002). Dyke et al. (2002b) noted that Preboreal cooling may have been particularly strong in the Beaufort Sea region, resulting in readvances of the northwest LIS between 9.8 and 9.6 ka BP. The chronology of final deglaciation of residual ice caps on the Ringnes Islands remains unknown. Nevertheless, the distribution of lateral meltwater channels suggests that these residual ice caps remained cold-based throughout deglaciation.

2.8 References

Alley, R.B., Mayewski, P.A., Sowers, T., Stuvier, M., Taylor, K.C., and Clark, P.U. 1997. Holocene climatic instability: a prominent, widespread event 8200 yr ago? Geology, **25**: 483-486.

Andrews, J.T. 1970. A geomorphic study of postglacial uplift with particular reference to Arctic Canada. Institute of British Geographers, London, England, Special Publication 2.

Atkinson, N. 1999. The last glaciation and relative sea-level history of central Baumann Fiord, SW Ellesmere Island, Canadian High Arctic. Unpublished M.Sc. Thesis, University of Alberta, Edmonton.

Balkwill, H.R., Roy, K.J., and Hopkins, W.S., Jr. 1974. Glacial features and pingos, Amund Ringnes Island, Arctic Archipelago. Canadian Journal of Earth Sciences, **11**: 1319-1325.

Balkwill, H.R. 1983. Geology of Amund Ringnes, Cornwall, and Haig Thomas islands, District of Franklin. Geological Survey of Canada, Memoir **390**.

Bard, E., Fairbanks, R.G., and Zindler, A. 1990. Comparison between radiocarbon and uranium series ages on glacial age Barbados corals. Nature, **345**: 405-409.

Bednarski, J.M. 1996. Surficial geology and sea level history of Bathurst Island, Northwest Territories. Geological Survey of Canada, Paper **96-B**, pp. 61-66.

Bednarski, J.M. 1998. Quaternary history of Axel Heiberg Island, bordering Nansen Sound, Northwest Territories, emphasizing the last glacial maximum. Canadian Journal of Earth Sciences, **35**: 520-533.

Bell, T. 1996. The last glaciation and sea level history of Fosheim Peninsula, Ellesmere Island, Canadian High Arctic. Canadian Journal of Earth Sciences, **33**: 1075-1086.

Benn, D.I., and Evans, D.J.A. (1998) Glaciers and Glaciation . Arnold, London.

Berger A. 1988. Milankovitch theory and climate. Reviews of Geophysics, **26**: 624-657.

Blake, W., Jr. 1970. Studies of glacial history in Arctic Canada. Canadian Journal of Earth Sciences, 7: 634-664.

Blake, W., Jr. 1972. Climatic implications of radiocarbon-dated driftwood in the Queen Elizabeth Islands, Arctic Canada. *In* Climatic change in the arctic areas during the last ten thousand years. *Edited by* Y. Vasari, H. Hyvarinen, and S. Hicks.

Blake, W., Jr. 1987. Geological Survey of Canada Radiocarbon Dates XXVI. Geological Survey of Canada, Paper **86-7**.

Blake, W., Jr. 1992. Holocene emergence at Cape Herschel, east-central Ellesmere Island, Arctic Canada: implications for ice sheet configuration. Canadian Journal of Earth Sciences, **29**: 1958-1980.

Bradley, R.S. 1985. Quaternary Paleoclimatology: Methods of paleoclimatic reconstruction. Allen & Unwin, Boston.

Bradley, R.S. 1990. Holocene paleoclimatology of the Queen Elizabeth Islands, Canadian High Arctic. Quaternary Science Reviews, **9**: 365-384.

Briffa, K., Korhola A., Snowball I, Koç N., and Nesje A. 2001. Holocene Climate Dynamics in High Latitude Europe and the North Atlantic. PAGES-PEPIII Past Climate Variability Through Europe and Africa: An International Conference, Program with Abstracts, Centre des Congrès, Aix-en-Provence, France.

Broecker, W.S., Andree, M., Wolfli, W., Oeschger, H., Bonani, G., Kennett, J., and Peteet, D. 1988. The chronology of the last deglaciation: Implications to the cause of the Younger Dryas event. Paleoceanography, **3**: 1-19.

Canadian Hydrographic Service 1976. Belcher Channel NT 12/13/14/15/16. Department of Energy, Mines and Resources, Ottawa. Scale 1: 1, 000, 000

Clark, P.U., and Mix, A.C. 2000. Ice sheets by volume. Nature, **406**: 689-690.

Clark, P.U., and Mix, A.C. 2002. Ice sheets and sea level of the Last Glacial Maximum. Quaternary Science Reviews, **21**: 1-7.

Darby, D.A., Bischof. J.F., Spielhagen, R.F., Marshall, S.A., and Herman, S.W. 2002. Arctic ice export events and their potential impact on global climate during the late Pleistocene. Paleoceanography, **17**: 1-17.

Dawes, P.R., and Christie, R.L. 1991. Geomorphic Regions. *In* Geology of the Innuitian Orogen and Arctic Platform of Canada and Greenland. *Edited by* H.P. Trettin. Geological Survey of Canada, Geology of Canada, No. 3, pp. 27-56.

Drewry, D.J. 1986. Glacial Geologic Processes. Arnold, London.

Dyke, A.S. 1993. Landscapes of cold-centred late Wisconsinan ice caps, Arctic Canada. Progress in Physical Geography, **71**: 223-247.

Dyke, A.S. 1998. Holocene delevelling of Devon Island, Arctic Canada: implications for ice sheet geometry and crustal response. Canadian Journal of Earth Sciences, **35**: 885-904.

Dyke, A.S. 1999 The last glacial maximum and the deglaciation of Devon Island: support for an Innuitian Ice Sheet. Quaternary Science Reviews, **18**: 393-420.

Dyke, A.S., and Prest, V.K. 1987. Late Wisconsinan and Holocene history of the Laurentide Ice Sheet. Géographie Physique et Quaternaire, **41**: 237-263.

Dyke, A.S., Dale, J.E., and McNeely, R. N. 1996. Marine molluscs as indicators of environmental change in glaciated North America and Greenland during the last 18 000 years. Géographie physique et Quaternaire, **50**: 125-184.

Dyke, A.S., and Savelle, J.M. 2000. Major end moraines of Younger Dryas age on Wollaston Peninsula, Victoria Island, Canadian Arctic: implications for paleoclimate and for formation of hummocky moraine. Canadian Journal of Earth Sciences, **37**: 601-619.

Dyke, A.S., Andrews, J.T., Clark, P.U., England, J.H., Miller, G.H., Shaw, J., and Veillette, J.J. 2002a. The Laurentide and Innuitian ice sheets during the Last Glacial Maximum. Quaternary Science Reviews, **21**: 9-31.

Dyke, A.S., St-Onge, D.A., and Savelle, J.M. 2002b. Younger Dryas and Preboreal end moraines, readvances, and recession rates, western Canadian Arctic. Quaternary Sciences from Land to Sea II: In honor of John T. Andrews. Geological Society of America Annual Meeting, Denver, Colorado, Paper **180-6**.

England, J. 1998. Support for the Innuitian Ice Sheet in the Canadian High Arctic during the Last Glacial Maximum. Journal of Quaternary Science, **13**: 275-280.

England, J. 1999. Coalescent Greenland and Innuitian ice during the Last Glacial Maximum: revising the Quaternary of the Canadian High Arctic. Quaternary Science Reviews, **18**: 421-556.

England, J., and Ó Cofaigh, C. 1998. Deglacial sea level along Eureka Sound: The effects of ice retreat from a central basin to alpine margins (abstract). Joint Meeting of the Geological Association of Canada/Mineralogical Association of Canada, Quebec, Canada 16, A-52., Northwest Territories. Geological Survey of Canada, Bulletin **346**.

England, J., Atkinson, N., Dyke, A.S., Evans, D.J.A., and Zreda, M. in press. Late Wisconsinan buildup and wastage of the Innuitian Ice Sheet across southern Ellesmere Island, Nunavut. Canadian Journal of Earth Sciences.

Fairbanks, R.G. 1989. A 17,000 year glacio-eustatic sea level record: influence of glacial melting rate on the Younger Dryas event and deep ocean circulation. Nature, **342**: 637-642.

Fisher, D.A., Reeh, N., and Langley, K. 1985. Objective reconstructions of the late Wisconsinan Laurentide Ice Sheet and the significance of deformable beds. Géographie physique et Quaternaire, **43**: 229–238.

Fisher, T.G., Smith, D.G., and Andrews, J.T. 2002. Preboreal oscillation: North Atlantic cooling caused indirectly by a glacial Lake Agassiz flood, 11,300 years ago. Quaternary Science Reviews, **21**: 873-878.

Fyles, J.G. 1990. Beaufort Formation (Late Tertiary) as seen from Prince Patrick Island, Arctic Canada. Arctic, **43**: 393-403.

Hanebuth, T., Stattegger, K., and Grootes, P.M. 2000. Rapid flooding of the Sunda Shelf: a late-glacial sea-level record. Science, **288**: 1033-1035.

Hart, J.K., and Boulton, G.S. 1991. The inter-relation of glaciotectonic and glaciodepositional processes within the glacial environment. Quaternary Science Reviews, **10**: 335-350.

Hodgson, D.A. 1977. A preliminary account of surficial materials, geomorphological processes, terrain sensitivity and Quaternary history of King Christian and southern Ellef Ringnes islands, District of Franklin. Geological Survey of Canada, Paper **77-1A**, pp. 485-493.

Hodgson, D.A. 1981. Surficial geology, Lougheed Island, northwest Arctic Archipelago. Geological Survey of Canada, Paper **81-1C**, pp. 27-34.

Hodgson, D.A. 1982. Surficial materials and geomorphological processes, western Sverdrup and adjacent islands, District of Franklin. Geological Survey of Canada, Paper 81-9.

Hodgson, D.A. 1985. The last glaciation of west-central Ellesmere Island, Arctic Archipelago, Canada. Canadian Journal of Earth Sciences, **22**: 347-368.

Hodgson, D.A. 1990. Were erratics moved by glaciers or icebergs to Prince Patrick Island, western Arctic Archipelago, Northwest Territories? Geological Survey of Canada, Paper **90-1D**, pp. 67-70.

Hodgson, D.A. 1994. Episodic ice streams and ice shelves during the retreat of the northwest sector of the late Wisconsinan Laurentide Ice Sheet over the central Canadian Arctic Archipelago. Boreas, **23**: 14-28.

Hodgson, D.A., and Vincent, J-S. 1984. A 10,000 yr BP extensive ice shelf over Viscount Melville Sound, Arctic Canada. Quaternary Research, **22**: 18-30.

Hodgson, D.A., Vincent, J-S., and Fyles, J.G. 1984. Quaternary geology of central Melville Island, Northwest Territories. Geological Survey of Canada, Paper **83-16**.

Horn, D.R. 1963. Marine geology, Peary Channel, District of Franklin. Geological Survey of Canada, Paper **63-11**.

Koerner, R.M., and Fisher, D.A. 1990. A record of Holocene summer climate from a Canadian high-Arctic ice core. Nature, **343**: 630-631.

Lamoureux, S.F., and England, J. 2000. Late Wisconsinan of the central sector of the Canadian High Arctic. Quaternary Research, **54**: 182-188.

Lemmen, D.S., Aitken, A.E., and Gilbert, R. 1994. Early Holocene deglaciation of Expedition and Strand fiords, Canadian High Arctic. Canadian Journal of Earth Sciences, **31**: 943-958.

Lowdon, J.A., and Blake, W., Jr. 1967. Geological Survey of Canada Radiocarbon Dates VI. Geological Survey of Canada, Paper **87-2B**.

Mangerud, J. 1980. Ice-front variations of different parts of the Scandinavian Ice Sheet, 13,000-10,000 years BP. *In* Studies in the Lateglacial of North-west Europe. *Edited by* J.J. Lowe, J.M. Gray, and J.E. Robinson. Pergamon Press, Oxford, pp. 23-30.

Mangerud, J., Anderson, S.T., Berglund, B.E., and Donner, J.J. 1974. Quaternary Stratigraphy of Norden, a proposal for terminology and classification. Boreas, **3**: 109-126.

Maxwell, J.B. 1981. Climatic regions of the Canadian Arctic Islands. Arctic, **34**: 224-240.

McNeely, R. 1989. Geological Survey of Canada Radiocarbon Dates XXVIII. Geological Survey of Canada, Paper **88-7**.

Mikolajewicz, U., Crowley, T.J., Schiller, A., and Voss, R. 1997. Modelling teleconnections between the North Atlantic and North Pacific during the Younger Dryas. Nature, **387**: 384-387.

Miller, G.H., Bradley, R.S., and Andrews, J.T. 1975. The glaciation level and lowest equilibrium line altitude in the high Canadian Arctic: maps and climatic interpretation. Arctic and Alpine Research, **7**: 155-168.

Mix, A.C., Bard, E., and Schneider, R. 2001. Environmental Processes of the Ice Age: land, ocean, Glaciers (EPILOG). Quaternary Science Reviews, **20**: 627-657.

Morrison, C.A. 2000. Late Quaternary glacial and sea level history of west-central Axel Heiberg Island, High Arctic Canada. Unpublished M.Sc. thesis, University of Alberta, Edmonton.

Ó Cofaigh, C. 1997. Glaciation and sea level change, Raanes Peninsula, western Ellesmere Island, Arctic Canada. Quaternary Newsletter, **82**: 40-41.

Ó Cofaigh, C. 1999. Late Quaternary glaciation and postglacial emergence, southern Eureka Sound, High Arctic Canada. Unpublished PhD Thesis, University of Alberta, Edmonton.

Ó Cofaigh, C., Lemmen, D.S., Evans, D.J.A., and Bednarski, J. 1999. Glacial sediment/landform assemblages in the Canadian High Arctic and their implications for Late Quaternary glaciation. Annals of Glaciology, **28**: 195-207.

Ó Cofaigh, C., England, J., and Zreda, M. 2000. Late Wisconsinan glaciation of southern Eureka Sound: evidence for extensive Innuitian ice in the Canadian High Arctic during the Last Glacial Maximum. Quaternary Science Reviews, **19**: 1319-1341.

Paterson, W.S.B. 1994. The Physics of Glaciers. Pergamon, Oxford.

Reeh, N. 1984. Reconstruction of the glacial ice covers of Greenland and the Canadian arctic islands by three-dimensional, perfectly plastic ice-sheet modelling. Annals of Glaciology, **5**: 115-121.

Rogers, A. N., Bromwich, D. H., Sinclair, E. N., and Cullather, R. I. 2001. The atmospheric hydrologic cycle over the Arctic Basin from reanalyses. Part 2: Interannual variability. Journal of Climate, **14**: 2414-2429.

Roots, E.F. 1963. Physiography: Cornwall, Lougheed, Amund Ringnes and Ellef Ringnes Islands. In: Geology of north-central part of the Arctic Archipelago, Northwest Territories. Geological Survey of Canada, Memoir **320**.

Stokes, C.R., and Clark, C.D. 2002. Ice stream shear margin moraines. Earth Surface Processes and Landforms, **27**: 547-558.

Stott, D.F. 1969. Ellef Ringnes Island, Canadian Arctic Archipelago. Geological Survey of Canada, Paper **68-16**.

St-Onge, D.A 1965. La géomorphologie de I'lle Ellef Ringnes, Territoires du Nord-Ouest, Canada. Geographical Branch, Paper **38**.

Stuiver, M., and Reimer, P.J. 1993. Radiocarbon, **35**: 215-230.

Sugden, D.E. 1978. Glacial erosion by the Laurentide ice sheet. Journal of Glaciology, **20**: 367-391.

Van der Veen, C.J. 1996. Tidewater calving. Journal of Glaciology, **42**: 375-385.

Walcott, R.I. 1972. Late Quaternary vertical movements in eastern North America: quantitative evidence of glacio-isostatic rebound. Reviews of Geophysics and Space Physics, **10**: 849-884.

Yokoyama, Y., Lambeck, K., De Deckker, P., and Fifield, L.K. 2000. Timing of the Last Glacial constrained by lowest sea-level observations. Nature, **406**: 713-716.

CHAPTER THREE

A statistical technique for source area determination of glacially transported granite erratics in the Queen Elizabeth Islands

3.1 Introduction

In formerly glaciated regions, glacial erratic dispersal trains can be used to reconstruct ice sheet configuration and extent by tracing indicator debris in an up-ice direction to its source outcrop. Such debris can include distinctive erratics, as well as lithic, mineral or metal grains (cf. Klassen and Thompson, 1993; Shilts 1993; Darby and Bischof 1996; Bischof and Darby 1999). Reconnaissance studies of the glacial history of the western Queen Elizabeth Islands (QEI) have demonstrated that granite erratics provide a conspicuous indication of widespread glaciation (St-Onge 1965; Balkwill et al. 1974; Hodgson, 1982; Balkwill 1983; Figure 3.1). However, it remained uncertain whether these were deposited by the Late Wisconsinan Innuitian Ice Sheet (IIS) from the east, or by pre-Late Wisconsinan advances of the Laurentide Ice Sheet (LIS) from the south.

Research in the eastern QEI has demonstrated that granite erratics originating from the Precambrian Shield of eastern Ellesmere Island were dispersed westward along two major flowlines within the IIS (Bell 1996; Ó Cofaigh et al. 2000; England et al. in press; Figures 3.1 and 3.2). A recent study in the northwest QEI has attributed granite erratics dispersed along northeast Amund Ringnes Island to one of these flowlines, which was inferred to have extended across southwest Ellesmere Island to Massey Sound, via Norwegian Bay (Atkinson 2003, Chapter 2, this volume; Figure 3.1). However, the

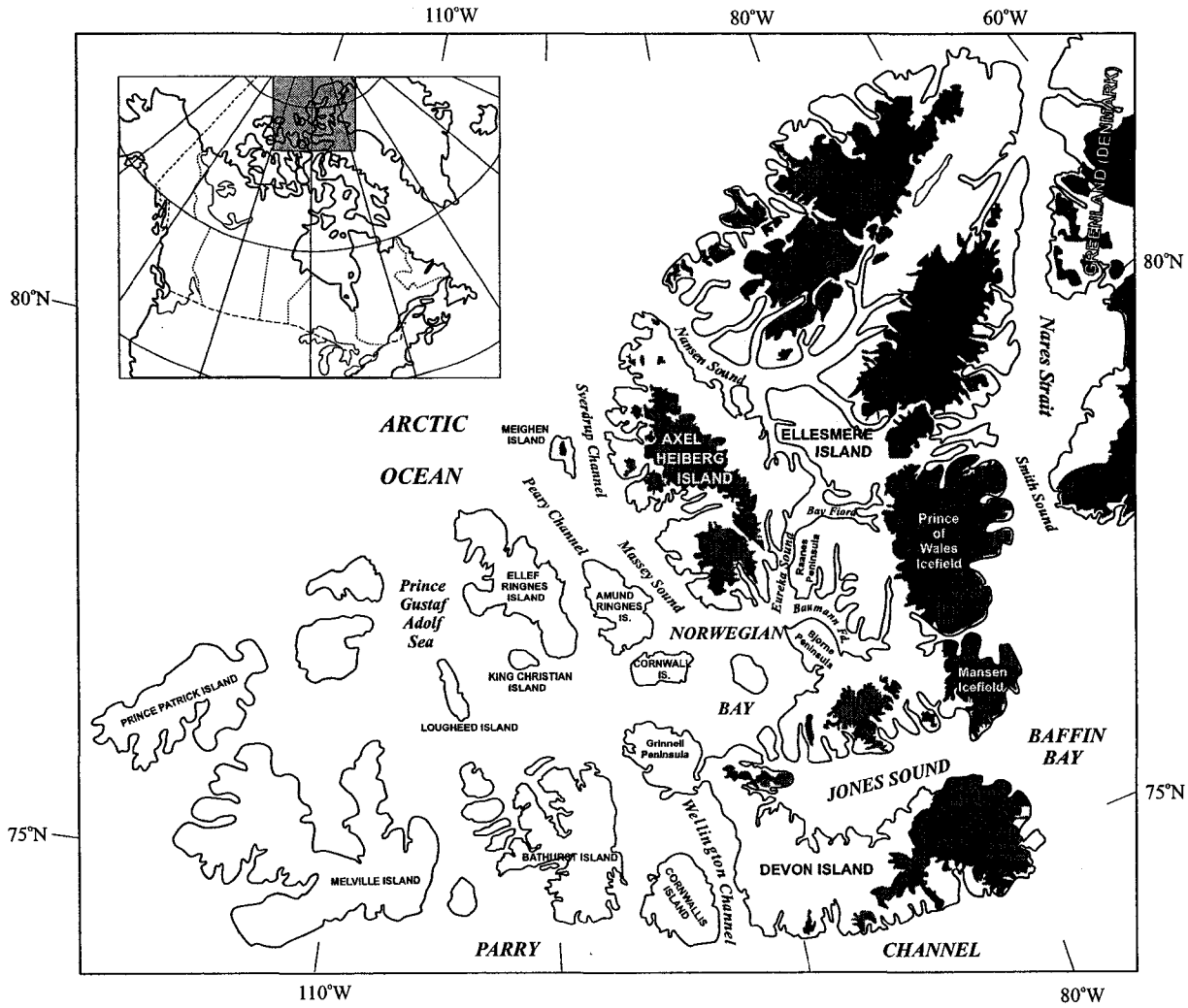

Figure 3.1. Regional map of the Queen Elizabeth Islands and the adjacent coast of Greenland. Contemporary ice caps are shaded dark gray.

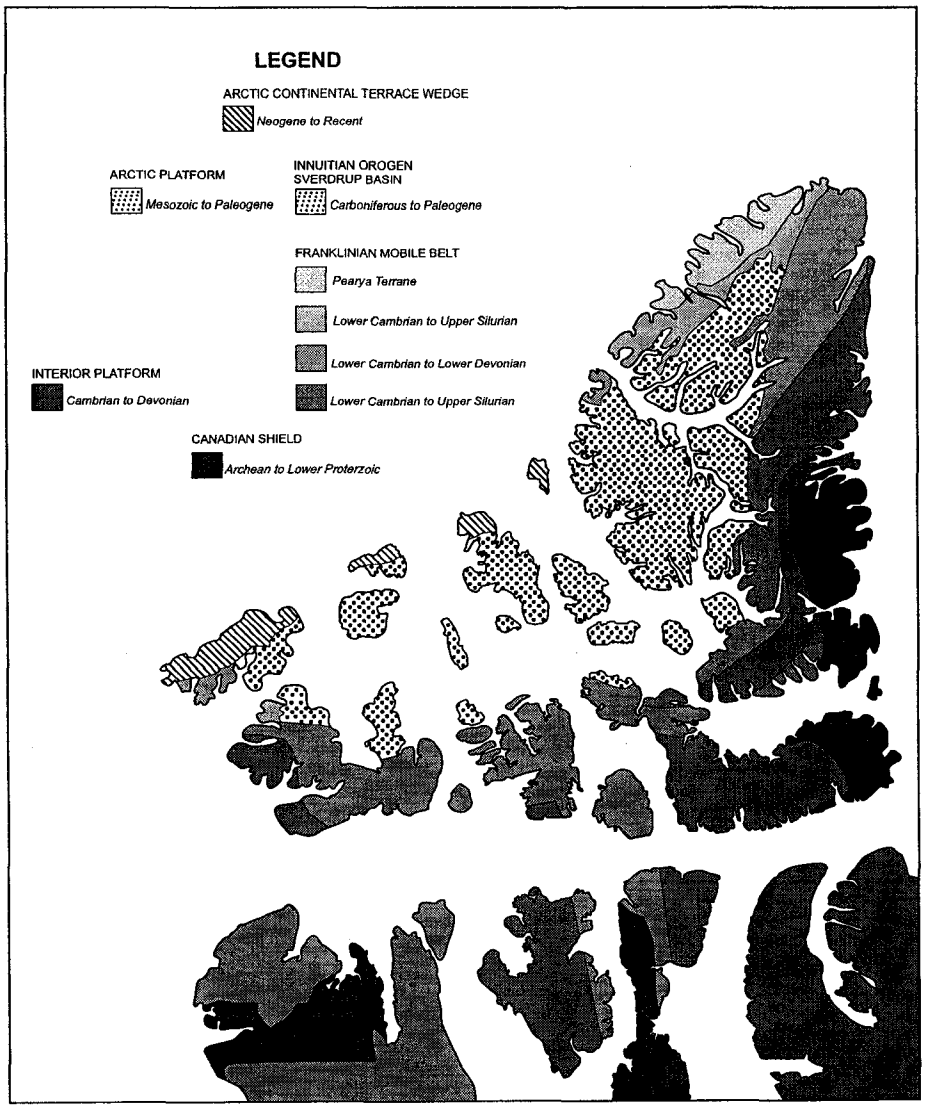

Figure 3.2. Geological provinces of the Arctic Archipelago (Trettin 1991). For place names, see Figure 3.1.

evidence for the proposed origin of granite erratics on Amund Ringnes Island is circumstantial, and remains to be demonstrated quantitatively. This paper utilizes statistical analyses of major element composition of granite erratics from southwest Ellesmere and Amund Ringnes islands and outcrops from the Precambrian Shield to determine whether any compositional trends exist that support the proposed configuration of this Innuitian flowline. To increase the size of the erratic population used in this analysis, it includes granite erratics recently mapped and collected on Meighen Island, which have also been attributed to this flowline (England unpublished). Results of this study may have implications for determining whether granite erratics of presently unknown provenance elsewhere in the Canadian Arctic islands are of Laurentide or Innuitian origin, particularly in areas where other glacial indicators are scarce.

3.2 Previous Research

Most of the Canadian Arctic islands south of Parry Channel contain a wide range of glacigenic sediments and landforms that were formed during repeated glaciation by the LIS through the Quaternary (Hodgson 1989; Figure 3.1). However, in the QEI to the north, the most conspicuous glacigenic sediments and landforms are restricted to their alpine eastern margin, which remains extensively glaciated (Figure 3.1).

Granite erratics originating from the Precambrian Shield of eastern Ellesmere Island occur within two prominent dispersal trains that extend westward across Ellesmere Island (Figure 3.3). A northern dispersal train extends through Bay Fiord to Eureka and Nansen sounds (Bell 1996; Bednarski 1998; Ó Cofaigh et al. 2000). A southern train follows Baumann Fiord and extends across Bjorne Peninsula into Norwegian Bay (Ó

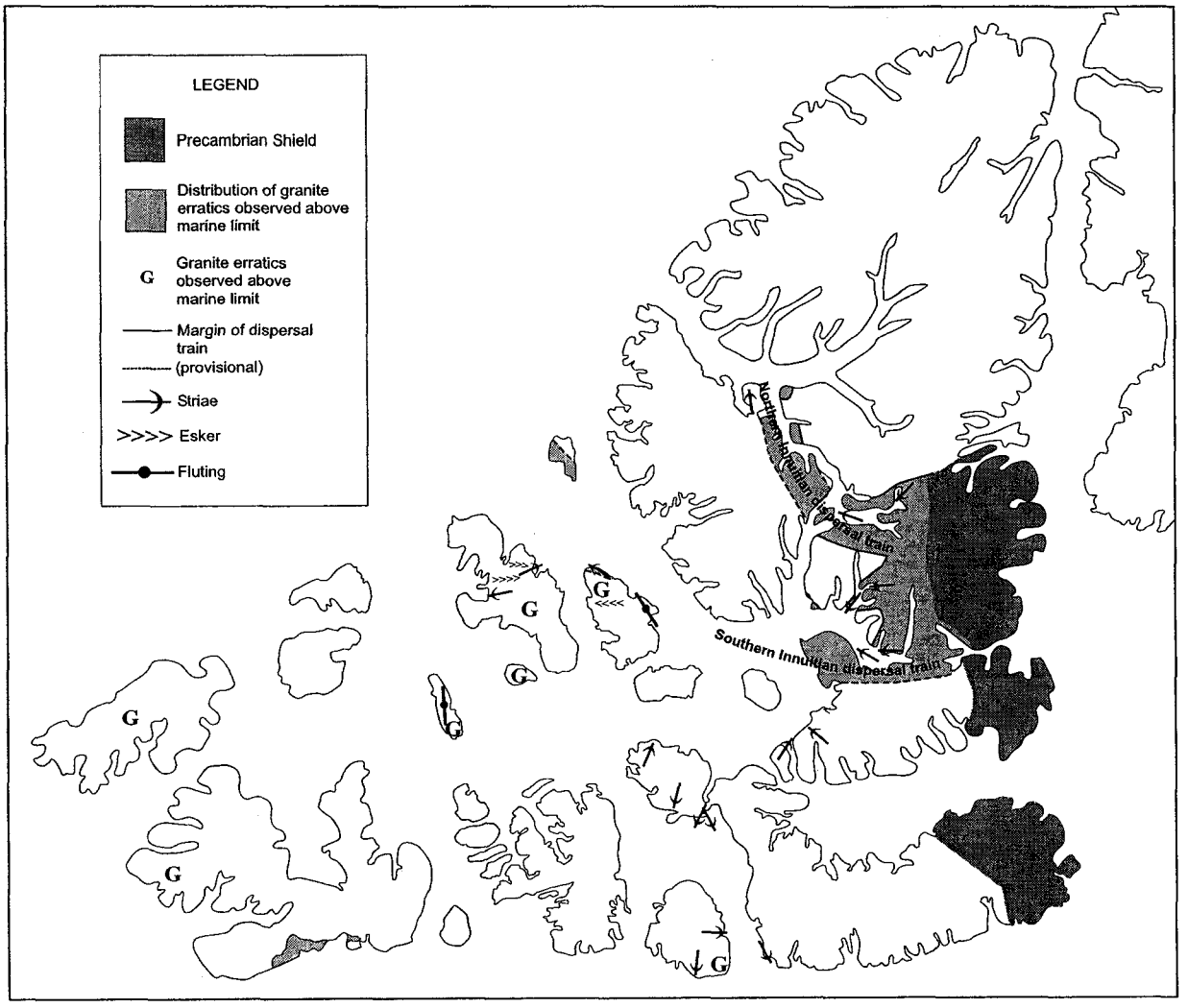

Figure 3.3. Distribution of granite erratics and available ice-flow indicators across the Queen Elizabeth Islands (St-Onge 1965; Balkwill et al. 1974; Hodgson 1977, 1981, 1982, 1990; Edlund 1991; Bell 1996; Hättestrand & Stroeven 1996; Bednarski 1998; Dyke 1999; Ó Cofaigh et al. 2000; Atkinson 2003; England et al. in press; England unpublished). For place names, see Figure 3.1.

Cofaigh et al. 2000; England et al. in press; Figure 3.3). Accelerator mass spectrometry dates on subtill organic deposits on southeast Ellesmere Island suggest that the westward dispersal of granite erratics accompanied the buildup of a precursor of the Prince of Wales Icefield after 19.8 ka BP (Blake 1992; Ó Cofaigh et al. 2000; Figure 3.1). A Late Wisconsinan chronology of granite dispersal is also supported by cosmogenic ^{36}Cl surface-exposure dates on erratics and surrounding bedrock on Raanes Peninsula (Ó Cofaigh et al. 2000; Figure 3.1). These data, together with glacial geomorphic and sedimentological evidence, suggest that granite erratics were transported from the Precambrian Shield by the westward flow of the IIS from a former divide that was centered over the present Prince of Wales Icefield (Hodgson 1985; Bell 1996; Ó Cofaigh et al. 2000; England et al. in press; Figures 3.1 and 3.3).

Studies in the lowlands of the western QEI have reported granite erratics on Amund and Ellef Ringnes, Meighen, Lougheed, King Christian and Prince Patrick islands, (St-Onge 1965; Balkwill et al. 1974; Hodgson 1977, 1981, 1982, 1990; England personal communication 2003; Figure 3.3). However, because of the paucity of supporting glacial geological evidence, it remained unclear whether these were deposited by the westward flow of ice from the eastern QEI (Craig and Fyles 1960; St-Onge 1965), or northward flow of the LIS from the Canadian mainland (Hodgson 1989). Recent research in the northwest QEI has proposed that granite erratics distributed across northeast Amund Ringnes Island relate to the northwest extension of the southern Innuitian dispersal train from the Precambrian Shield of eastern Ellesmere Island (Atkinson 2003, Chapter 2, this volume; Figure 3.3). This paper assesses the validity of this proposal. Its objectives are to: 1) describe the distribution and major element

composition of glacially transported granite erratics across the eastern and northwest QEI; 2) compare the major element composition of granite erratics within the southern Innuitian dispersal train to those along its proposed extension across the northwest QEI; 3) establish the location of compositionally similar outcrops of the Precambrian Shield; 4) identify what spatial trends in erratic composition, if any, can be related to the proposed configuration of the northwest IIS.

3.3 Study area

3.3.1 Pre-Quaternary geology

The QEI is a subplate containing sediments of the Innuitian Province, which is bordered to the northwest by the Cenozoic Arctic continental terrace wedge, and to the southeast by the Precambrian Shield (Trettin 1991; Figure 3.2). Amund and Ellef Ringnes islands are situated in the Sverdrup Basin of the northwest Innuitian Province (Dawes and Christie 1991). This basin contains weakly deformed and gently dipping Mesozoic clastic sediments that are poorly to moderately consolidated (Dawes and Christie 1991; Balkwill 1983). Southeast of the Ringnes Islands, deformed Middle to Upper Palaeozoic carbonate and clastic sedimentary rocks of the Franklinian mobile belt, and undeformed Paleozoic carbonates of the Arctic Platform, outcrop on southwest Ellesmere Island (Trettin 1987; Figure 3.2). Further east, the Precambrian Shield outcrops as nunataks within the Prince of Wales and Manson icefields (Frisch 1988; Figure 3.2). This is a crystalline terrane in the granulite facies, with retrograded amphibolites occurring locally (Frisch 1988; Frisch and Trettin 1991). The major units of this terrane are infracrustal quartzofeldspathic gneisses of granitic composition, closely associated with metasedimentary belts aligned along a northeasterly structural trend (Frisch 1988; Frisch and Trettin 1991).

3.3.2 Physiography

The major physiographic units of the QEI, including some of the fiords and inter-island channels, notably Parry Channel, either developed during, or were augmented by, Late Cretaceous and Tertiary orogenesis and rifting (Kerr 1980, 1982; Hodgson 1989; Figures 3.1 and 3.2). The physiography of the Ringnes Islands comprises lowland plains (<60 m asl), scarped lowlands (≤150 m asl) and piercement domes (150 to 265 m asl; Roots 1963). Scattered gravel that occurs between 100 to 200 m asl on both islands is thought to be the remnant of an extensive sheet of Late Tertiary fluvial sediment, possibly the Beaufort Formation, and indicate that this physiography developed through Late Tertiary and Quaternary fluvial planation and dissection (Hodgson 1982). These deposits must predate the development of the interisland channels (Thorsteinsson and Tozer 1970; England 1987; Hodgson 1989).

Southwest Ellesmere Island marks a transition between the low relief western QEI, and the alpine regions (up to 2000 m asl) that support the Prince of Wales and Manson icefields. South of Baumann Fiord, rocks of the Franklinian Mobile Belt form isolated uplands (>150 m asl) interspersed within the lowlands of Bjorne Peninsula. North of Baumann Fiord, the Franklinian Mobile Belt imparts a northeast-southwest physiographic grain, forming ridges and valleys (>600 m asl; Trettin 1987). Tertiary tectonic rifting augmented this structural trend (Kerr 1981).

3.3.3 Distribution and origin of granite erratics

Although granite erratics are widely scattered across the QEI, variations in clast size, morphology and associated deposits suggest that they occur within two distinct populations.

Granite erratics exhibiting evidence of glacial transport extend across Svendsen and Bjorne peninsulas (southwest Ellesmere Island), northern Raanes Peninsula (west-central Ellesmere Island) and east-central Axel Heiberg Island, covering all terrain, including inter-fiord highlands (>600 m asl) surrounding Eureka Sound and Bay and Baumann fiords (Bell 1996; Bednarski 1998; Ó Cofaigh et al. 2000; England et al. in press; Figure 3.3). On Amund Ringnes Island, ~300 km to northwest, Balkwill et al. (1974) described a large granite erratic (~1 m^3) on the summit of a piercement dome (245 m asl). Elsewhere on Amund Ringnes Island, Atkinson (2003, Chapter 2, this volume) described granite erratics within glaciofluvial gravel and till <15 km to the south and east of this piercement dome. Approximately 100 km to the north, England (unpublished) mapped granite erratics across the southwestern half of Meighen Island (Figure 3.3). Farther west, on Prince Patrick Island, Hodgson (1990) described granules to 4 m blocks of granite scattered up to 190 m asl across outcrops of the Beaufort Formation (Figure 3.3). The most southerly observation of glacially transported granite erratics in the QEI is on central Melville Island, where erratics were deposited by advances of the LIS from the Canadian mainland (Hodgson and Vincent 1984; Hodgson et al. 1984; Hodgson 1989; Figure 3.3). Despite extensive research to the east, no granite erratics have been observed above marine limit on Bathurst Island, northern Cornwallis Island and Grinnell Peninsula (Bednarski 1996; Edlund, 1991; Dyke 1999; Figure 3.3).

Granite erratics that do not exhibit any features characteristic of glacial transport are reported on the scarped lowlands of Ellef Ringnes Island, and mostly occur within scattered veneers of well-rounded gravel (St-Onge 1965; Atkinson 2003, Chapter 2, this volume; Figure 3.3). Similarly, granite erratics reported on King Christian Island are

restricted to plateau gravels that occur on topographic highs, particularly primary watersheds (Hodgson 1982). Isolated granite erratics that appear too large to be residuals of a non-glacial deposit occur on east-central Ellef Ringnes Island (Atkinson 2003, Chapter 2, this volume). However, these lie below Holocene marine limit, and therefore have likely been transported by rafting, either by sea ice or icebergs. Similarly, granite erratics reported within stream beds incised through till on Lougheed Island (Hodgson 1981; Figure 3.3) also occur below marine limit, and it is unclear whether they originated from dissection of till, or relate to non-glacial deposits.

3.4 Field methods

Sites lying on the proposed route of the southern Innuitian dispersal train on southwest Ellesmere, Amund Ringnes and Ellef Ringnes islands were inspected for granite erratics during ground traverses and helicopter surveys through four field seasons (1997-2001). To eliminate the possibility of mapping granite erratics transported by rafting, traverses were conducted above marine limit. The location and elevation of granite erratics observed in the field area was recorded with a GPS and a micro-altimeter (accuracy ±2m). Altimeter readings were corrected for variations in temperature and pressure, and measured relative to high tide (tidal range in the region is ~1 m). A sample of each granite erratic mapped on the Ringnes Islands was collected. On Ellesmere Island, where granite erratics are abundant, samples were collected randomly, although emphasis was placed on those exhibiting evidence of glacial transport, principally striae and faceting. Although some erratics collected from the study area exhibited minor grussification, most had fresh, unweathered surfaces.

3.5 Laboratory analysis

To determine the weight percentage of major and trace elements, the outer layers of each erratic sample were removed with a rock saw to produce a ~10 g cube of granite that was then ground to a 2 μm powder in a stainless steel shatter box. Powders were then submitted for X-ray fluorescence (XRF) analysis at the GeoAnalytical Laboratory, Washington State University. Details of sample preparation and analytical procedure are described by Johnson et al. (1999).

3.6 Statistical treatment

Two statistical analyses were used to determine whether the composition of granite erratics on Ellesmere, Amund Ringnes and Meighen islands are consistent with the proposed provenance and configuration of the southern Innuitian dispersal train. To identify the different components of granite composition, a Principal Components Analysis (PCA) was conducted on the major element composition of the granites collected from Ellesmere, Amund Ringnes and Meighen islands, and on compositional data from the Precambrian Shield of Ellesmere Island (Frisch 1988). However, to determine whether the composition of the granite erratics has closer affinities with Laurentide source areas to the south, the PCA also included data from outcrops of the Precambrian Shield on Somerset Island (Blackadar 1967; Figure 3.2). K-means cluster analysis, based on the component scores, was used to group together compositionally similar erratics and outcrops. By examining the distribution of the members of each cluster, it may be possible to determine whether compositional trends exist between granite dispersal trains originating from different parts of the Precambrian Shield.

3.7 Results

3.7.1 Mean composition of granite

The major element oxides in the granite population of the QEI are SiO_2 and Al_2O_3. Variation in element concentration was large, with standard deviations close to 100% relative to TiO_2, FeO, MnO, MgO and CaO.

3.7.2 Components of the granite population

To determine the different components of the granite population from Ellesmere, Somerset, Amund Ringnes and Meighen islands, a Varimax normalized PCA was performed on 9 components of granite composition (SiO_2, TiO_2, Al_2O_3, FeO, MnO, MgO, CaO, Na_2O and K_2O) from 45 erratic and 167 outcrop samples (Figure 3.4). Two principal components (F1, F2) with eigenvalues >1 were extracted from the correlation matrix of 9 variables, accounting for 73% of the variance within the original dataset (Table 3.1).

F1 loads strongly on FeO and MnO, with high loadings on MgO and CaO, and strong negative loadings on SiO_2 and K_2O. This factor accounts for 59% of the variance in the dataset. F2 loads strongly on Al_2O_3 and Na_2O, with moderate loadings on K_2O and MgO and accounts for 14% of the variance in the dataset.

3.7.3 Granite populations

K-means cluster analysis based on the component scores for factors F1 and F2 was used to separate the erratic and outcrop samples into distinctive compositional clusters. This technique groups samples into a cluster whose members exhibit minimal compositional variation, while maximizing the compositional variability between each

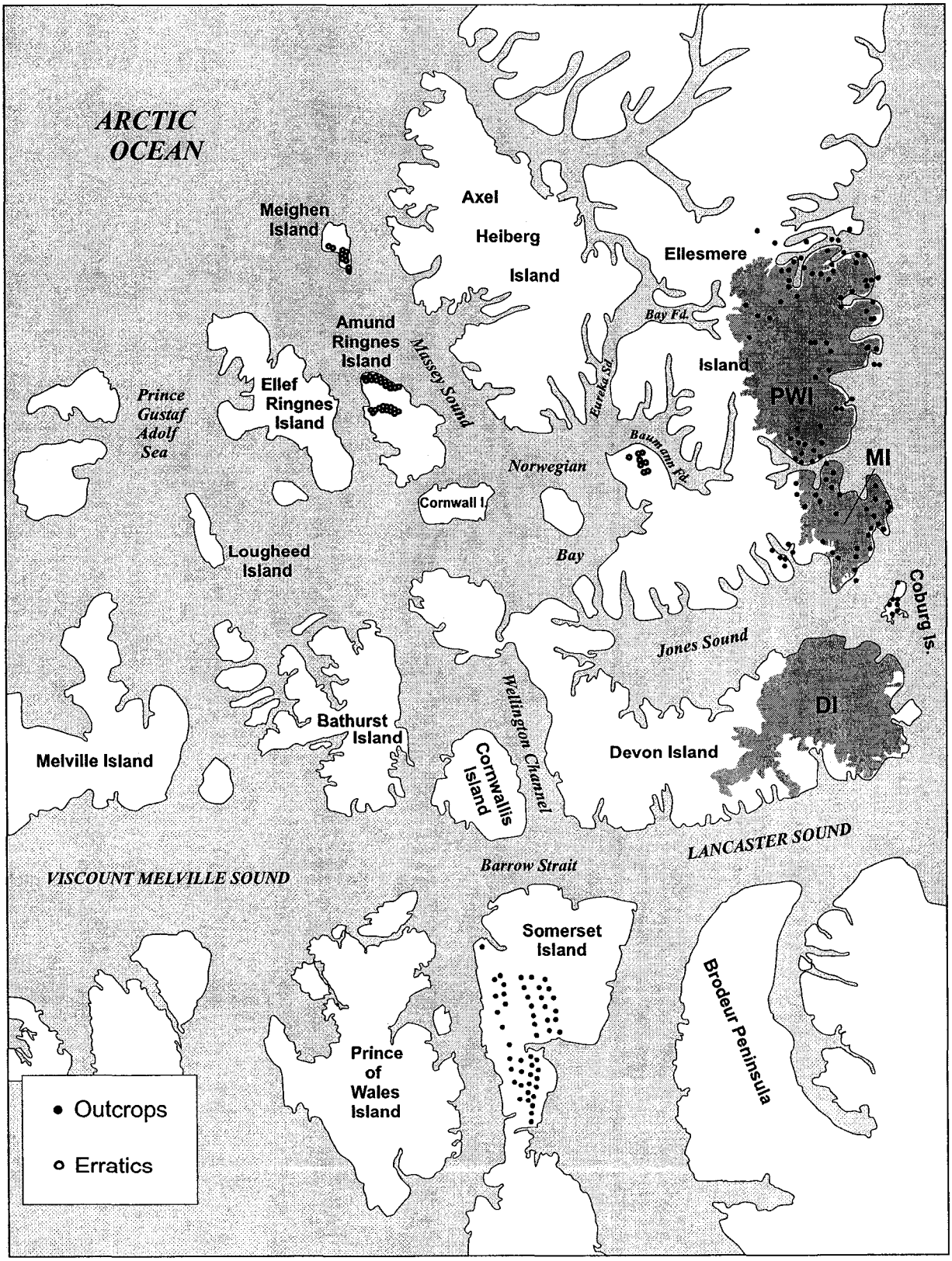

Figure 3.4. Distribution of granite erratics and outcrops analysed in this study. Contemporary ice caps are shaded (PWI, MI and DI; Prince of Wales Icefield, Manson Icefield and Devon Island ice cap).

	F1	F2
SiO_2	-0.94	0.1
TiO_2	0.71	0.176
Al_2O_3	0.16	-0.727
FeO	0.93	0.13
MnO	0.9	0.16
MgO	0.86	0.246
CaO	0.89	-0.11
Na_2O	-0.3	-0.77
K_2O	-0.76	0.27
Eigenvalue	5.34	1.34
%	59	14
Cumulative %	59	73

Table 3.1 Results of the Varimax normalized Principal Components Analysis

cluster. The best separation between clusters was when 5 clusters were used (Figure 3.5, Table 3.2).

C1

From the original dataset of 212 samples, 64 occur within Cluster 1, of which 39 are erratics (Figure 3.6a). *C1* erratics are distributed across Bjorne Peninsula (7), Amund Ringnes (24) and Meighen (8) islands, and collectively account for 82% of the erratics presented in this paper (Figure 3.6a). The remaining samples are from outcrops on Ellesmere and Somerset islands (Figure 3.6a). Cluster 1 is characterized by a low amount (3.2% ± 1.6%) of F1 components (FeO, MnO, MgO and CaO) with a moderate amount (19.2% ± 1.26%) of F2 components (Al_2O_3 and Na_2O; Table 3.3).

C2

Sixty-two samples fall into Cluster 2 (Figure 3.6b). Only 5 of these are erratics (11% of the erratic population), which are distributed across Bjorne Peninsula (1), Amund Ringnes (3) and Meighen (1) islands. The remaining samples are from outcrops distributed on Ellesmere and Somerset islands (Figure 3.6b). Cluster 2 is characterized by a moderate percentage of F1 components (8.1% ± 4.2) and a moderate-high amount of F2 components (20.4% ± 2.7%; Table 3.3).

C3

Cluster 3 accounts for 20 samples, 19 of which are from outcrops on Somerset Island (Figure 3.6c). There are no erratics within this cluster. Cluster 3 is characterized by a moderate percentage of F1 components (14.5% ± 5.3%) and CaO and a relatively high amount of F2 components (24.1% ± 3.1%; Table 3.3).

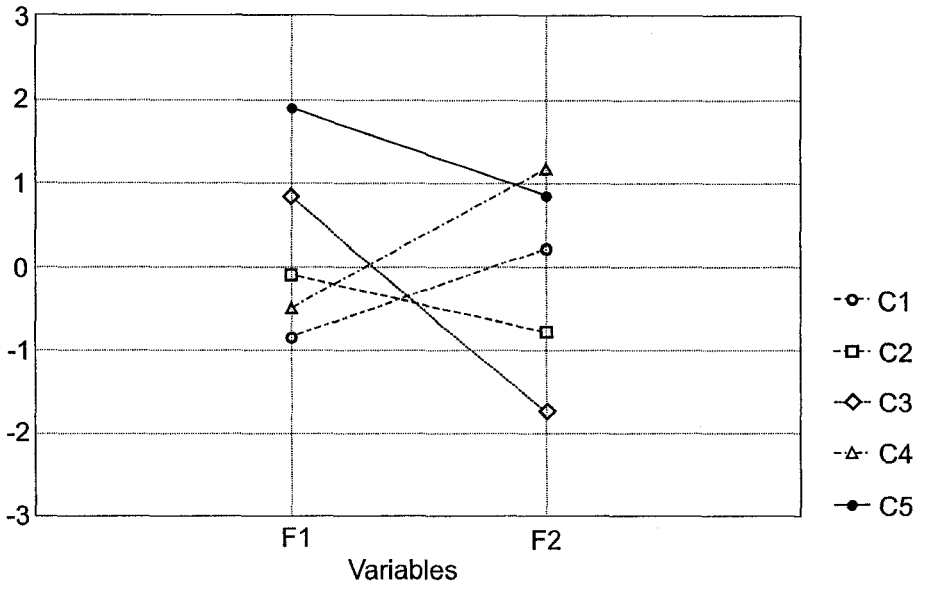

Figure 3.5. Graph of mean distances between clusters and factors.

Table 3.2. Results of the K-means cluster analysis for outcrops and erratics in the QEI. Erratic designations: ***AR***, Amund Ringnes Island; ***BP***, Bjorne Peninsula (SW Ellesmere Island); ***MI***, Meighen Island. Somerset Island outcrop designations: BE, TA and BR (cf. Blackadar 1967). Ellesmere Island outcrops have numeric designations (cf. Frisch 1988)

Cluster 1

Sample	SiO_2	TiO_2	Al_2O_3	FeO	MnO	MgO	CaO	Na_2O	K_2O
1	74.3	0.18	13.3	0.7	0.02	0.41	1.07	3.1	5.06
2	69.82	0.72	14.56	1.85	0	0.9	2.82	3.02	4
3	72.9	0.18	13.8	0	0.02	0.72	1.15	3.23	5.13
121-1	75.2	0.04	15	0.5	0.02	0.24	0.82	3.1	4.17
160	76.7	0.08	14.8	0.7	0.06	0.23	1.12	3.8	1.86
65-2	67.8	0.44	15.8	2.4	0.05	1.45	2.57	3.4	4.2
113-9	70	0.42	14.7	1.7	0.07	1.2	2.66	3.5	3.17
141	67.1	0.54	15.2	2.3	0.07	1.92	3.79	3.2	3.57
22	69.8	0.41	14.8	2.6	0.04	1.06	2.85	3.5	3.46
83-2	73.9	0.17	13.9	0.7	0.01	0.44	2.12	4.2	2.56
13	72.3	0.22	13.8	0.8	0.02	0.25	1.62	2.9	5.21
302	73.7	0.16	14.5	0.3	0.01	0.27	0.85	3.9	5.19
151	73	0.25	14	1	0.03	0.42	1.27	3.1	5.86
67-2	74.1	0.08	14.3	0.5	0.01	0.21	0.83	3.3	5.78
303-1	73.5	0.14	14.1	0.6	0.01	0.45	0.73	3.2	5.28
9	73.7	0.24	14.5	0.8	0.02	0.53	1.7	3.9	3.52
167	71.4	0.24	14.8	1.7	0.03	0.96	1.6	3.5	4.03
260	77.1	0.01	13.3	0.5	0.12	0.11	0.54	3.8	4.08
349	74.3	0.14	14.3	0.7	0.01	0.33	0.96	3	4.77
AR-30-99	*73.52*	*0.121*	*14.61*	*1.63*	*0.017*	*0.24*	*0.75*	*3.36*	*5.59*
AR-32-99	*72.77*	*0.025*	*15.11*	*1.08*	*0.004*	*0.01*	*0.5*	*3.54*	*6.85*
AR-37-99	*74.7*	*0.003*	*14.33*	*0.55*	*0.056*	*0*	*0.44*	*4.26*	*5.49*
AR-38-99	*72.97*	*0.137*	*14.84*	*1.77*	*0.009*	*0.45*	*0.72*	*3.42*	*5.53*
AR-39-99	*72.67*	*0.244*	*14.76*	*1.99*	*0.025*	*0.45*	*1.73*	*3.9*	*4.13*
AR-40-99	*72.58*	*0.219*	*14.99*	*1.78*	*0.027*	*0.37*	*0.97*	*3.27*	*5.55*
AR-42-99	*71.92*	*0.085*	*15.71*	*1.48*	*0.013*	*0.16*	*0.83*	*3.96*	*5.66*
AR-44-99	*71.45*	*0.35*	*14.86*	*2.56*	*0.01*	*0.6*	*0.89*	*2.73*	*6.28*
AR-45-99	*72.89*	*0.17*	*14.97*	*1.31*	*0.006*	*0.12*	*0.92*	*3.72*	*5.78*
AR-46-99	*71.4*	*0.148*	*15.8*	*1.71*	*0.014*	*0.17*	*1.08*	*4.07*	*5.46*
AR-48-99	*71.39*	*0.336*	*14.83*	*2.73*	*0.01*	*0.32*	*1.06*	*3.35*	*5.9*
BP-1-2-99	*71.88*	*0.234*	*15.39*	*2.06*	*0.015*	*0.35*	*0.82*	*3.46*	*5.62*
BP-2-99	*76.07*	*0.154*	*12.65*	*2.12*	*0.021*	*0.23*	*1.06*	*3.55*	*4.1*
BP-3-2-99	*73.73*	*0.18*	*14.32*	*1.68*	*0.005*	*0.34*	*0.88*	*3.13*	*5.61*
BP-2-99	*73.23*	*0.182*	*14.24*	*2.14*	*0.017*	*0.24*	*0.89*	*3.28*	*5.62*
BP-1-99	*72.83*	*0.2*	*14.7*	*1.99*	*0.025*	*0.36*	*1.26*	*3.54*	*4.97*
BP-2-99	*72.36*	*0.208*	*15.16*	*1.88*	*0.01*	*0.31*	*1.24*	*3.76*	*4.95*
BE62-66	73.8	1	14.6	0.5	0.01	0.6	2	3.4	3.3
TA62-4	70.8	0.32	15.8	1.7	0.01	0.5	2.6	3.3	4.8
TA62-44	73	0.15	15.3	0.6	0.01	0.5	1.4	2.7	6.2
BE62-38	67.8	0.45	15.9	2.1	0.03	0.5	1.3	2.8	6.2
BE62-42	75	0.2	16.2	1.1	0.01	0.5	0.5	3.1	3.2
BE62-45	73.6	0.41	14.5	1.6	0.02	0.3	1	2.9	5.5
BE62-52	74.6	0.05	12.8	1.7	0.02	1	1	4.3	4.3
BE62-87	71.7	0.25	14.8	0.8	0.01	0.9	1.2	4	5.3
BR62-31	71.5	0.05	16.3	1.1	0.02	0.5	1.6	2.4	5.5
BE62-46	69.2	0.25	16.5	1	0.02	0.5	1.9	3.5	6
TA62-100	71.6	0.9	15.3	1	0.01	0.5	1.6	3.9	5
AR-3-01	*73.83*	*0.120*	*15.39*	*0.91*	*0.006*	*0.32*	*0.77*	*3.46*	*5.27*
AR-2-01	*69.04*	*0.092*	*17.08*	*0.84*	*0.006*	*0.25*	*0.78*	*3.40*	*8.31*
AR-1-01	*73.11*	*0.191*	*15.08*	*1.59*	*0.013*	*0.58*	*0.84*	*3.17*	*5.95*
AR-5-01	*74.09*	*0.197*	*14.18*	*1.85*	*0.012*	*0.47*	*0.59*	*3.05*	*5.78*
AR-7-01	*73.60*	*0.015*	*15.21*	*1.25*	*0.100*	*0.23*	*0.66*	*3.55*	*6.26*
AR-8-01	*74.93*	*0.068*	*14.65*	*0.81*	*0.009*	*0.19*	*0.99*	*4.15*	*4.63*
AR-9-01	*73.81*	*0.113*	*15.07*	*0.94*	*0.029*	*0.22*	*0.90*	*3.94*	*5.05*
AR-10-01	*72.73*	*0.194*	*14.75*	*1.82*	*0.008*	*0.31*	*0.78*	*3.33*	*5.88*
AR-11-01	*71.27*	*0.176*	*16.03*	*1.50*	*0.019*	*0.39*	*1.02*	*3.97*	*5.59*
AR-11-01	*70.74*	*0.294*	*15.59*	*2.27*	*0.015*	*0.86*	*0.65*	*3.32*	*5.98*
AR-13-01	*73.65*	*0.177*	*14.63*	*1.61*	*0.014*	*0.42*	*0.91*	*3.33*	*5.44*
MI-5C-00	*73.23*	*0.261*	*14.49*	*1.86*	*0.013*	*0.49*	*0.80*	*2.99*	*5.64*
MI-5B-00	*72.45*	*0.200*	*15.21*	*1.67*	*0.019*	*0.53*	*0.80*	*3.38*	*5.58*
MI-5A-00	*73.66*	*0.215*	*14.95*	*1.76*	*0.015*	*0.58*	*0.84*	*3.54*	*4.79*
MI-1A-00	*72.05*	*0.158*	*15.36*	*1.52*	*0.006*	*0.42*	*0.66*	*3.04*	*6.46*
MI-4B-00	*72.47*	*0.237*	*15.16*	*1.72*	*0.024*	*0.59*	*0.82*	*3.15*	*5.75*
MI-4A-00	*73.12*	*0.150*	*14.99*	*1.41*	*0.011*	*0.45*	*1.27*	*3.72*	*4.91*
MI-6A-00	*73.47*	*0.195*	*14.51*	*1.69*	*0.010*	*0.35*	*0.76*	*3.11*	*5.47*
MI-6B-00	*74.24*	*0.189*	*14.56*	*1.54*	*0.006*	*0.42*	*0.77*	*3.15*	*5.49*
AR-2-01	*69.04*	*0.092*	*17.08*	*0.84*	*0.006*	*0.25*	*0.78*	*3.40*	*8.31*
AR-2-00	*69.22*	*0.082*	*17.13*	*0.78*	*0.005*	*0.20*	*0.75*	*3.34*	*8.33*
BP-4-1-99	*75.33*	*0.13*	*14.31*	*1.44*	*0.008*	*0.17*	*0.77*	*3.05*	*4.67*
Ave	**75.9**	**0.2**	**15.6**	**1.4**	**0.02**	**0.5**	**1.2**	**3.6**	**5.3**
SD	**2**	**0.2**	**0.9**	**0.6**	**0.02**	**0.3**	**0.6**	**0.4**	**1.2**

Cluster 2

Sample	SiO_2	TiO_2	Al_2O3	FeO	MnO	MgO	CaO	Na_2O	K_2O
214	56.9	0.81	21	7.8	0.1	3.49	1.22	2	4.57
245-1	61.8	0.62	20	5.8	0.09	2.26	1.4	1.8	3.83
218-1	57.3	0.83	20.3	7.5	0.07	4.05	0.94	1.8	4.97
307	71.1	0.36	14.9	0	0.03	0.7	2.51	4.1	2.77
143	58.6	0.77	20.7	5.3	0.07	2.6	0.98	2.1	5.32
175	57.9	0.86	20.3	6.5	0.09	3.17	1.5	1.1	3.31
79	65	0.57	16.3	3.5	0.06	1.83	4.5	4.3	1
85	67	0.59	16	2.3	0.03	1.65	3.91	3.9	1.43
87	65.4	0.64	16.2	2.5	0.03	1.95	3.9	4.3	1.42

Cluster 2 (continued i)

Sample	SiO_2	TiO_2	Al_2O_3	FeO	MnO	MgO	CaO	Na_2O	K_2O
116-1	76.4	0.2	12.8	1.3	0.03	0.22	1.86	4.9	1.21
126	71.1	0.21	16.5	0.9	0.03	0.57	4.16	4.7	1.01
128	67.3	0.37	13.6	5.1	0.08	2.95	2.76	4.2	1.2
203-1	68.1	0.38	16.5	1.8	0.04	1.66	4.18	5	1.18
219	63.3	0.55	16.7	2.9	0.09	2.66	4.38	4.3	1.71
309	64.8	0.46	17.3	2.7	0.07	2.02	4.86	4.6	1.3
318	69.3	0.42	16.1	1.8	0.04	1.15	3.54	4.3	1.45
350	69.3	0.36	16.3	2.1	0.05	1.28	3.52	3.8	1.28
361	67.7	0.45	16.9	1.9	0.05	1.22	3.68	4.8	1.58
131	66.9	0.52	14.8	3.3	0.06	3.57	4.23	3.1	1.85
226	65.2	0.59	15.3	3	0.08	2.82	4.74	4.3	1.02
261	66.2	0.41	16.2	2	0.05	1.77	4.89	4.3	0.98
205	69.1	0.47	15.3	2	0.06	1.79	4.03	3.9	1.16
366	58.1	0.73	18.1	6	0.14	5.02	6.98	2.4	1.08
104	63.2	0.64	15.2	3.5	0.08	3.75	5.6	4.2	1.02
76	64.9	0.5	16.3	4.4	0.08	1.81	3.97	3.2	3
172	73.2	0.28	14.1	1.2	0.04	0.72	3.01	4.1	1.5
215-1	65.8	0.65	15.6	2.7	0.07	1.95	3.73	3.4	2.38
315-1	66.5	0.45	15.7	2.1	0.05	1.93	3.85	3.7	2.52
317	64.9	0.56	16.7	2.5	0.06	1.99	3.8	3.8	2.61
296	69.1	0.13	16.7	0.6	0.02	0.38	3.11	4.5	3.06
44	63.5	0.78	16.2	2.5	0.06	2.8	4.81	3.5	2.95
153	69.7	0.33	13.8	1.3	0.04	1.42	3.07	4.7	2.08
301	72.4	0.27	14.7	1.1	0.02	0.64	2.39	4.4	2.87
28	66.4	0.42	16.7	2.3	0.07	1.09	3.93	4.6	2.99
115-1	64.9	0.91	16.3	3.2	0.07	1.78	4.5	4.6	1.67
156-1	64.4	0.69	16	3	0.09	2.33	5.35	4.4	1.13
213	63.4	0.57	16.4	3.1	0.09	2.74	4.53	4.2	1.23
266	64.3	0.54	16	2.7	0.07	2.88	5.44	4.2	0.95
68	71.1	0.33	15.1	1.4	0.03	0.87	2.84	4.1	2.38
235	68.4	0.41	16	1.7	0.05	1.29	3.28	4.9	1.95
225	70.4	0.26	14.6	1	0.03	1.27	2.71	5	2.41
AR-8-99	***74.23***	***0.113***	***14.65***	***2.14***	***0.087***	***0.35***	***2.46***	***4.77***	***1.16***
AR-47-99	***70.2***	***0.332***	***15.62***	***3.15***	***0.025***	***0.89***	***2.63***	***4.17***	***2.89***
BP-3-1-99	***73.15***	***0.218***	***15.26***	***1.38***	***0.005***	***0.39***	***1.31***	***4.44***	***3.78***
TA62-89	59.1	0.65	16.8	3.9	0.06	1.3	8.4	3.9	3.8
BE62-68	73.2	0.35	13.9	4	0.1	1.5	2.7	3.7	0.3
TA62-33	63.6	0.63	21	2.4	0.03	0.6	4.6	3.5	3.2
TA62-35	64.7	0.58	19.2	3.4	0.05	0.8	2.8	4	4.3
TA62-37	66.3	0.47	19.6	2.4	0.02	0.5	4.2	3.2	3.4
TA62-21	62.8	0.88	19.2	4.9	0.05	2	4.4	2.7	2.9
BE62-33	69.8	0.28	17.5	1.7	0.01	0.5	3.4	3.7	3.2
BE62-14	60.6	0.76	17.5	4.8	0.06	2.3	5.7	3.7	3.5
BE62-43	72	0.31	15.2	1.8	0.05	0.5	2.4	4.7	2.9
BE62-55	67	0.69	15.9	1.9	0.03	0.5	3.4	3.8	4.8
BE62-70	71.7	0.34	16.7	0.5	0.01	0.5	3.3	4.6	2.1
BE62-86	66.4	0.66	16.5	3.9	0.07	0.5	5	4.7	1.2
BE62-91	70.6	0.12	15.7	0.8	0.01	1.2	3.4	5	1.9
TA62-28	63	0.88	19.2	4.5	0.04	2	3.5	3.7	2.3
BE62-29	67.3	0.42	19.4	1.9	0.01	0.6	4.2	4	2
TA62-80	60.1	0.56	18.4	2.5	0.05	2.7	6.6	3.8	5.5
AR-6-01	***73.14***	***0.217***	***15.18***	***1.68***	***0.017***	***0.52***	***1.40***	***4.56***	***3.41***
MI-1C-00	***72.80***	***0.153***	***15.57***	***1.33***	***0.007***	***0.36***	***1.43***	***4.53***	***3.95***
Ave	**66.6**	**0.5**	**16.5**	**2.8**	**0.05**	**1.6**	**3.6**	**3.9**	**2.4**
SD	**4.6**	**0.2**	**1.9**	**1.7**	**0.02**	**1.1**	**1.5**	**0.8**	**1.2**

Cluster 3

Sample	SiO_2	TiO_2	Al_2O_3	FeO	MnO	MgO	CaO	Na_2O	K_2O
250	62	0.5	17.3	3.7	0.1	3.13	4.87	4.4	0.72
BE62-1	58.5	1.3	27.5	4.7	0.03	3.9	0.5	0.8	1.9
TA62-27	58.4	0.67	19	4.5	0.13	2.2	6.5	4.1	2.2
TA62-38	48.5	1.4	19.7	6.7	0.21	3	11.4	4.1	1
TA62-41	51.2	1	21.2	7	0.16	0.6	10.8	3.9	1.3
TA62-90	56.7	0.71	17.6	3.3	0.08	2.5	8.7	4.8	3.6
BE62-50	52.2	1.6	18.4	7.2	0.19	2.7	7.6	4.9	0.8
BE62-27	61.1	1.3	17.8	5.2	0.19	1.4	4.8	4.8	1.6
BR62-41	34	0.54	19.3	3.5	0.02	0.5	4.8	3.3	3.3
BE62-62	62.3	0.46	19.2	3.7	0.06	1.8	5.5	4.7	1.7
TA62-9	48.8	1.5	20.7	9.6	0.2	2.9	8.9	4.4	1.7
TA62-91	55.9	0.94	21.4	6.7	0.13	0.5	7.2	4.5	1.6
TA62-93	56.7	1.1	20.4	6.1	0.13	2.2	7	4	1.4
BE62-34	53.6	1	21.3	6.1	0.16	1	7.3	4.2	2.5
BE62-37	52.7	0.94	20.6	4.7	0.13	3	6.5	5.3	3.1
TA62-42	63	0.56	18.7	4.2	0.09	2.9	5	4.4	1.1
BE62-17	57.6	0.84	19.5	5	0.12	0.5	7.7	5.2	1.9
BE62-6	57	1.1	19.9	7	0.09	4	5.6	3.3	1.8
BE62-107	61.5	1	18.4	6.1	0.1	0.5	5.8	4.6	1
TA62-11	50.4	1.6	19.8	8.9	0.26	3.7	6.5	3.9	0.9
Ave	**55.1**	**1**	**19.9**	**5.7**	**0.1**	**2.1**	**6.6**	**4.2**	**1.8**
SD	**6.7**	**0.4**	**2.2**	**1.7**	**0.1**	**1.2**	**2.3**	**0.9**	**0.8**

Cluster 4

Sample	SiO_2	TiO_2	Al_2O_3	FeO	MnO	MgO	CaO	Na_2O	K_2O
4	62.4	0.85	17.6	6.3	0.07	3.34	0.97	1.4	2.58
72-4	77.1	0.4	12	2	0.01	1.22	0.64	1.7	4.19
75	72.2	0.56	13.4	4.2	0.07	2.93	0.37	0.4	3.02
273-4	67.5	0.62	17	4.6	0.06	1.95	1.14	1.6	4.17
59	74.1	0.2	12	6.7	0.2	1.96	0.26	1.3	1.11
62	78.2	0.41	9.5	3.1	0.32	1.15	0.31	0.8	4.12
153	57.1	1	20.2	7.1	0.08	4.15	0.64	0.9	3.97
268	70.7	0.61	14.4	4.2	0.09	1.66	1.01	1.8	3.1
177	72.1	0.53	12.2	3.2	0.08	1.17	1.89	2.1	2.85
202	65.9	0.61	16.3	5.4	0.11	2.48	1.19	2.4	3.43
208	64.2	0.71	16.8	5.4	0.06	2.08	0.96	2	3.9
114-1	69.2	0.43	13.8	3.9	0.1	2.68	3.9	2.1	1.11
47	71	0.42	14.5	2.4	0.04	1.35	2.69	2.5	4.71
103-1	71.3	0.47	12.8	2.7	0.05	0.59	1.79	2	5.55
140	63.1	0.41	15	5	0.11	5.8	0.91	2	5.81
215-2	74.2	0.17	13.5	0.7	0.02	0.54	1.43	2.6	5.02
265	75.1	0.17	12.4	1	0.02	0.77	0.88	3.3	4.49
58	76.3	0.17	12.4	0.8	0.01	0.2	0.59	2.9	5.39
318	73	0.2	13.6	0.7	0.01	0.29	1.12	2.7	5.52
20-1a	73.2	0.24	13.7	1.6	0.02	0.38	1.77	2.6	5.1
181	72.8	0.23	14.3	0.7	0.01	0.26	0.63	2.3	6.37
207-2	71.5	0.42	13.9	1.8	0.04	0.73	0.97	2.8	5.61
295	72.8	0.2	14	1.4	0.06	0.54	0.9	2.5	6.16
317-3	71.6	0.18	14.7	1.9	0.03	0.82	0.64	2.1	6.87
278	68.2	0.93	13.8	2.7	0.05	0.97	2.24	2.5	5.48
312	58.1	1.64	14.6	3.8	0.09	2.43	4.56	2.8	3.62
AR-36-99	***70.73***	***0.416***	***15.22***	***2.85***	***0.014***	***0.77***	***0.96***	***2.58***	***6.14***
BP-1-1-99	***74.51***	***0.03***	***13.75***	***0.79***	***0.003***	***0.01***	***0.32***	***1.97***	***†8.61***
BE62-11	77.1	0.42	13.5	2	0.01	2	0.3	0.9	3.6
BE62-97	82.7	0.4	8.9	2.1	0.03	0.4	1.2	1.4	1.5
BE62-49	75.9	0.07	14	0.1	0.01	0.5	1.1	2.3	5
BE62-53	74.8	0.12	12.7	0.5	0.1	1	2.9	2.9	2.6
MI-1B-00	***70.81***	***0.346***	***15.26***	***1.90***	***0.007***	***0.61***	***0.76***	***2.54***	***7.22***
Ave	**46**	**0.2**	**8.7**	**1.1**	**0.02**	**0.6**	**0.9**	**1.5**	**3.1**
SD	**4.9**	**0.3**	**1.4**	**1.2**	**0.03**	**1.2**	**1**	**0.5**	**1.4**

Cluster 5

Sample	SiO_2	TiO_2	Al_2O_3	FeO	MnO	MgO	CaO	Na_2O	K_2O
119	58.8	0.93	14.6	10.5	0.17	6.43	1.33	1	2.35
211-3	59.8	1.16	22.5	9.3	0.24	4.02	0.41	0.8	2.51
10	60.6	0.68	15.8	6	0.12	5.72	6.69	2	0.92
24-1a	47.2	1.06	14.2	10.5	0.26	7.64	15.5	0.9	0.39
63-4	47.8	1.04	13.3	9.3	0.25	10.2	8.79	2.6	1.05
113-2	47.7	1.65	14.7	11.7	0.26	8.28	11	1.1	0.75
108	50.4	0.9	11.5	6.8	0.18	8.68	10.2	3.1	3.11
117	52.8	1.48	15	10.2	0.19	4.62	8.18	3.1	1.41
21	51.8	1.53	15.5	8.7	0.15	6.44	6.42	3.1	0.83
36	53	0.96	14.6	6.8	0.14	9.41	7.8	2.9	1.37
157	49.7	1.5	14.8	9.7	0.2	8.35	9.65	2.8	0.52
257	46.3	0.72	16.6	7.6	0.16	9.78	13.1	1.8	0.49
346	45.8	0.77	11.4	7.2	0.19	13.9	13	2.1	0.82
319	48.1	0.53	16.9	5.4	0.16	7.82	16	1.8	0.49
259	48.6	0.91	14.7	9	0.24	7.76	14	1.1	0.13
213	45.6	2.18	13.9	9.8	0.33	6.84	10.5	1.9	0.58
215	47.8	1.06	14.6	8.5	0.25	10.7	9.82	2.7	0.76
276	47.8	0.92	16.8	9.5	0.21	7.86	12.3	1.8	0.41
279	48.5	1.04	12.8	10.7	0.17	8.61	10.8	1.1	0.8
293	47.8	0.97	13.9	9.2	0.28	8.08	11.3	2.1	0.87
114A	48.25	4.92	11.75	9.1	0.27	5.43	8.37	2.83	1.02
114B	47.78	5.01	11.98	8.8	0.26	5.86	8.42	2.56	1.07
115	48	4.96	11.98	10.3	0.19	5.65	9.13	2.59	1.04
128	48.4	5	12.71	9.1	0.26	5.59	8.69	2.45	0.55
129	47.79	4.71	12.52	10.8	0.22	5.53	8.74	2.48	0.82
137	48.05	3.99	13.32	7.2	0.19	5.39	8.93	2.61	0.66
165	49.9	4.14	12	12.5	0.21	4.25	8.39	2.1	1.2
11-4a	42	4.99	11.77	9.3	0.28	5.88	10.9	2.4	1.38
BE62-35	43.4	1.3	16.8	12.6	0.17	7.5	15.2	1.1	0.2
BE62-47	49.7	0.31	14.2	6.2	0.15	10.2	15.1	1.2	1.7
BE62-65	50.4	0.52	15.5	10	0.17	7	12.5	3.1	0.7
BE62-88	50.5	1.2	14.6	11.4	0.21	3.2	14.1	2.4	0.2
TA62-48	49.9	1.3	18.5	9.7	0.17	5.4	9.7	2.2	1.4
Ave	**49.4**	**1.9**	**14.4**	**9.2**	**0.2**	**7.2**	**10.1**	**2.1**	**0.9**
SD	**4**	**1.6**	**2.3**	**1.8**	**0.05**	**2.2**	**3.5**	**0.7**	**0.7**

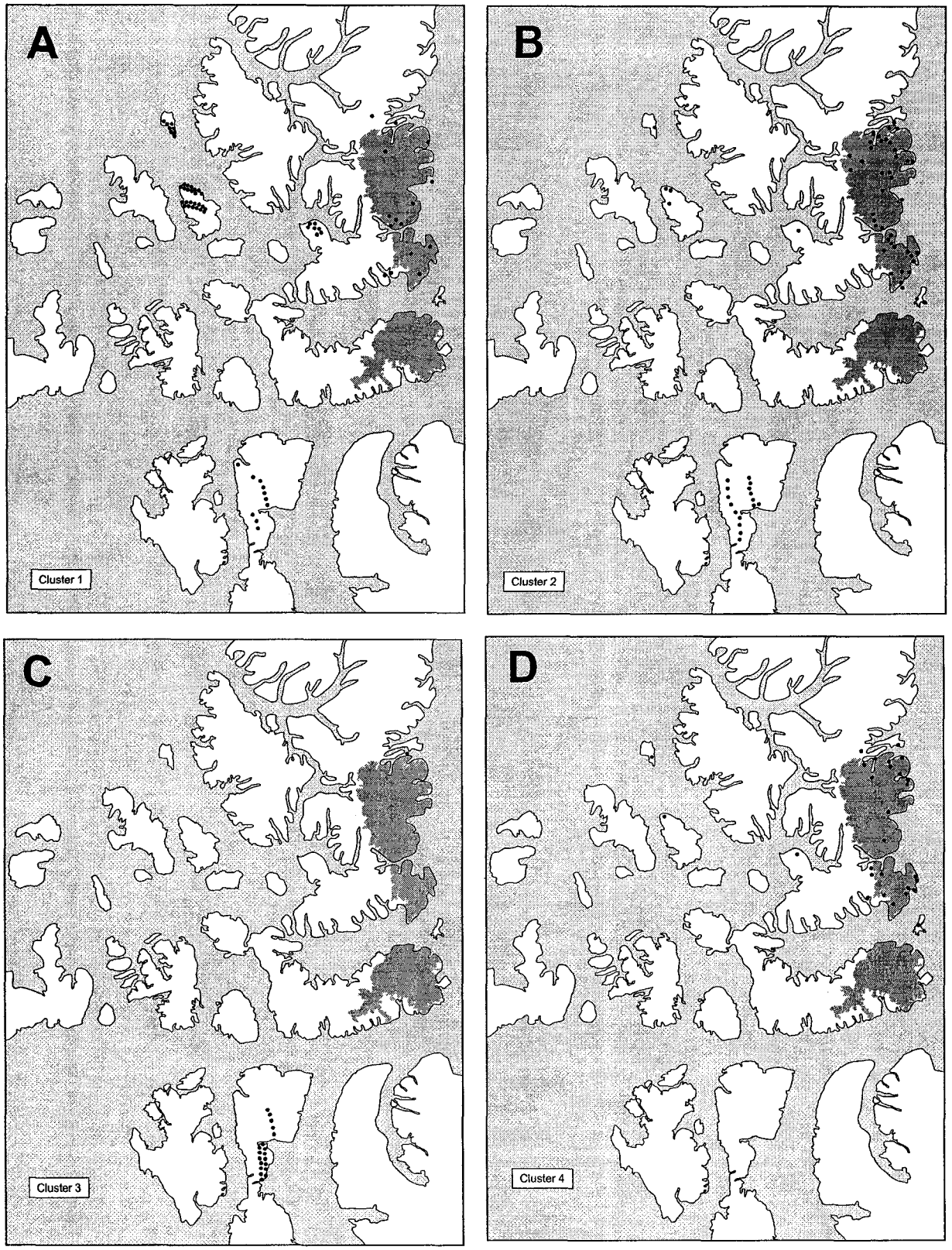

Figure 3.6. Location of erratic and outcrop samples within Clusters 1-5.

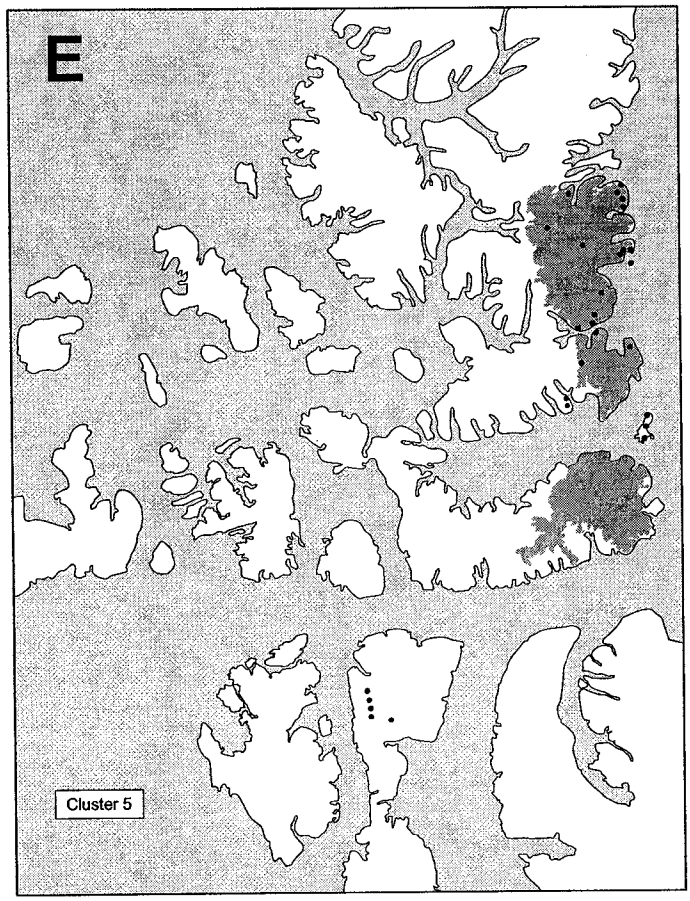

Figure 3.6 (continued).

Factor	Principal components	Cluster				
		C1	C2	C3	C4	C5
F1	FeO, MnO, MgO, CaO	3.2 (1.57)	8.1 (4.2)	14.6 (5.3)	5.6 (4.2)	26.8 (7.6)
F2	Al_2O_3, NaO	19.2 (1.26)	20.4 (2.7)	24.1 (3.1)	16.1 (2.8)	16.5 (3.0)

Table 3.3. Percentage abundance of element oxides that load most strongly on F1 and F2 principal components (based on totalled averages from Table 3.2) within each of the five granite clusters (standard deviations shown in brackets).

C4

Of the 33 samples in Cluster 4, only 3 are erratics (Figure 3.6d). The rest are from outcrops on eastern Ellesmere Island. This cluster is characterized by a low percentage of F1 components (5.6% ± 4.2%) and a relatively low amount of F2 components (16.1% ± 2.8%; Table 3.3).

C5

Cluster 5 accounts for 33 samples, all of which are outcrops distributed on Ellesmere and Somerset islands (Figure 3.6e). This cluster is characterized by a high percentage of F1 components (26.7% ± 7.6%) and a relatively low amount of F2 components (16.5% ± 2.8%; Table 3.3).

3.8 Interpretation and discussion

Glacially transported granite erratics in the eastern and northwest QEI are found in a dispersal train that extends from the Precambrian Shield of eastern Ellesmere Island to Meighen Island (Figure 3.3). Their spatial distribution defines a coherent pattern of regional dispersal, in so far as their trajectory appears logically connected (cf. Klassen and Thompson 1993). This simple pattern has been used in part, to propose a major flow trajectory of the Late Wisconsinan IIS (cf. Ó Cofaigh et al. 2000; Atkinson 2003, Chapter 2, this volume; England et al. in press).

Results of the PCA and cluster analyses demonstrate that there is little variation in the composition of granites distributed along the proposed route of the southern Innuitian dispersal train, with 82% of erratics on southwest Ellesmere, Amund Ringnes and Meighen islands clustering in the same compositional group (*C1*). The remaining

members of *C1* consist of granite outcrops on Somerset and eastern Ellesmere islands, which define the location of possible sources of the *C1* dispersal train. However, these results demonstrate that there are difficulties in determining the source area of *C1* erratics by PCA and cluster analyses of outcrops of the Precambrian Shield of eastern Ellesmere Island. Firstly, there is no apparent glaciological, geological or topographic reason why the southern Innuitian dispersal train is dominated by *C1* outcrops relative to *C2* outcrops, since the distribution of outcrops belonging to either occur in close proximity with each other throughout the Prince of Wales Icefield (Figure 3.6a and b). This may instead reflect a weakness in the statistical technique when applied to outcrops that do not contain significant compositional variations. Secondly, it is not possible to identify a specific source area for the *C1* dispersal train, since the northeasterly strike of the Precambrian Shield is approximately parallel to the inferred orientation of the former Innuitian ice divide, thus *C1* erratics could have originated from any outcrop distributed along strike. However, it is more likely that the *C1* dispersal train described in this paper originated from outcrops beneath a former divide over the southern Prince of Wales Icefield, since erratics originating from northerly outcrops would likely have been transported west by ice flowing along Bay Fiord (cf. Bell 1996; Bednarski 1998; Ó Cofaigh et al. 2000; Figures 3.1 and 3.4). However, analysis of granite erratics distributed along the northern Innuitian dispersal train is required to assess the validity of this proposal. Nevertheless, this technique does indicate that *C3* outcrops characterize a composition that is unique to Somerset Island and does not contribute to the erratic population presented in this paper. This, together with the absence of granite on Bathurst Island, northern Cornwallis Island and Grinnell Peninsula (Bednarski 1996; Edlund 1991;

Dyke 1999), suggests Somerset Island is an unlikely source of any of the erratics on southwest Ellesmere, Amund Ringnes and Meighen islands.

The possibility that the dispersal pattern described in this paper records cycles of glacial and/or fluvial erosion, transport and deposition that have been succeeded by Late Wisconsinan glaciation requires consideration. For example, granite re-entrainment by Innuitian ice-flow would reinforce the compositional record of any pre-Late Wisconsinan glaciation(s), and increase the net distance of granite dispersal, particularly if there was no significant shift in glacial transport direction (cf. Klassen and Thompson 1993). However, there is currently no evidence of pre-Late Wisconsinan glaciation in the stratigraphic record of southwest Ellesmere Island or Amund and Ellef Ringnes islands (cf. Hodgson 1985; Ó Cofaigh et al. 2000; Atkinson 2003, Chapter 2, this volume; England et al. in press). Alternatively, Quaternary glaciers may have redeposited granite erratics from Late Tertiary fluvial gravels. Future PCA and cluster analysis may determine what differences, if any, exist between the composition and provenance of granites attributed in this paper to the southern Innuitian dispersal train, and those from in situ plateau gravels deposited by rivers draining a formerly contiguous Tertiary landmass (cf. Hodgson 1982).

3.9 Implications

Results presented in this paper complement the spatial pattern of granite dispersal, which collectively suggest that the distribution of granite erratics across the eastern and northwest QEI define a coherent former ice-flow trajectory of the IIS. These data suggest that the spatial and compositional trends of granite dispersal may constitute the most geographically and geologically recognizable signature of the IIS across the western QEI.

However, analyses of granite erratics distributed elsewhere in the region are required to assess the suitability of this technique in differentiating compositional trends between other glacial dispersal trains.

Although this technique does not enable specific source areas in the Precambrian Shield of eastern Ellesmere Island to be identified, preliminary results suggest that *C3* characterizes granite outcrops that are unique to Somerset Island, and may provide a distinctive compositional cluster for identifying Laurentide granite dispersal trains in any future study. If validated, this technique may be useful in correlating granite erratics of presently unknown origin on Lougheed and Prince Patrick islands to Laurentide or Innuitian source areas. However, it is acknowledged that age determinations of granite erratics by U-Pb dating of zircon or monazite can be used to diagnose source provenance more reliably. Nevertheless, the statistical treatment of geochemical data described in this paper may be useful in clustering erratics into distinctive compositional groups that limit their possible source areas. By focussing on individual samples from each of these groups, this technique therefore has the potential to reduce the number of samples needed to determine erratic provenance by geochronological analyses.

Finally, the shape of the southern Innuitian dispersal train across southwest Ellesmere and northeast Amund Ringnes islands appears, at least in part, to be controlled by topography, with some boundaries coinciding with upland edges or fiord margins. These likely acted as barriers or conduits within the northwest IIS that influenced the configuration of its flow. This distribution reinforces interpretations that the physiography of the eastern and northwest QEI predates Late Wisconsinan glaciation (cf. Ó Cofaigh et al. 2000). It is not yet possible to determine whether the fiords and

interisland channels of the QEI represent Tertiary dendritic drainage systems overdeepened by glacial erosion or submerged grabens resulting from Tertiary block-faulting. However, this paper provides further geological evidence for the occupation of these channels by Late Wisconsinan trunk glaciers. Although the role of these glaciers in the landscape evolution of the QEI is presently unknown, future models could be constrained by estimating spatial and temporal variations in glacial erosion depth from cosmogenic radionuclide inheritance (cf. Fabel and Harbor 1999).

3.10 References

Atkinson, N. 2003. Late Wisconsinan glaciation of Amund and Ellef Ringnes islands, Nunavut: evidence for the configuration, dynamics and deglacial chronology of the northwest sector of the Innuitian Ice Sheet. Canadian Journal of Earth Sciences, **40**: 351-363.

Balkwill, H.R., Roy, K.J., and Hopkins, W.S., Jr. 1974. Glacial features and pingos, Amund Ringnes Island, Arctic Archipelago. Canadian Journal of Earth Sciences, **11**: 1319-1325.

Balkwill, H.R. 1983. Geology of Amund Ringnes, Cornwall, and Haig Thomas islands, District of Franklin. Geological Survey of Canada, Memoir **390**.

Bednarski, J.M. 1996. Surficial geology and sea level history of Bathurst Island, Northwest Territories. Geological Survey of Canada, Paper **96-B**, pp. 61-66.

Bednarski, J.M. 1998. Quaternary history of Axel Heiberg Island, bordering Nansen Sound, Northwest Territories, emphasizing the last glacial maximum. Canadian Journal of Earth Sciences, **35**: 520-533.

Bell, T. 1996. The last glaciation and sea level history of Fosheim Peninsula, Ellesmere Island, Canadian High Arctic. Canadian Journal of Earth Sciences, **33**: 1075-1086.

Bischof, J., and Darby, D. A. 1999. Quaternary ice transport in the Canadian Arctic and extent of Late Wisconsinan Glaciation in the Queen Elizabeth Islands. Canadian Journal of Earth Sciences, **36**: 2007-2022.

Blackadar, R.G. 1967. Precambrian geology of Boothia Peninsula, Somerset Island, and Prince of Wales Island, District of Franklin. Geological Survey of Canada, Bulletin **151**.

Blake, W., Jr. 1992. Holocene emergence at Cape Herschel, east-central Ellesmere Island, Arctic Canada: implications for ice sheet configuration. Canadian Journal of Earth Sciences, **29**: 1958-1980.

Craig, B.G., and Fyles, J.G. 1960. Pleistocene geology of Arctic Canada. Geological Survey of Canada, Paper **60-10**.

Darby, D.A., and Bischof, J.F. 1996. A statistical approach to source determination of lithic and Fe Oxide grains: An example from the Alpha Ridge, Arctic Ocean. Journal of Sedimentary Research, **66**: 599-607.

Dawes, P.R., and Christie, R.L. 1991. Geomorphic Regions. *In* Geology of the Innuitian Orogen and Arctic Platform of Canada and Greenland. *Edited by* H.P. Trettin. Geological Survey of Canada, Geology of Canada, No. 3, pp. 27-56.

Dyke, A.S. 1999 The last glacial maximum and the deglaciation of Devon Island: support for an Innuitian Ice Sheet. Quaternary Science Reviews, **18**: 393-420.

Edlund, S. A. 1991. Preliminary surficial geology of Cornwallis and adjacent islands, Northwest Territories Geological Survey of Canada, Paper **89-12**.

England, J. 1987. Glaciation and the evolution of the Canadian high arctic landscape. Geology, **15**: 419-424.

England, J., Atkinson, N., Dyke, A.S., Evans, D.J.A., and Zreda, M. (in press) Late Wisconsinan buildup and wastage of the Innuitian Ice Sheet across southern Ellesmere Island, Nunavut. Canadian Journal of Earth Sciences.

Fabel, D., and Harbor, J. 1999. Applications of in situ produced cosmogenic radionuclide techniques in glaciology and glacial geomorphology, Annals of Glaciology, 28: 103-110.

Frisch, T. 1988. Reconnaissance geology of the Precambrian Shield of Ellesmere, Devon and Coburg islands, Canadian Arctic Archipelago. Geological Survey of Canada, Memoir **409**.

Frisch, T., and Trettin, H.P. 1991. Precambrian successions in the northernmost part of the Canadian Shield. *In* Geology of the Innuitian Orogen and Arctic platform of Canada and Greenland, Trettin, H.P. (editor), Geological Survey of Canada, Geology of Canada, No 3, pp. 103-108.

Hodgson, D.A. 1977. A preliminary account of surficial materials, geomorphological processes, terrain sensitivity and Quaternary history of King Christian and southern Ellef Ringnes islands, District of Franklin. Geological Survey of Canada, Paper **77-1A**, pp. 485-493.

Hodgson, D.A. 1981. Surficial geology, Lougheed Island, northwest Arctic Archipelago. Geological Survey of Canada, Paper **81-1C**, pp. 27-34.

Hodgson, D.A. 1982. Surficial materials and geomorphological processes, western Sverdrup and adjacent islands, District of Franklin. Geological Survey of Canada, Paper **81-9**.

Hodgson, D.A. 1985. The last glaciation of west-central Ellesmere Island, Arctic Archipelago, Canada. Canadian Journal of Earth Sciences, **22**: 347-368.

Hodgson, D.A. 1989. Quaternary stratigraphy and chronology (Queen Elizabeth Islands). *In* Quaternary Geology of Canada and Greenland, Fulton, R.J. (ed), Geological Survey of Canada, Geology of Canada, No 1, pp. 452-459.

Hodgson, D.A. 1990. Were erratics moved by glaciers or icebergs to Prince Patrick Island, western Arctic Archipelago, Northwest Territories? Geological Survey of Canada, Paper **90-1D**, pp. 67-70.

Hodgson, D.A. 1994. Episodic ice streams and ice shelves during the retreat of the northwest sector of the late Wisconsinan Laurentide Ice Sheet over the central Canadian Arctic Archipelago. Boreas, **23**: 14-28.

Hodgson, D.A., and Vincent, J-S. 1984. A 10,000 yr BP extensive ice shelf over Viscount Melville Sound, Arctic Canada. Quaternary Research, **22**: 18-30.

Hodgson, D.A., Vincent, J-S., and Fyles, J.G. 1984. Quaternary geology of central Melville Island, Northwest Territories. Geological Survey of Canada, Paper **83-16**.

Johnson, D. M., Hooper, P. R., and Conrey, R. M. 1999. XRF Analysis of Rocks and Minerals for Major and Trace Elements on a Single Low Dilution Li-tetraborate Fused Bead. Advances in X-ray Analysis, **41**: 843-867.

Kerr, J.W. 1981. Evolution of the Canadian Arctic Islands: transition between the Atlantic and Arctic Oceans. In *The Ocean Basin Margin, Volume 5, The Arctic Ocean.* Nairn, A.E.M., Churkin, M. Jr., Stehli, F.G. (eds) Plenum Press, New York, 115-199.

Klassen, R.A., and Thompson, F.J. 1993. Glacial history, drift composition, and mineral exploration, central Labrador. Geological Survey of Canada, Bulletin **435**.

Morrison, C.A. 2000. Late Quaternary glacial and sea level history of west-central Axel Heiberg Island, High Arctic Canada. Unpublished M.Sc. Thesis, University of Alberta, Edmonton, Alberta.

Ó Cofaigh, C., England, J., and Zreda, M. 2000. Late Wisconsinan glaciation of southern Eureka Sound: evidence for extensive Innuitian ice in the Canadian High Arctic during the Last Glacial Maximum. Quaternary Science Reviews, **19**: 1319-1341.

Shilts, W.W. 1993. Geological Survey of Canada's contributions to understanding the composition of glacial sediments. Canadian Journal of Earth Sciences, **30**: 333-353.

St-Onge, D.A 1965. La géomorphologie de I'lle Ellef Ringnes, Territoires du Nord-Ouest, Canada. Geographical Branch, Paper **38**.

Thorsteinsson, R., and Tozer, E.T. 1970. Geology of the Arctic Archipelago. *In* Geology and Economic Minerals of Canada, Douglas, R.J.W. (ed) Geological Survey of Canada, Economic Geology Report 1, 5th edition, 549-590.

Trettin, H.P. 1987. Pearya: a composite terrain with Caledonian affinities in northern Ellesmere Island. Canadian Journal of Earth Sciences, **24**: 224-245.

Trettin, H.P. 1991. Tectonic Framework *In* Geology of the Innuitian Orogen and Arctic Platform of Canada and Greenland, H.P. Trettin (ed), Geological Survey of Canada, Geology of Canada, No 3, pp. 59-66.

CHAPTER FOUR

Postglacial emergence of Amund and Ellef Ringnes islands, Nunavut: implications for the northwest sector of the Innuitian Ice Sheet[2].

4.1 Introduction

Amund and Ellef Ringnes islands lie northwest of the Innuitian uplift, a ridge of glacioisostatic recovery corresponding to the axis of maximum former thickness of the Innuitian Ice Sheet (IIS; cf. Blake 1970; Walcott 1972; Dyke 1998; Dyke and Peltier 2000; Figure 4.1). In a related paper, Atkinson (2003, Chapter 2, this volume) described ice-flow features and early Holocene deglacial sediments that record the advance, and subsequent retreat of the northwest sector of the IIS across Amund Ringnes Island and through its adjacent channels (Figures 4.1 and 4.2). However, the glacial geologic record of Amund Ringnes Island provides only a *minimum* estimate for the extent and thickness of the northwest IIS. Ice-flow features and deglacial landforms on adjacent Ellef Ringnes Island indicate that it supported a local ice cap that retreated from its coast during the early Holocene (Atkinson 2003, Chapter 2, this volume). However, it remains uncertain whether this was a fully independent ice cap or simply a late-glacial remnant of northward-flowing Innuitian ice that crossed the island before the breakup of marine-based ice in Hassel Sound and Prince Gustaf Adolf Sea (Figure 4.1).

This paper describes Holocene delevelling of Amund and Ellef Ringnes islands, focussing on the postglacial relative sea-level history following the removal of their Late Wisconsinan ice loads. The objectives of this paper are to: 1) determine the form and

[2] A version of this chapter has been accepted for publication in the Canadian Journal of Earth Sciences.

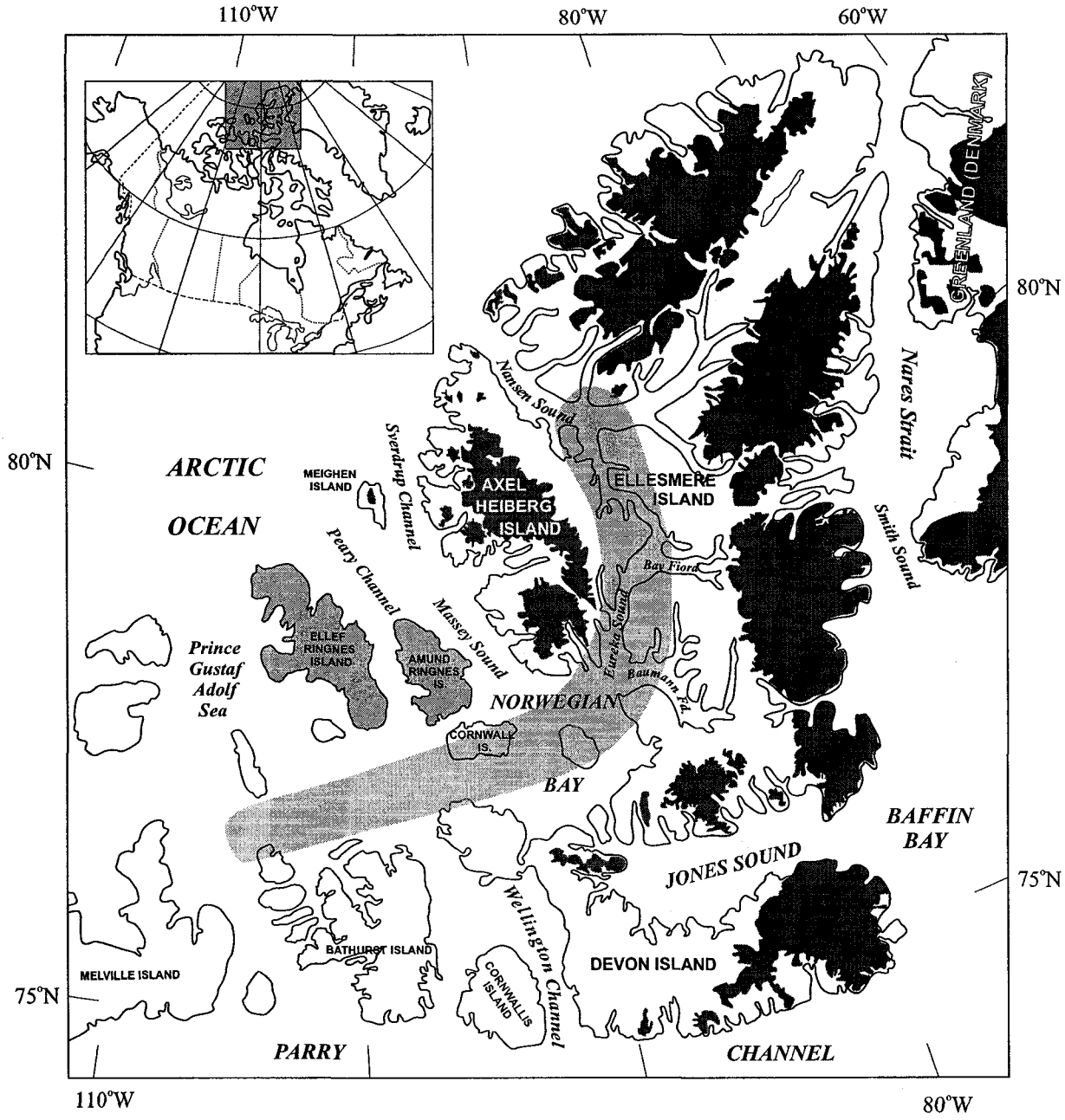

Figure 4.1. Regional map of the Queen Elizabeth Islands and the adjacent coast of Greenland. Closed cell shows the axis of the Innuitian uplift. Contemporary ice caps are shaded dark gray. The Ringnes Islands are illustrated with light shading.

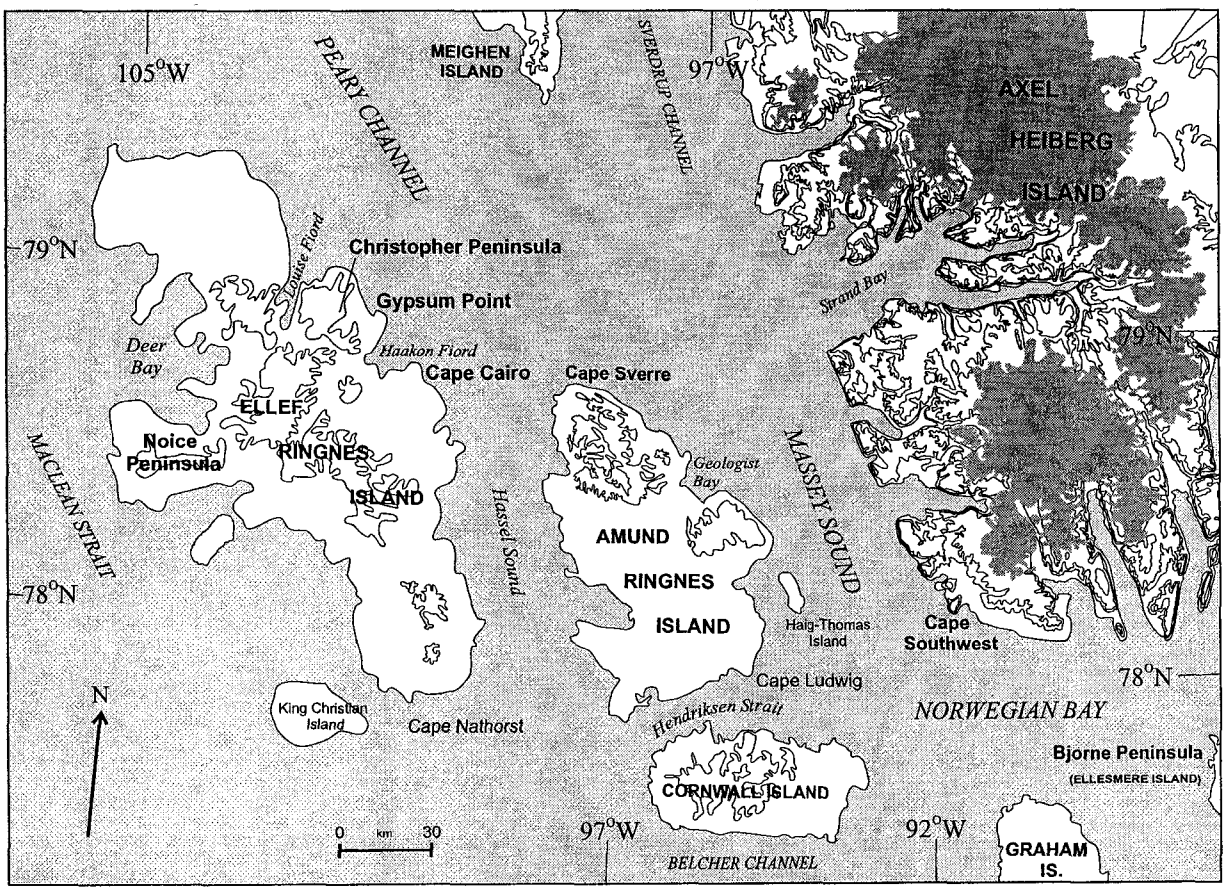

Figure 4.2. Northwest Queen Elizabeth Islands, showing Amund and Ellef Ringnes islands and place names referred to in the text. Contour interval is 100 m. Contemporary ice caps are shaded.

response times, described with respect to their half-lives, of postglacial relative sea-level curves from sites where chronological control is available; 2) reconstruct the pattern of shoreline delevelling and integrate these data with published work concerning the Innuitian uplift; and 3) assess the implications of these data for former ice sheet configuration across Amund and Ellef Ringnes islands.

Determining the extent and dynamics of the IIS along the polar margin of the Queen Elizabeth Islands (QEI), particularly along axes of enhanced ice-flow such as Massey Sound, is important because increased iceberg export from the IIS has implications for glacial sedimentation and climate variability in the Arctic Ocean and North Atlantic during the Late Wisconsinan glacial maximum (cf. Bond and Lotti 1995; Dowdeswell et al. 1995; Bischof et al. 1996; Bischof and Darby 1997; Clark and Stokes 2001; Darby et al. 2002). The IIS must also be considered as a possible source for streamlined bedforms of enigmatic origin described by Polyak et al. (2001) on the Lomonosov Ridge in the Arctic Ocean Basin. Moreover, improving geologically based reconstructions of former ice sheet extent and dynamics are critical in resolving the current imbalance (up to 40%) between the global estimate of ice volume, expressed as ice-equivalent sea level lowering at the Last Glacial Maximum, and the sum of present estimates of individual ice-sheet volumes inferred from regional rebound analysis (cf. Lambeck et al. 2000; Clark and Mix 2002).

4.2 Previous Research

Previous reconstructions favouring extensive Late Wisconsinan glaciation in the QEI were based largely on the postglacial relative sea-level (RSL) history of the archipelago (Blake 1970; Walcott 1972; Tushingham 1991; Tushingham and Peltier

1991). However, the geophysical interpretation of this sea-level record in the QEI, which inferred a pan-archipelago ice sheet, was initially challenged due to the lack of supporting glacial geological evidence (cf. England 1976; Boulton 1979; England et al. 1991). Recent studies have now reconciled the pattern of Holocene emergence throughout the eastern and central QEI with geological evidence of extensive Late Wisconsinan glaciation (Ó Cofaigh 1999; Ó Cofaigh et al. 2000; Bednarski 1998; Dyke 1998, 1999; England 1998; Bischof and Darby 1999; Lamoureux and England 2000). These RSL curves exhibit continuous Holocene emergence, with the highest shorelines (~140 m asl) occurring along the axis of the Innuitian uplift (Blake 1970, 1972; Walcott 1972; Dyke 1998; England and Ó Cofaigh 1998; Ó Cofaigh 1999; Figure 4.1). The integration of these data from Devon Island (Figure 4.1) enabled Dyke (1998) to reconstruct glacioisostatic recovery within the southeastern radius of the Innuitian uplift, and infer the distribution of ice loading within that part of the IIS by inverting Holocene RSL data.

Dyke (1998) observed that the forms of RSL curves from Devon Island are generally described by the exponential function $y = ae^{bx}$, where y is elevation (m), x is age (ka), b is the proportionality constant, which is related to mantle viscosity and ice sheet size, a is a constant that yields the least-squares fit and e is the base of natural logarithms. The pattern of isobases drawn on dated, delevelled shorelines exhibits a rise from southeast to northwest, towards Norwegian Bay, consistent with the uplift pattern originally used to propose the IIS (Blake 1970, 1972). The isobases also record the southeastward migration of the axis of the Innuitian uplift across Devon Island throughout the Holocene, indicating that maximum Late Wisconsinan ice thickness occurred over the low islands and wide channels of the central QEI (Dyke 1998). Glacial

geologic evidence in this area records divergent ice-flow on either side of the uplift axis, reinforcing Dyke's (1998) proposal that in the lowland relief of the central QEI, the Innuitian uplift would coincide with the position of a former ice divide. However, the location of Innuitian divides elsewhere in the QEI does not coincide with the position of the Innuitian uplift (cf. Andrews 1982; Andrews and Peltier 1989). In the alpine eastern QEI, convergent ice-flow from Innuitian divides that encircled Eureka Sound formed an interior basin of maximum former ice thickness, now recorded by the north-south trend of the Innuitian uplift between Ellesmere and Axel Heiberg islands (Ó Cofaigh 1999; Ó Cofaigh et al. 2000; Figure 4.1).

A further finding was that the response times of RSL curves from Devon Island, described with respect to their half-lives ($0.693/b$), or exponential relaxation times, range from ~2 ka near the uplift centre, to ~1 ka near the margin. These results contradicted an earlier hypothesis that response times for Canadian Arctic RSL curves were uniform (Andrews 1970). Subsequent research by Dyke and Peltier (2000) demonstrated that this response time pattern is regionally coherent. This radial gradient of half-lives extending outward from the former centre of ice sheet loading was explained by relaxation times becoming increasingly insensitive to mantle viscosity, due to the increased control of lithospheric thickness at sites covered by progressively thinner ice towards the ice sheet margin (Dyke 1998; Dyke and Peltier 2000). This paper describes the pattern of Holocene emergence in a region where RSL curves have not been previously published, and considers what linkages, if any, exist between glacioisostatic adjustments northwest of the Innuitian uplift, and the former configuration of the northwest IIS. This

reconstruction complements previous studies on the southeastern radius of the Innuitian uplift, and further clarifies the configuration of the IIS across the QEI.

4.3 Study Area

Amund and Ellef Ringnes islands occupy the northwest QEI, a lowland (<265 m asl) separating the mountains of Ellesmere and Axel Heiberg islands from the polar continental shelf and adjacent Arctic Ocean Basin (Figure 4.2). The Ringnes Islands are separated by broad, northwest-oriented channels, 200-500 m deep, that contain elongate troughs up to 700 m deep (Horn 1963). The physiography of the Ringnes Islands is characterized by lowland plains (<60 m asl) accented by scarps of basic igneous intrusions (≤150 m asl), and piercement domes of diapiric gypsum and anhydrite (150 to 265 m asl; Roots 1963; Balkwill et al. 1983). The islands lie below the modern glacial equilibrium line altitude (300-400 m asl; Miller et al. 1975) and are therefore ice-free. During the Late Wisconsinan, parts of the Ringnes Islands were overridden by the northwest sector of the IIS (Atkinson 2003, Chapter 2, this volume). Erratic dispersal and ice-flow features along eastern Amund Ringnes Island indicate that convergent outflow from Innuitian divides spanning both the eastern and central QEI filled Norwegian Bay, and sustained trunk glacier (≥440 m thick) which flowed northwestward through Massey Sound. The interior of Amund Ringnes Island was overridden by northward-flowing ice from an Innuitian divide that extended westward across the central QEI, in the vicinity of Belcher Channel (Figure 4.1). Whether Ellef Ringnes Island was also overridden by Innuitian ice, or covered by a local ice cap remains unclear. Deglaciation of the Ringnes Islands was preceded by the breakup of marine-based ice in Massey and Hassel sounds and Prince Gustaf Adolf Sea between 10 and 9 ka BP (Figure 4.2). Following the

evacuation of marine-based ice, residual ice caps persisted on Amund and Ellef Ringnes islands and did not begin to retreat inland until 8.9 to 8.6 ka BP, respectively (Atkinson 2003). This radial retreat is widely recorded by ice-contact and raised marine shorelines that are discussed in this paper.

4.4 Methodology and techniques

Throughout Arctic Canada, sites that were heavily ice-loaded during the last glaciation exhibit continuous emergence from marine limit, the highest shoreline along a formerly glacioisostatically depressed coastline (Andrews 1970). In contrast, for sites proximal to the ice margin, initial emergence is followed by submergence, while sites more distal to the ice margin experience continuous submergence (Quinlan and Beaumont 1981). The elevation of marine limit and the form of the subsequent RSL curve is a function of the ice thickness, distance from the ice margin and the age of deglaciation (Andrews 1970; Quinlan and Beaumont 1981; Dyke and Peltier 2000). Hence, RSL curves are important because they can be used to describe the relaxation process of the crust due to deglaciation, and can also be used to draw isobases on postglacial shorelines that portray the spatial and temporal pattern of glacial unloading and allow inverse modelling of ice sheet history (Andrews and Peltier 1989; Dyke 1998). However, because RSL curves include the combined effects of glacial rebound and global eustatic sea level rise, it is not yet possible to convert RSL curves into uplift curves, because there is no single or unique eustatic correction for hydroisostatic deformation (cf. Andrews and Peltier 1988; Dyke 1998; Dyke and Peltier 2000).

Marine limit on Amund and Ellef Ringnes islands is often without geomorphic expression, and at several locations, a minimum estimate can only be determined by the

highest marine shells. Where marine limit is identifiable, it is recorded either by the highest raised marine delta or beach, or the lowest elevation of undisturbed residuum, marking a former washing limit. Paleoshoreline elevations on the Ringnes Islands were determined by micro-altimetry. Measurements were corrected for changes in temperature and pressure and calibrated to a datum of high tide. These elevations are considered accurate to within ±2 m. To determine the age of raised shorelines, shells and driftwood collected from raised marine sediments were submitted for radiocarbon dating by Accelerator Mass Spectrometry (AMS).

To avoid possible errors associated with post-stranding displacement of datable materials (principally by sea-ice push and gelifluction; Dyke et al. 1991), relative sea-level histories are ideally constrained by embedded driftwood and bowhead whale remains, because both are buoyant and likely to be stranded on a contemporaneous raised beach. Shells in growth position are equally informative when they can be stratigraphically related to specific paleoshorelines, as when collected in growth position from well-preserved deltas. However, whalebone and deltas were rarely encountered on the Ringnes Islands. Instead, most of the radiocarbon dates were obtained on surface shells, which are difficult to relate to contemporaneous former sea levels. Rather, surface shells provide a maximum age for the paleoshoreline on which they occur, and a minimum age for marine limit if found below the highest raised shoreline. These data can be used to determine the form of postglacial emergence by assembling data points that must lie on or below the RSL curve, since all molluscs live in some depth of water, hence must fall below their contemporaneous sea level. Samples that represent conspicuous data outliers consist of shells that may have lived in water depths of tens of meters, or shells

and driftwood that are interpreted to reflect post-stranding displacement or sinking. These data are discussed in the text, but are removed from form and response time calculations of RSL curves from the Ringnes Islands. The remaining data are fitted by exponential regressions to draw subjective RSL curves from the Ringnes Islands. This paper discusses 36 radiocarbon dates, 16 of which are new. Due to the nonlinear radiocarbon year-calendar year relationship that results from long-term changes in oceanic and atmospheric ^{14}C content, all radiocarbon dates from the Ringnes Islands are calibrated to calendar years, and are presented in Table 2.1. However, in order to integrate the Ringnes Islands RSL data with RSL data elsewhere in the QEI (Dyke 1998; Dyke and Peltier 2000), all ages reported in this chapter are quoted in radiocarbon years BP.

4.5 Results

4.5.1 Relative sea-level history

Northern Amund Ringnes Island

The highest marine limit on Amund Ringnes Island occurs at Cape Sverre, where whole valves of *Hiatella arctica* lie on the surface of wave-washed residuum at 106 m asl (sample 1, Figure 4.3; Table 4.1). A single valve from this site dated 10.1 ka BP, which provides a minimum age for the establishment of marine limit, which is taken to be ≥106 m asl. South of Anderson Bay, marine limit is recorded by coarse sand on-lapping bedrock to 87 m asl. Two and a half kilometers farther south, paired valves of *Mya truncata* at 76 m asl, that are considered to be in growth position, dated 9.2 ka BP (sample 2, Figure 4.3; Table 4.1). This date provides a minimum age for the 87 m marine limit. East of Anderson Bay, marine limit is marked by silt draping evaporite outcrops up to 68 m asl (sample 3). Directly downslope, whole valves of *M. truncata* at 60 m asl

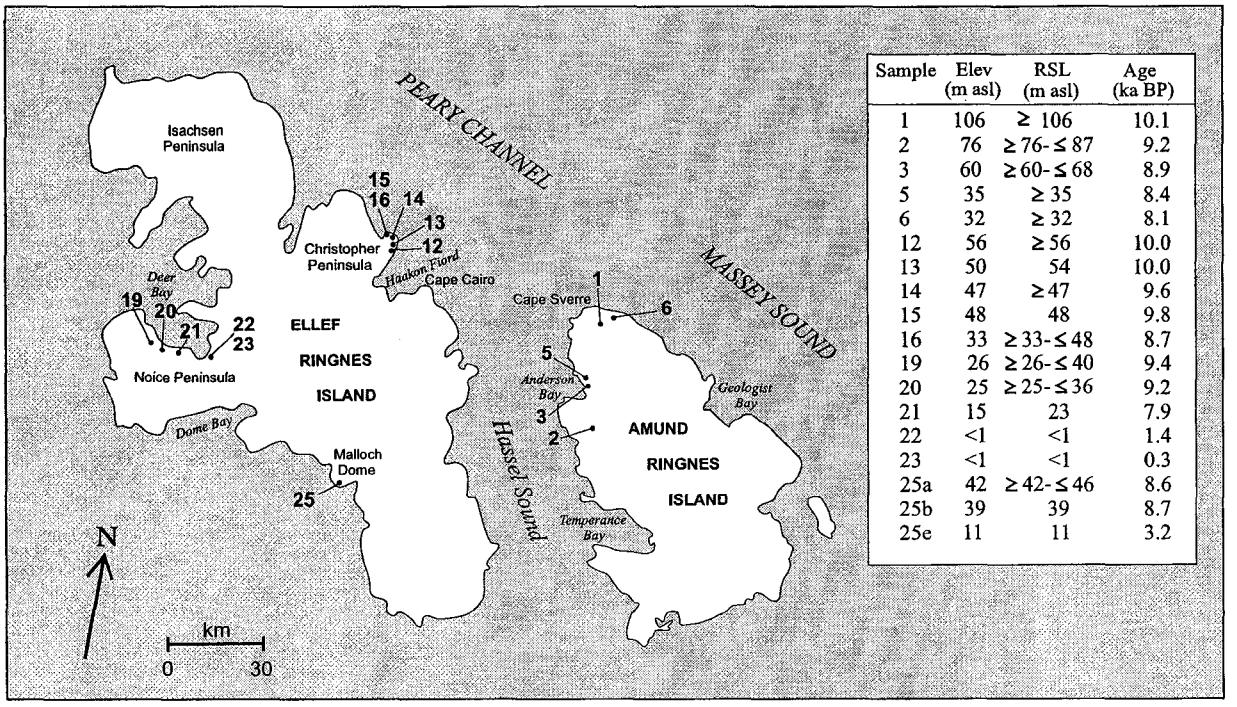

Sample	Elev (m asl)	RSL (m asl)	Age (ka BP)
1	106	≥ 106	10.1
2	76	≥ 76-≤ 87	9.2
3	60	≥ 60-≤ 68	8.9
5	35	≥ 35	8.4
6	32	≥ 32	8.1
12	56	≥ 56	10.0
13	50	54	10.0
14	47	≥ 47	9.6
15	48	48	9.8
16	33	≥ 33-≤ 48	8.7
19	26	≥ 26-≤ 40	9.4
20	25	≥ 25-≤ 36	9.2
21	15	23	7.9
22	<1	<1	1.4
23	<1	<1	0.3
25a	42	≥ 42-≤ 46	8.6
25b	39	39	8.7
25e	11	11	3.2

Figure 4.3. Site names referred to in text and the locations of radiocarbon-dated samples used to construct RSL curves from the Ringnes Islands.

Table 4.1. Holocene Radiocarbon Dates (see Figure 4.3 for sample locations)

Sample	Location	Laboratory dating No.[a]	Material	Age (14C years BP)	Calibrated age[b] (cal. years BP)	Enclosing material	Sample elevation (m asl)	Relative sea level (m asl)	Lat. N	Long. W	References
Amund Ringnes Island											
1	Cape Sverre	CAMS-66145	*H. arctica*	10 060 ± 60	11 200	fine-grained residuum	106	≥106	78° 46'	97° 40'	Atkinson (2003)
2	Anderson Bay	Beta 141599	*M. truncata*	9230 ± 60	10 300	fine-grained residuum	76	≥76- ≤87	78° 28'	97° 48'	Atkinson (2003)
3	Anderson Bay	Beta-141600	*M. truncata*	8870 ± 60	9660	marine silt	60	≥60- ≤68	78° 33'	97° 58'	Atkinson (2003)
4	Cape Sverre		driftwood	8960 ± 60	10 260	marine silt	45	>45	78° 48'	98° 04'	this paper
5	NW Amund Ringnes Is.	GSC-1391	shell fragments	8430 ± 170	9460	marine silt	~35	>35	78° 34	97° 58'	Lowdon et al. (1977)
6	Cape Sverre		driftwood	8060 ± 70	9180	marine silt	32	>32	78° 48'	98° 04'	this paper
7	NW Amund Ringnes Is.	GSC-1834	shells	2930 ± 270	3365	unknown	70	unknown	78° 35'	98° 04'	Lowdon et al. (1977)
8	Panarctic Central Dome	GSC-2551	shells	9010 ± 110	9900	unknown	60	unknown	78° 19'	96° 15'	McNeely (1989)
9	Cape Ludwig	GSC-1973	shells	7710 ± 120	9030	unknown	~30	unknown	78° 02'	95° 14'	Lowdon et al. (1977)
10	Temperance Bay	GSC-2624	organics	6900 ± 100	7990	unknown	28	unknown	78° 02'	97° 45'	McNeely (1989)
11	Temperance Bay	GSC-2625	shells	8340 ± 90	9030	unknown	19	unknown	78° 03'	96° 46'	McNeely (1989)
Ellef Ringnes Island											
12	Haakon Fiord	TO-9503	*M.truncata*	10 010 ± 70	11 140	gravelly residuum	56	≥56	78° 52'	101° 10'	Atkinson (2003)
13	Haakon Fiord	TO-9501	*M. truncata*	10 000 ± 70	11 140	marine sand	50	54	78° 56'	101° 01'	Atkinson (2003)
14	Haakon Fiord	TO-9502	*M. truncata*	9600 ± 70	10 630	gravelly residuum	47	≥47	78° 52'	101° 08'	this paper
15	Gypsum Point	TO-9500	shell fragments	9830 ± 70	10 850	gravelly sand	48	48	78° 58'	101° 06'	this paper
16	Gypsum Point	TO-9499	*M. trucata*	8740 ± 70	9480	marine silt	33	≥33- ≤48	78° 58'	101° 07'	this paper
17	Cape Cairo	TO-9750	*H. arctica*	9690 ± 90	10 680	fine-grained residuum	60	≥60	78° 45'	100° 15'	Atkinson (2003)
18	Cape Cairo	TO-9807	whalebone	10 370 ± 60	11 680	marine silt	41	≥41	78° 44'	100° 10'	this paper
19	N. Noice Peninsula	TO-9748	*H.arctica*	9400 ± 70	10 260	marine-reworked sand	26	≥26- ≤40	78° 31'	104° 14'	Atkinson (2003)
20	N. Noice Peninsula	TO-9747	*H. arctica*	9190 ± 90	10 080	marine-reworked sand	25	≥25- ≤36	78° 30'	103° 43'	Atkinson (2003)
21	N. Noice Peninsula	TO-9746	*H.arctica*	7860 ± 90	8440	marine-reworked sand	15	23	78° 29'	103°32'	this paper
22	N. Noice Peninsula	TO-9806	driftwood	1400 ± 50	1400	marine sand	<1	<1	78° 31'	103°27'	this paper
23	N. Noice Peninsula	TO-9805	driftwood	270 ± 50	480	marine sand	<1	<1	78° 31'	103°27'	this paper
24	N. Noice Peninsula	L-643 B	*A. borealis*	7350 ± 200	8030	unknown	22	unknown	77° 55'	99° 30'	St-Onge (1965)
25a	Malloch Dome	TO-9751	*H.arctica*	8560 ± 110	9415	beach gravel	42	42	78° 11'	101°18'	Atkinson (2003)
25b	Malloch Dome	TO-10595	*M. truncata*	8680 ± 70	9460	beach gravel	39	≥39- ≤46	78° 11'	101°18'	this paper
25c	Malloch Dome	TO-10594	*H.arctica*	8740 ± 70	9480	beach gravel	34	≥34- ≤46	78° 11'	101°18'	this paper
25d	Malloch Dome	TO-9804	*A. borealis*	7700 ± 70	8280	beach gravel	24	24	78° 11'	101°18'	this paper
25e	Malloch Dome	TO-9803	*H.arctica*	3170 ± 60	3090	beach gravel	11	11	78° 11'	101°18'	this paper
25f	Malloch Dome	TO-10593	*H.arctica*	6600 ± 60	7250	beach gravel	2	2	78° 11'	101°18'	this paper
26	Dome Bay	GSC-2572	plant material	7520 ± 90	8590	unknown	26	unknown	78° 27'	102°37'	McNeely (1989)
27	Jackson Bay	GSC-2383	shells	7690 ± 120	8440	unknown	25	unknown	78° 12'	100°46'	Lowdon & Blake (1978)
28	Cape Nathorst	GSC-999	driftwood	8320 ± 140	9650	unknown	95	unknown	77° 40'	99°37'	Lowdon et al. (1971)
29	Cape Nathorst	GSC-1846	shells	8370 ± 200	9450	unknown	~32	unknown	77° 53'	99°38'	Lowdon & Blake (1976)
30	Cape Nathorst	GSC-2537	shells	8880 ± 110	9830	unknown	32	unknown	77° 56'	90°54'	McNeely (1989)
31	Cape Nathorst	L-643 A	*A. borealis*	8500 ± 200	9450	unknown	33	unknown	77° 55'	99°30'	St-Onge (1965)

Notes: m asl, metres above sea level.

[a] Laboratory designations: CAMS, Lawrence Livermore; Beta, Beta Analytic; GSC, Geological Survey of Canada; TO, IsoTrace Laboratory; L, Lamont-Doherty. Samples of marine shells were corrected for isotopic fractionation to a base of ^{13}C=-25°/$_{oo}$ and corrected for a marine reservoir effect of 410 years. Quoted errors represent 68% confidence limits.

[b] All ages calibrated using CALIB4.4 (Stuvier and Reimer 1986-2002).

dated 8.9 ka BP, which provides a minimum age for the 68 m marine limit. The rate of subsequent emergence of northern Amund Ringnes Island is provided by three radiocarbon-dated samples that lack a clear relationship to their related paleoshorelines. Five kilometers east of Cape Sverre, samples of driftwood collected from the surface of marine silt at 45 m asl and 32 m asl dated 8.9 ka BP and 8.1 ka BP (samples 4 and 6, respectively). North of Anderson Bay, shell fragments at 35 m asl dated 8.4 ka BP (sample 5).

Christopher Peninsula, eastern Ellef Ringnes Island

At the mouth of Haakon Fiord, shell fragments lie on the surface of residuum, up to 56 m asl, which is interpreted as marine limit. A single fragment of *M. truncata* from this surface dated 10.0 ka BP, which provides a minimum age on this marine limit (sample 12, Figure 4.3; Table 4.1). Two kilometers farther north, marine limit is defined by a raised beach at 54 m asl, and a fragment of *M. truncata* collected downslope at 50 m asl dated 10.0 ka BP (sample 13). The similarity of these two shorelines (56 and 54 m asl) and their concordant ages (10 ka BP) suggest that this age closely approximates deglaciation and the establishment of marine limit. The rate of subsequent emergence is constrained by radiocarbon-dated samples from three lower shorelines. At the mouth of Haakon Fiord, fragments of *M. truncata* on the surface of fine-grained residuum at 47 m asl dated 9.6 ka BP, which provides a maximum estimate for a 47 m paleoshoreline (sample 14). Four kilometers northwest, marine limit at Gypsum Point is recorded by a gravel beach at 48 m asl, where a single, unidentified shell fragment dated 9.8 ka BP (sample 15). Downslope, a valve of *M. truncata* from silt at 33 m asl dated 8.7 ka BP (sample 16).

Noice Peninsula, western Ellef Ringnes Island

Extensive fans of fine-grained, poorly indurated, seaward-dipping sandstone fringe the coast of northern Noice Peninsula, and are likely part of the Eureka Sound Formation (cf. Balkwill et al. 1983). The sandstone is mantled by a fossiliferous veneer of marine reworked sand that forms a featureless coastal plain extending to a break in slope at 40 m asl. This sand is interpreted to be the product of mixed erosional-depositional regression (cf. Bednarski 1988) derived from the underlying sandstone, and the break in slope is thus considered to mark marine limit. A minimum age for this marine limit is provided by whole valves of *H. arctica* on the surface of the coastal plain at 26 m asl which dated 9.4 ka BP (sample 19, Figure 4.3; Table 4.1). Thirteen kilometers east, the upper limit of similar sand is considered to mark marine limit, at 36 m asl (sample 20). A minimum age estimate is provided by whole valves of *H. arctica*, at 25 m asl, dated 9.2 ka BP. Four kilometers farther east, sandstone is mantled by raised beaches to 23 m asl, which is interpreted to be marine limit. A minimum age estimate for this marine limit is provided by a single valve of *H. arctica* collected immediately downslope, at 15 m asl, which dated 7.9 ka BP (sample 21). Two kilometers north, an embedded driftwood log (3 m long) collected above a micro-cliff (<1 m asl) dated 1.4 ka BP (sample 22). Below the micro-cliff, a smaller sample of driftwood collected close to high tide dated 270 years (sample 23).

Malloch Dome, western Ellef Ringnes Island

Malloch Dome is a diapir mantled on its southwest flank by raised beaches up to 46 m asl, which mark local marine limit. A fragment of *H. arctica* collected from a berm at 42 m asl dated 8.6 ka BP, which provides a minimum age for marine limit (sample 25a,

Figure 4.3; Table 4.1), although dated shell fragments from two lower berms suggest that it was established at least 100 years earlier (samples 25b and c). Control on the rate of subsequent emergence is provided by berms at 24 and 11 m asl which contain whole valves of various taxa (samples 25d and 25e, respectively). Single valves of *H. arctica* and *Astarte borealis* dated 7.7 (24 m asl) and 3.2 ka BP (11 m asl).

4.5.2 Relative sea-level curves

The Holocene radiocarbon database available from the Ringnes Islands is presented in Table 4.1. These data are used to reconstruct the RSL history of the Ringnes Islands by assembling data points that must lie on or below the RSL curve. The database also includes outliers that poorly constrain the RSL curve, such as spurious samples that lie either well above the curve (e.g., sample 7), or below it, such as old-but-low samples of redeposited shells or driftwood (e.g., samples 4 and 25f) or marine shells living in an unknown depth of water. Consequently, only the curves based on culled data are presented in this section, corresponding to the sample numbers in Figure 4.3 and Table 4.1.

Beaches or deltas necessary for relating dated samples to their contemporaneous former sea-level are poorly developed in the Ringnes Islands, possibly reflecting pervasive, land-fast sea ice and generally arid conditions that produced little runoff. Hence, the RSL assignment of these samples is subjective, since the form of the curves is assumed to be generally exponential (cf. Andrews 1970; Andrews and Peltier 1989; Dyke and Peltier 2000). This assumption may over simplify postglacial emergence of the Ringnes Islands, which could include other controls on Holocene RSL, including glacial readvances, tectonic adjustments or forebulge migration. Nevertheless, these data allow

generalized reconstructions of glacioisostatic adjustments and former ice sheet configuration in an area of the northwest QEI for which no other data or regional syntheses exist.

Northern Amund Ringnes Island

The proximity of samples 1, 2 and 3 (Figure 4.3), each related to their respective marine limits, allows them to be used to constrain the form of the emergence curve between 10.1 and 8.9 ka BP (Figure 4.4a). This segment of the curve is well described by the exponential function $y = ae^{bx}$, with a coefficient of determination (r^2) of 0.99, and an exponential relaxation time (half-life) of 1.8 ka. Although this curve underestimates the RSL assignment of sample 2, its slope is compatible with the elevational range of the RSL attributed to the sample. This curve was not forced through the origin (modern sea-level), however its y axis intercept is close to zero (+2 (±1.5) m asl). The curve provides a minimum slope for the RSL history of northern Amund Ringnes Island, and suggests that marine molluscs (sample 5) were living in ~20 m of water, while the driftwood (sample 6) may have either sunk, or was displaced ~18 m downslope after stranding. A second RSL curve that is forced through these lower samples (samples 5 and 6) is also presented (Figure 4.4a). This curve provides a maximum slope for the RSL history of northern Amund Ringnes Island and approximates ($r^2 = 0.92$) an exponential curve with half-life of 1.06 ka.

These curves constitute end members for the RSL history of northern Amund Ringnes Island based on available dated shorelines. They indicate continuous emergence of northern Amund Ringnes Island from 10 ka BP to present. However, the curve with the maximum slope underestimates both the elevation and the RSL assignment of shells

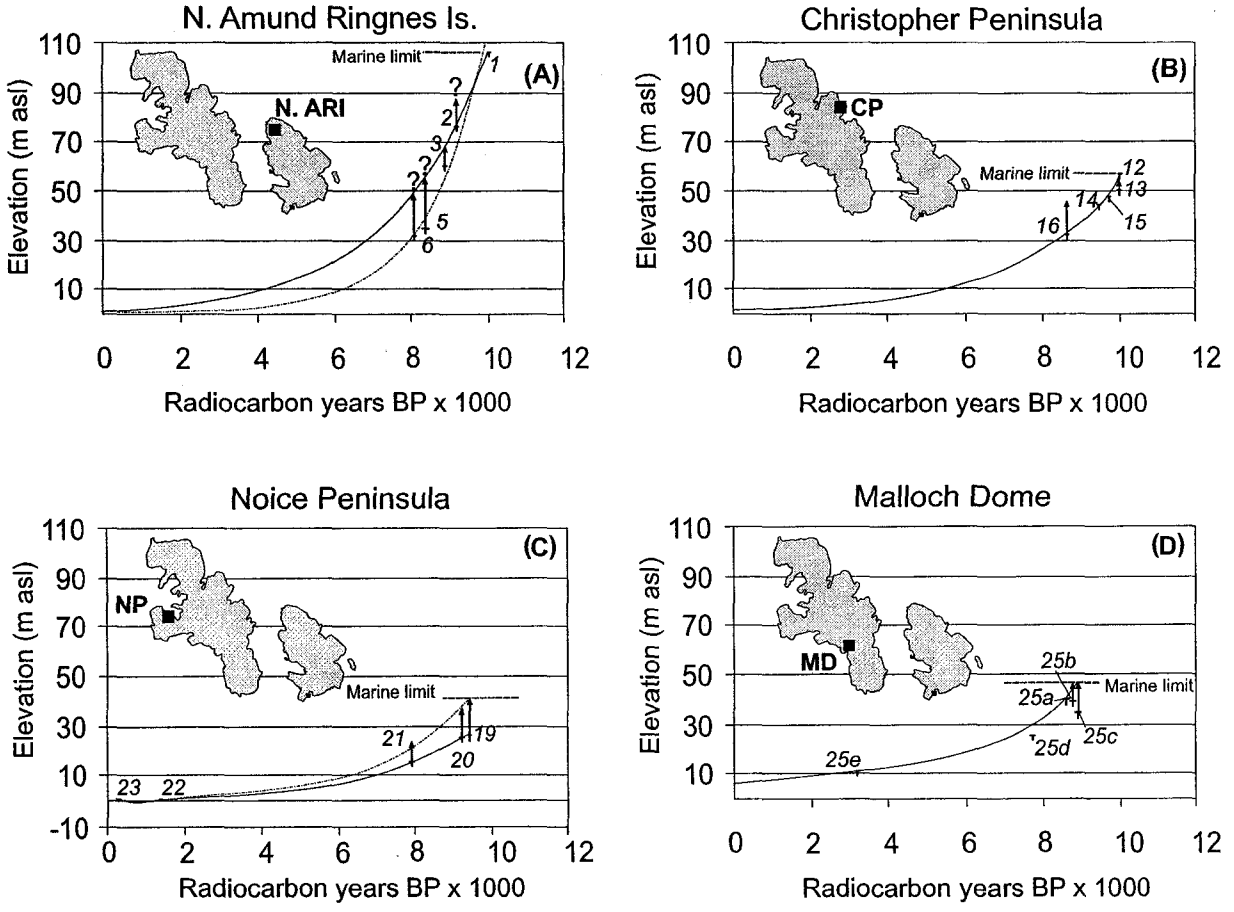

Figure 4.4. Least squares regression RSL curves from the Ringnes Islands based on numbered samples referred to in text, Figure 4.3 and Table 4.1. Minimum and maximum slopes are shown by solid and dashed lines, respectively. Horizontal bars correspond to standard errors on radiocarbon dates. Vertical bars denote instrument accuracy (±2 m) and the elevational range of the sample vis-à-vis its related RSL.

in growth position (sample 2), thereby erroneously placing these molluscs above sea-level at the time of their colonization. Therefore, the form and response time of the minimum curve is favoured. The amount of emergence in the first half-life of the curve is 52 m, with an average emergence rate of 2.9 m/century. However, it is important to note that the sampling area extends for 36 km in the direction of postglacial delevelling (tilting), which increases southwards, towards Norwegian Bay. This reduces the quality of the curve more significantly than when the sampling area is extended normal to the direction of tilt (cf. Dyke and Peltier 2000), because coeval shorelines will experience differential emergence, depending on their proximity to the uplift centre. This may explain why the minimum slope, which is largely constrained by samples from northern Amund Ringnes Island, shows the curve passing through sample 2 (the southernmost site), rather than above it, as would be expected with molluscs dating a correlative RSL at a more northern site. Accordingly, it is possible that the half-life of the curve based on the minimum slope could be somewhat shorter (<1.8 ka).

Christopher Peninsula, eastern Ellef Ringnes Island

Five dates are used to constrain the form of the RSL curve from 10.0 to 8.7 ka BP (Figure 4.4b). These data closely approximate (r^2 = 0.98) an exponential curve with a half-life of 1.8 ka (Figure 4.4b). The *y* axis intercept of this curve is close to zero (+1 (±1.2) m asl), without being forced through the intercept, and suggests continuous emergence of east-central Ellef Ringnes Island from 10 ka BP to present, although this is untested by data younger than 8.7 ka BP. The amount of emergence within the first half-life was 28 m, at a rate of 1.5 m/century.

Noice Peninsula, western Ellef Ringnes Island

Five dates are used to constrain two RSL curves that bracket the emergence history of west-central Ellef Ringnes Island between 9.2 and 1.4 ka BP (Figure 4.4c). The maximum slope is based on RSL assignments of the uppermost samples, which are related to marine limit, and is well described ($r^2 = 0.99$) by an exponential function with a half-life of 1.25 ka. The minimum slope corresponds to the elevations of the samples, rather than their inferred RSL's, and also exhibits a simple exponential decay ($r^2 = 0.98$), with a half-life of 1.36 ka. However, the minimum slope underestimates the RSL assignment of sample 21, which clearly relates to a marine limit that is 8 m above the sample. Therefore, the form and response time of the maximum slope, which better incorporates the 23 m marine limit, is considered more representative of the RSL history of northern Noice Peninsula. The amount of emergence within the first half-life of this curve was 20 m, at a rate of 1.6 m/century. The juxtaposition of samples 22 and 23, <1 m above sea-level, suggests that little net emergence has occurred between 1.4 ka and 270 BP. Sample 22 is driftwood embedded within the low-gradient, vegetated backshore of southeast Deer Bay, and is considered to represent the RSL at the time of its stranding because there is no apparent mechanism for its displacement from upslope sources, and it lies above high tide and the limit of ice-push. The form of the maximum slope, which includes the RSL assignment of sample 22, suggests that when sample 23 was stranded 270 BP, its RSL was below modern sea-level. Therefore, the present position of sample 23 on a modern intertidal zone suggests that it has been displaced upslope by marine transgression, concomitant with the truncation of the older (1.4 ka BP) shoreline by modern high tide, currently eroding the adjacent micro-cliff.

Malloch Dome, western Ellef Ringnes Island

Five dates are used to constrain the form of the RSL curve from 8.8 to 3.2 ka BP (Figure 4.4d). The upper segment of this curve is based on the inferred RSL of samples 25b and c, which are ascribed to marine limit (46 m asl). These data approximate (r^2 = 0.93) an exponential curve with half-life response time of 2.9 ka, and indicates continuous emergence of Malloch Dome since deglaciation. Emergence within the first half-life was 23 m, at a rate of 0.8 m/century. This curve is not as well described by regression expressions as other curves from the Ringnes Islands, and its rate of emergence and *y* axis intercept (+5 (±2.5) m asl) deviate significantly from them.

4.5.3 Postglacial Isobases and shoreline delevelling

Time series isobase maps for the Ringnes Islands are based on three curves presented in this paper (Figures 4.4a-c), as well as published data from Lougheed, Bathurst, Devon, Axel Heiberg and Ellesmere islands (Hodgson 1981; Lemmen et al. 1994; Dyke 1998; Ó Cofaigh 1999; Morrison 2000; Bednarski 2003; England et al. in press; Figure 4.5). Since widespread deglaciation of the northwest QEI did not occur until ~9.2 ka BP (Atkinson 2003, Chapter 2, this volume), the 10 ka BP shoreline can only be defined for the northwest part of the Ringnes Islands. However, shoreline establishment after 9 ka BP permits comparison of all younger shorelines across the region.

Isobases trend NE-SW across Ellef and Amund Ringnes islands, from Prince Gustaf Adolf Sea to Peary Channel, and rise towards an elongate ridge centered on Norwegian Bay (Figures 4.1 and 4.5). East of the Ringnes Islands, isobases curve northward across Massey Sound and Peary Channel, towards northwest Axel Heiberg

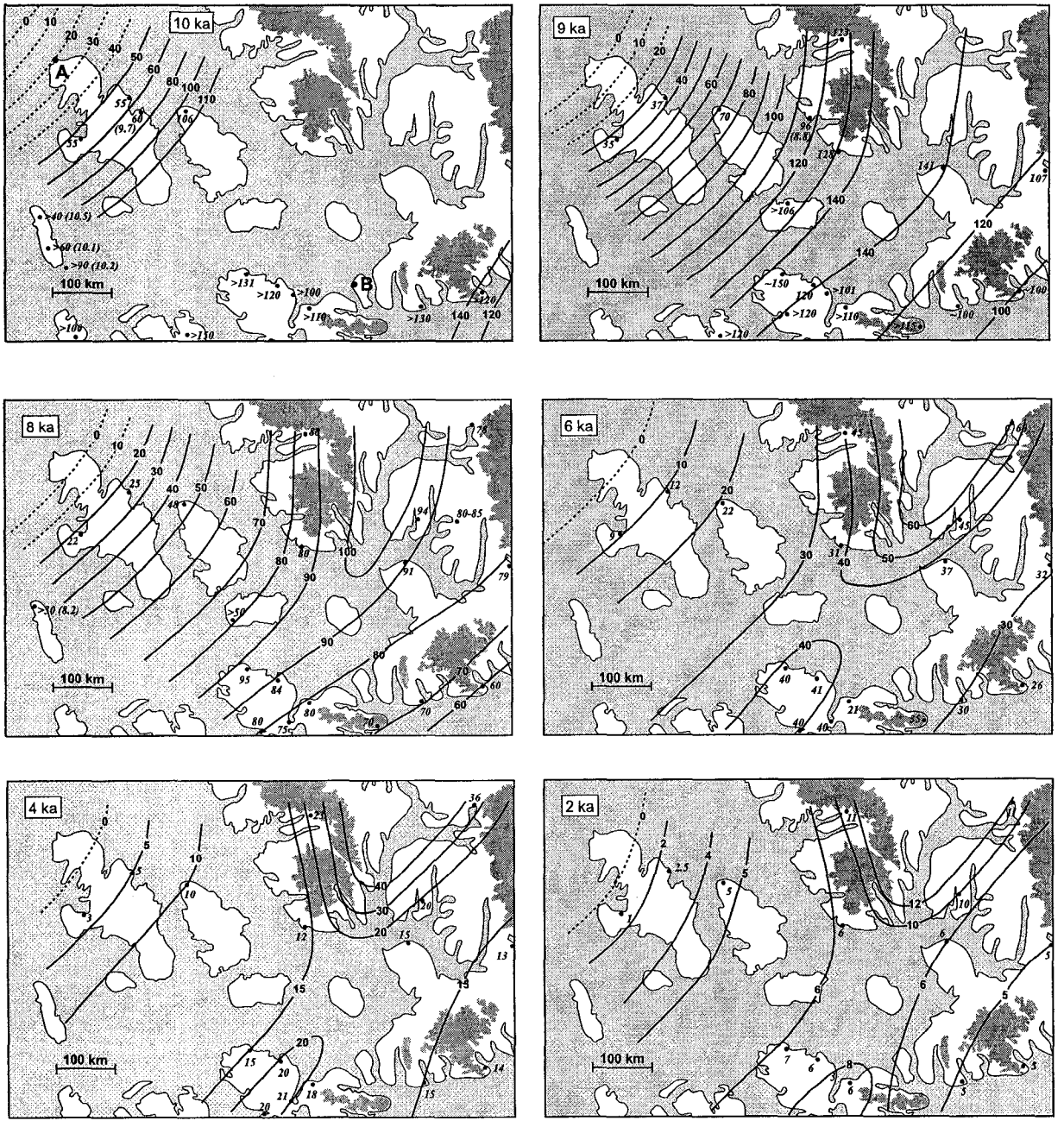

Figure 4.5. Time-series isobase maps of the northwest QEI. Points A and B show the transect used to construct shoreline profiles in Figure 4.6.

Island, where Morrison (2000) documented the N-S orientation of the ~8.5 ka BP isobase (Figure 4.5).

A 430 km transect of shoreline profiles is drawn across the Ringnes Islands to Dyke's (1998) isobase pattern around Devon Island (A to B, Figure 4.5). These profiles illustrate an increase in the elevation of delevelled shorelines of all ages from northwest to the southeast (Figure 4.6). At the time of initial deglaciation, these place the uplift axis over Norwegian Bay. Dyke (1998) documented the subsequent southeast migration of this uplift axis towards Devon Island, concomitant with the diminution of all shoreline gradients from 10 ka BP.

The position of the zero isobase in the western archipelago at the onset of deglaciation is estimated by projecting the decreasing gradient of the 10 ka shoreline forward linearly, northwestward from the Ringnes Islands (Figures 4.5a and 4.6). This shoreline places the zero isobase on the continental shelf, and indicates that the Ringnes Islands were at least 50 km inboard of the margin of the Innuitian uplift at 10 ka BP. Younger shorelines record the migration of the zero isobase ~150 km to the southeast, progressing across Isachsen Peninsula to southeast Deer Bay, between 9 and 2 ka BP, at a rate of ~19 km/1000 years.

4.6 Discussion

Four new RSL curves are presented for the Ringnes Islands. Three of these record exponential crustal relaxation across the region due to early Holocene deglaciation, and indicate continuous, ongoing emergence of northern Amund Ringnes Island and east-central Ellef Ringnes Island. However, the current data indicate that west-central Ellef Ringnes Island has experienced a late Holocene transgression. Despite the limitations of

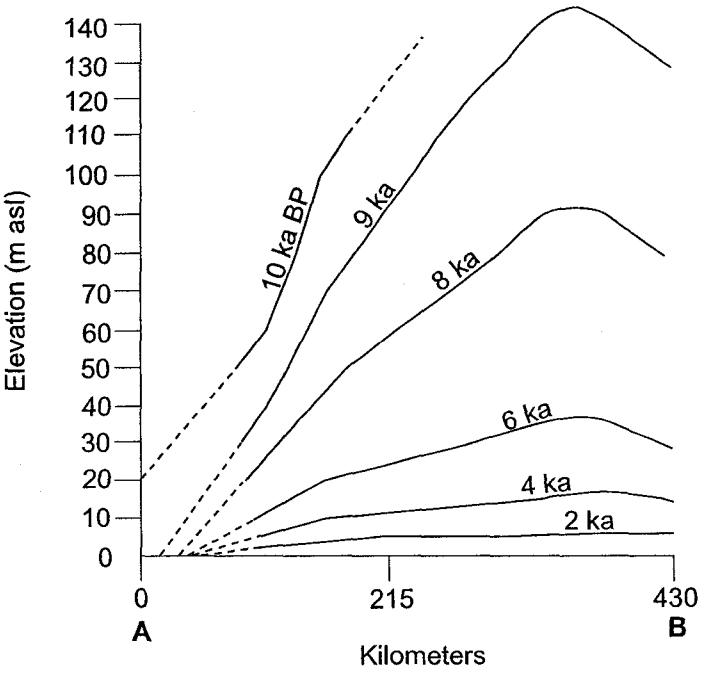

Figure 4.6. Shoreline profiles along line A-B in Figure 4.5.

assigning subjective RSL's to some samples based on the assumption that the emergence curve is exponential, the only site where geomorphic evidence suggests a significant fluctuation in Holocene RSL is on Noice Peninsula.

The half-lives of these three curves range from 1.8 ka adjacent to Massey Sound, to 1.25 ka at Deer Bay. This pattern is broadly consistent with the half-lives (1.75 to 1.5 ka adjacent to Massey Sound, and 1.5 ka on Noice Peninsula) presented by Dyke and Peltier (2000). However, despite the similarity in response time of curves bordering Massey Sound, the magnitude of emergence occurring within the first half-life of each curve decreases markedly from northern Amund Ringnes Island (52 m) to Christopher Peninsula (28 m). It is important to note that the timing of initial emergence at both sites is similar (10 ka BP). Therefore it is unlikely that these differences result from incorrectly comparing the first half-life of the Amund Ringnes curve with the second half-life of the Christopher Peninsula curve. Because such differences reflect a diminishing ice load, northwest across the Ringnes Islands, these data suggest that the proportionality constant for both curves is uniform, since their half-lives do not reflect the apparent differences in the magnitude of the ice load.

The fourth curve from the Ringnes Islands also records continuous, ongoing emergence of Malloch Dome, but its form and response time (2.9 ka) depart significantly from those of the other curves presented in this paper. This may be the result of errors in the measurement, RSL assignment or interpretation of the Malloch Dome data. Alternatively, the RSL history of Malloch Dome may have been influenced by the persistence of a local ice cap, which continued to load part of Ellef Ringnes Island after the early Holocene, thereby partially countering rebound within the Innuitian uplift.

However, Dyke (1998) and England et al. (in press) reported no discernible effect of the Neoglacial expansion of ice caps on Devon and Ellesmere islands on postglacial emergence curves in those regions (Figure 4.1). Whether postglacial emergence of Malloch Dome reflects non-glacioisostatic factors, such as a reduction in the rate diapirism during the Holocene, due to disturbances in the lateral gradient of evaporite extrusion, especially in response to prior loading and unloading, is also unknown. Interpretation of the postglacial emergence history of the Ringnes Islands is further complicated by the use of RSL data that do not account for hydroisostatic deformation, since there is no single or unique eustatic correction. This is problematic when comparing the regional pattern of half-lives, since hydroisostatic deformation associated with rising sea-levels (~55 m since 10 ka BP) may have influenced the form and response times of the Ringnes Islands RSL curves, particularly at Noice Peninsula and Malloch Dome, where the onset of emergence occurred between 0.6 and 1.4 ka years after northern Amund Ringnes Island and Christopher Peninsula. Hence, it is possible that the half-lives of curves where initial emergence occurred later are underestimated.

Isobase maps and the pattern of shoreline delevelling demonstrate that both Amund and Ellef Ringnes islands occupied the northwest radius of the Innuitian uplift, lying at least 50 km inboard of its margin at the time of initial deglaciation (10 ka BP). There is no unequivocal evidence of a local glacioisostatic signature on Amund or Ellef Ringnes islands that can presently be separated from the progressive southeastward shrinkage of the Innuitian uplift throughout the Holocene. This pattern of shoreline delevelling supports earlier reconstructions that maximum Late Wisconsinan ice thickness in the central QEI occurred over Norwegian Bay (Dyke 1998). Glacial geologic

evidence on Devon, Cornwall and Amund Ringnes islands records divergent ice-flow on either side of this uplift axis, reinforcing earlier proposals that in the central QEI, this axis of maximum ice thickness coincides with the position of an ice divide (cf. Dyke 1998, 1999; Lamoureux and England 2000; Atkinson 2003, Chapter 2, this volume). The zero isobase which, as Dyke (1998) noted, lies on the proximal side of the crustal forebulge, has migrated ~150 km southeast since 10 ka BP, thus explaining the submergence of western Ellef Ringnes Island

Due to the scarcity of control points, isobases drawn across the Ringnes Islands provide a provisional reconstruction of the extent and thickness of the northwest IIS, which is otherwise poorly constrained. These record the diminishing thickness of the northwest IIS across the Ringnes Islands, from Norwegian Bay to the Arctic Ocean (Figure 4.5). The continuity of the isobases across Massey Sound is consistent with the glacial geologic evidence that suggests that Massey Sound was fully occupied by grounded ice (≥440 m thick) during the last glaciation (Atkinson 2003). Similarly, the absence of an isobase embayment across Amund and Ellef Ringnes islands suggests that there was no significant difference between the Late Wisconsinan ice loads of both islands and Hassel Sound, although on this length scale (~35 km), flexural rigidity may be sufficient to conceal such differences. Parallel isobases across Peary Channel would also suggest that this grounded ice extended beyond Massey Sound, although their northward deflection towards Axel Heiberg Island requires that ice thickness was greater on the eastern side of the channel, likely due to the increasing influence of ice-flow from Axel Heiberg Island (Figure 4.1). However, in the absence of other islands, there are no control points to confirm the actual isobase pattern over the channels themselves.

The diminution of shoreline gradients and passage of the zero isobase across the Ringnes Islands record the shrinkage of the northwest radius of the Innuitian uplift, concomitant with the southeastward migration of the uplift centre. These data complement those from the southeast radius of the Innuitian uplift, although the isobase maps and pattern of shoreline delevelling presented in this paper indicate that migration of the uplift axis progressed slowly, and remained in the poorly constrained region of Graham Island until ~6 ka BP (Figures 4.2, 4.5 and 4.6). Migration of the uplift centre suggests that ablation of the IIS occurred asymmetrically, likely due to the combined effects of earlier and more rapid retreat of its northwest sector, and the proximity of its southeast sector to Baffin Bay, which favoured higher snow accumulation and greater ice thickness (cf. Dyke 1998). The glacial geomorphic, chronologic and RSL records of the Ringnes Islands document the vulnerability of the northwest IIS, much of which was grounded below sea-level, to break-up along marine-based margins, in part reinforcing this interpretation (Atkinson 2003, Chapter 2, this volume).

4.7 References

Andrews, J.T. 1970. A geomorphic study of postglacial uplift with particular reference to Arctic Canada. Institute of British Geographers, London, England, Special Publication 2.

Andrews, J.T. 1982. On the reconstruction of Pleistocene ice sheets: A review. Quaternary Science Reviews, **1**: 1-30.

Andrews, J.T., and Peltier, W.R. 1989. Quaternary geodynamics in Canada. *In* Quaternary Geology of Canada and Greenland. *Edited by* R.J. Fulton. Geological Survey of Canada, Geology of Canada, **1**.

Atkinson, N. 2003. Late Wisconsinan glaciation of Amund and Ellef Ringnes islands, Nunavut: evidence for the configuration, dynamics and deglacial chronology of the northwest sector of the Innuitian Ice Sheet. Canadian Journal of Earth Sciences, **40**: 351-363.

Bard, E., Fairbanks, R.G., and Zindler, A. 1990. Comparison between radiocarbon and uranium series ages on glacial age Barbados corals. Nature, **345**: 405-409.

Bednarski, J.M. 1988. The geomorphology of glaciomarine sediments in a high arctic fiord. Géographie physique et Quaternaire, **42**: 65-74.

Bednarski, J.M. 1998. Quaternary history of Axel Heiberg Island, bordering Nansen Sound, Northwest Territories, emphasizing the last glacial maximum. Canadian Journal of Earth Sciences, **35**: 520-533.

Bednarski, J.M. 2003. Deglaciation of Bathurst Island Group, Nunavut; Geological Survey of Canada, Map 2020A, scale 1:250 000.

Bischof, J.F., Clark, D.L., and Vincent, J-S. 1996. Origin of ice-rafted debris: Pleistocene paleoceanography in the western Arctic Ocean. Paleoceanography, **11**: 743-756.

Bischof, J.F., and Darby, D.A. 1997. Mid- to Late Pleistocene Ice Drift in the Western Arctic Ocean: Evidence for a different Circulation in the Past. Science, **277**: 74-78.

Bischof, J., and Darby, D. A. 1999. Quaternary ice transport in the Canadian Arctic and extent of Late Wisconsinan Glaciation in the Queen Elizabeth Islands. Canadian Journal of Earth Sciences, **36**: 2007-2022.

Blake, W., Jr. 1970. Studies of glacial history in Arctic Canada. Canadian Journal of Earth Sciences, **7**: 634-664.

Blake, W., Jr. 1972. Climatic implications of radiocarbon-dated driftwood in the Queen Elizabeth Islands, Arctic Canada. *In* Climatic change in the arctic areas during the last ten thousand years. *Edited by* Y. Vasari, H. Hyvarinen, and S. Hicks.

Bond, G.C., and Lotti, R. 1995. Iceberg discharges into the North Atlantic on millenial time scales during the last glaciation. Science, **267**: 1005-1010.

Boulton, G.S. 1979. A model of Weichselian glacier variation in the North Atlantic regions. Boreas, **8**: 373-395.

Clark, C.D., and Stokes, C.R. 2001. Extent and basal characteristics of the M'Clintock Ice Stream. Quaternary International, **86**: 81-101.

Darby, D.A., Bischof. J.F., Spielhagen, R.F., Marshall, S.A., and Herman, S.W. 2002. Arctic ice export events and their potential impact on global climate during the late Pleistocene. Paleoceanography, **17**: 1-17.

Dowdeswell, J.A., Maslin, M.A., Andrews, J.T., and McCave, I.N. 1995. Iceberg production, debris rafting, and the extent and thickness of Heinrich layers (H-1, H-2) in North Atlantic sediments. Geology, **23**: 301-304.

Dyke, A.S. 1998. Holocene delevelling of Devon Island, Arctic Canada: implications for ice sheet geometry and crustal response. Canadian Journal of Earth Sciences, **35**: 885-904.

Dyke, A.S. 1999. The last glacial maximum and the deglaciation of Devon Island: support for an Innuitian Ice Sheet. Quaternary Science Reviews, **18**: 393-420.

Dyke, A.S., Morris, T.F., and Green, D.E.C. 1991. Postglacial tectonic and sea-level history of the central Canadian Arctic. Geological Survey of Canada, Bulletin **397**.

Dyke, A.S., and Peltier, W.R. 2000. Forms, response times and variability of relative sea-level curves, glaciated North America. Geomorphology, **32**: 315-333.

England, J. 1976. Late Quaternary glaciation of the eastern Queen Elizabeth Islands, northwest territories, Canada: alternative models. Quaternary Research, **6**: 185-202.

England, J. 1998. Support for the Innuitian Ice Sheet in the Canadian High Arctic during the Last Glacial Maximum. Journal of Quaternary Science, **13**: 275-280.

England, J., Sharp, M., Lemmen, D.S., and Bednarski, J. 1991. On the extent and thickness of the Innuitian Ice Sheet: a postglacial adjustment approach: Discussion. Canadian Journal of Earth Sciences, **28**: 1689-1695.

England, J., and Ó Cofaigh, C. 1998. Deglacial sea level along Eureka Sound: The effects of ice retreat from a central basin to alpine margins (abstract). Joint Meeting of the Geological Association of Canada/Mineralogical Association of Canada, Quebec, Canada 16, A-52., Northwest Territories. Geological Survey of Canada, Bulletin **346**.

England, J., Atkinson, N., Dyke, A.S., Evans, D.J.A., and Zreda, M. in press. Late Wisconsinan buildup and wastage of the Innuitian Ice Sheet across southern Ellesmere Island, Nunavut. Canadian Journal of Earth Sciences.

Hodgson, D.A. 1981. Surficial geology, Lougheed Island, Northwest Arctic Archipelago. Geological Survey of Canada, Paper **81-1C**.

Horn, D.R. 1963. Marine geology, Peary Channel, District of Franklin. Geological Survey of Canada, Paper **63-11**.

Lambeck, K., Yokoyama, Y., Johnston, P., and Purcell, A. 2000. Global ice volumes at the Last Glacial Maximum and early Lateglacial. Earth and Planetary Science Letters, **181**: 513-527.

Lamoureux, S.F., and England, J. 2000. Late Wisconsinan of the central sector of the Canadian High Arctic. Quaternary Research, **54**: 182-188.

Lemmen, D.S., Aitken, A.E., and Gilbert, R. 1994. Early Holocene deglaciation of Expedition and Strand fiords, Canadian High Arctic. Canadian Journal of Earth Sciences, **31**: 943-958.

Lowdon, J.A., Robertson, I.M., and Blake, W., Jr. 1971. Geological Survey of Canada Radiocarbon Dates XI. Geological Survey of Canada, Paper **71-7**.

Lowdon, J.A., and Blake, W., Jr. 1976. Geological Survey of Canada Radiocarbon Dates XVI. Geological Survey of Canada, Paper **76-7**.

Lowdon, J.A., Robertson, I.M., and Blake, W., Jr. 1977. Geological Survey of Canada Radiocarbon Dates XVII. Geological Survey of Canada, Paper **77-7**.

Lowdon, J.A., and Blake, W., Jr. 1978. Geological Survey of Canada Radiocarbon Dates XVIII. Geological Survey of Canada, Paper **78-7**.

McNeely, R. 1989. Geological Survey of Canada Radiocarbon Dates XXVIII. Geological Survey of Canada, Paper **88-7**.

Miller, G.H., Bradley, R.S., and Andrews, J.T. 1975. The glaciation level and lowest equilibrium line altitude in the high Canadian Arctic: maps and climatic interpretation. Arctic and Alpine Research, **7**: 155-168.

Morrison, C.A. 2000. Late Quaternary glacial and sea level history of west-central Axel Heiberg Island, High Arctic Canada. Unpublished M.Sc. thesis, University of Alberta, Edmonton.

Ó Cofaigh, C. 1999. Holocene emergence and shoreline delevelling, southern Eureka Sound, High Arctic Canada. Géographie physique et Quaternaire, **53**: 235-247.

Ó Cofaigh, C., Lemmen, D.S., Evans, D.J.A., and Bednarski, J. 1999. Glacial sediment/landform assemblages in the Canadian High Arctic and their implications for Late Quaternary glaciation. Annals of Glaciology, **28**: 195-207.

Ó Cofaigh, C., England, J., and Zreda, M. 2000. Late Wisconsinan glaciation of southern Eureka Sound: evidence for extensive Innuitian ice in the Canadian High Arctic during the Last Glacial Maximum. Quaternary Science Reviews, **19**: 1319-1341.

Polyak, L., Edwards, M.H., Coakley, B.J., and Jokobsson, M. 2001. Ice shelves in the Pleistocene Arctic Ocean inferred from glaciogenic deep-sea bedforms. Nature, **401**: 453-457.

Quinlan, G., and Beaumont, C. 1981. A comparison of observed and theoretical postglacial relative sea level in Atlantic Canada. Canadian Journal of Earth Sciences, **18**: 1146-1163.

Roots, E.F. 1963. Physiography: Cornwall, Lougheed, Amund Ringnes and Ellef Ringnes Islands. In: Geology of north-central part of the Arctic Archipelago, Northwest Territories. Geological Survey of Canada, Memoir **320**.

St-Onge, D.A 1965. La géomorphologie de l'Ile Ellef Ringnes, Territoires du Nord-Ouest, Canada. Geographical Branch, Paper **38**.

Stuiver, M., and Reimer, P.J. 1993. Radiocarbon, **35**: 215-230.

Tushingham, A.M. 1991. On the extent and thickness of the Innuitian Ice Sheet: a postglacial adjustment approach. Canadian Journal of Earth Sciences, **28**: 231-239.

Tushingham, A.M., and Peltier, W.R. 1991. Ice-3G: a new global model of late Pleistocene deglaciation based on geophysical predictions of post-glacial relative sea level change. Journal of Geophysical Research, B, **96**: 4497-4523.

Walcott, R.I. 1972. Late Quaternary vertical movements in eastern North America: quantitative evidence of glacio-isostatic rebound. Reviews of Geophysics and Space Physics, **10**: 849-884.

CHAPTER FIVE

Conclusions

5.1 Introduction

This thesis describes the glacial and relative sea-level history of Amund and Ellef Ringnes islands, northwest Queen Elizabeth Islands (QEI), where early reconnaissance work has not been updated in the most recent reconstruction of Northern Hemisphere ice sheets (cf. EPILOG Project; Clark and Mix 2002). The only refinement of reconnaissance studies in the western QEI is by Bischof and Darby (1999), who reconstructed the extent of Late Wisconsinan glaciation based on the distribution of ice transported debris. Bischof and Darby (1999) proposed that Ellesmere, Axel Heiberg, Devon, Cornwallis, Bathurst and Melville islands were covered by island-based ice caps that flowed radially into the adjacent interisland channels, forming trunk glaciers up to 600 m thick (Figure 5.1). Although Bischof and Darby (1999) indicated that trunk ice extended as far north as Peary Channel, their reconstruction did not identify any ice cover on Ringnes Islands during the Late Wisconsinan. However, this reconstruction was based largely on the mineralogy of third-order glacigenic sediments collected below the limit of postglacial emergence, which could therefore have been transported by early Holocene ice-rafting rather than a Late Wisconsinan ice sheet. Data presented in this thesis directly address the style and chronology of glaciation and its isostatic and eustatic effects across the northwest QEI during the Last Glacial Maximum (LGM). However, determining the glacial history of the Ringnes Islands and their adjacent marine channels is more significant than merely filling a gap in the reconstruction of the glacial history of the QEI.

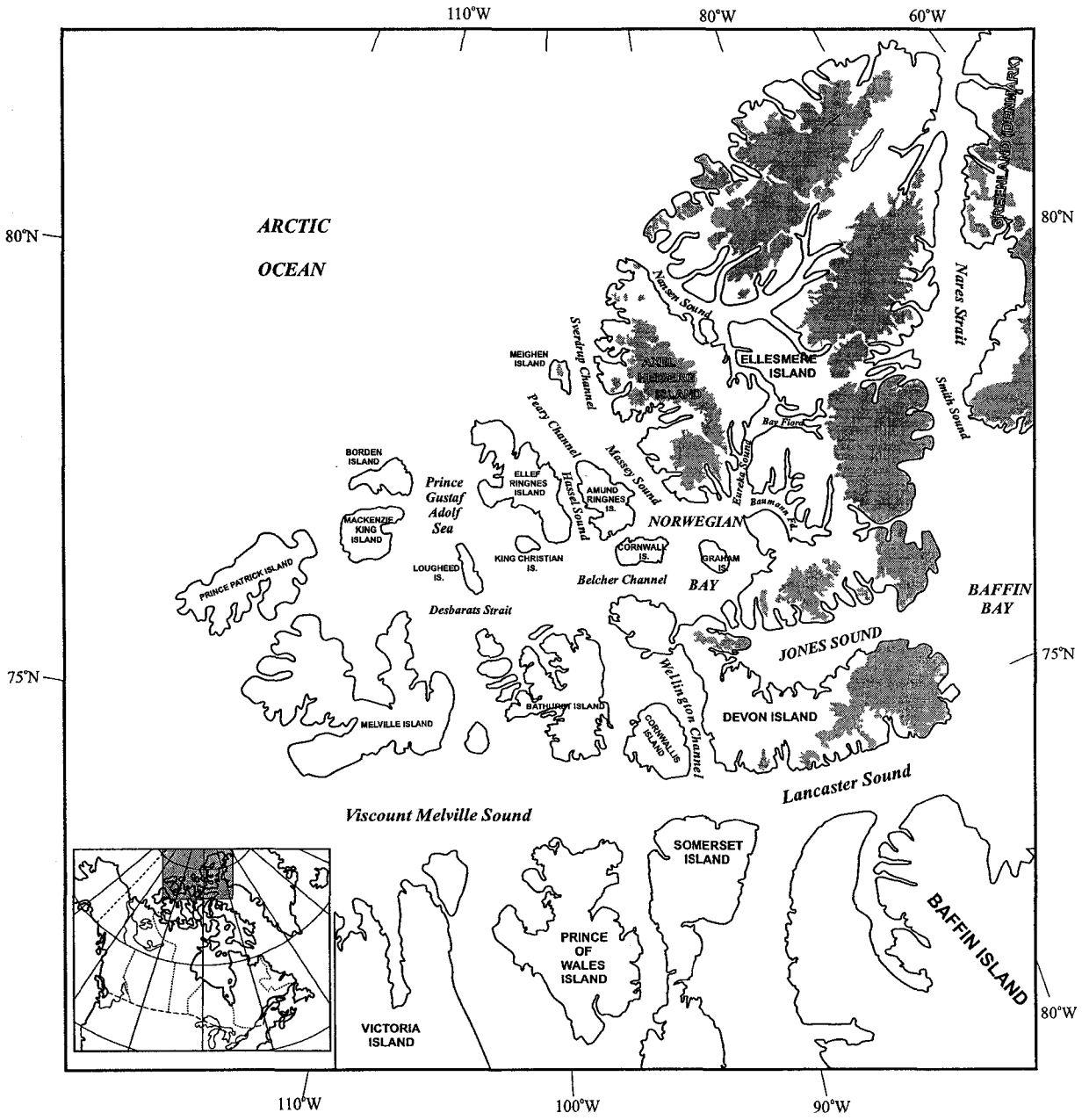

Figure 5.1. Regional map of the Canadian Arctic Archipelago and the adjacent coast of Greenland. Contemporary ice caps are shaded dark gray.

Their location relative to Norwegian Bay, which is proposed to have been an important conduit within Innuitian Ice Sheet (IIS; England 1998) provides the opportunity to determine the glacial history of the northwest QEI, which may have been a focus of significant ice-flux towards the Arctic Ocean Basin during the last glaciation (Figure 5.1). By presenting the chronology, extent and dynamics of glaciation across the Ringnes Islands, this thesis further clarifies the glacial history of the QEI, which contributes to a better understanding of the external forcings and internal feedbacks, as well as the linkages between the climate subsystems, that drive paleoenvironmental change around the margin of the Arctic Ocean (cf. Clark and Mix 2002; Dyke et al. 2002a; Brigham-Grette et al. 2003).

5.2 Configuration of ice cover on and bordering the Ringnes Islands

Northwesterly flow of a ≥440 m thick trunk glacier along Massey Sound is recorded by granite erratics resting on striated and ice-moulded bedrock along eastern Amund Ringnes Island. These granite erratics occur within a dispersal train that extends from eastern Ellesmere Island to Meighen Island, which is inferred to document a major flow trajectory of the former IIS from an alpine divide over the Precambrian Shield (Figure 5.1). Statistical analyses of granite geochemistry suggest that there is little variation in the composition of granites distributed along this dispersal train, and support the proposal that they originated from the Shield of eastern Ellesmere Island. The interior of Amund Ringnes Island was overridden by predominantly granite-free, non-erosive ice flowing north into Peary Channel. It is proposed that this flowline originated from an Innuitian divide occupying Belcher Channel, and represents the northward extension of lowland ice that first crossed Cornwall Island (Dyke 1998; Lamoureux and England

2000; Figure 5.1). This flowline may have overtopped Piercement Dome (up to 245 m asl), and converged with the Massey Sound trunk glacier along eastern Amund Ringnes Island, thereby keeping granite-carrying ice largely offshore. There is no unequivocal evidence that granite-bearing flowlines, either within the Late Wisconsinan IIS, or possibly the pre-LGM Laurentide Ice Sheet (LIS), have ever crossed Ellef Ringnes Island. Nevertheless, eskers, rare striae and lateral meltwater channels do record widespread glaciation of Ellef Ringnes Island. This ice covered uplands (210 m asl) and extended at least as far as Peary Channel and Prince Gustaf Adolf Sea (Figure 5.1). However, it remains unknown whether this was a full-glacial, local ice cap, and/or Innuitian ice that flowed north through Hassel Sound from the lowland divide which extended through western Belcher Channel, north of Bathurst Island (Figure 5.1).

Evidence of basal sliding along eastern Amund Ringnes Island indicates that the Massey Sound trunk glacier was, at least locally, warm-based. This is attributed to ice-flow from alpine and lowland divides converging from a drainage basin of ~78, 000 km^2 into Norwegian Bay (~22, 000 km^2), where internal deformation and strain heating, together with subglacial deformation of marine sediment accelerated ice-flow along Massey Sound, forming an ice stream.

5.3 Chronology of ice buildup

Currently, the youngest radiocarbon date that constrains the advance of granite-carrying ice from the Precambrian Shield of eastern Ellesmere Island towards Amund Ringnes Island indicates that buildup of a precursor of the Prince of Wales Icefield established a regional westward ice-flow after 19.8 ka BP (Blake 1992; Ó Cofaigh et al. 2000; Figure 5.1).

Mid-Wisconsinan aged shelly diamicts deposited above marine limit on southwest Ellesmere, Graham and Cornwall islands provide maximum estimates for ice buildup immediately south of the Ringnes Islands (Figure 5.1; Hodgson 1985; Blake 1987; Lamoureux and England 2000; Ó Cofaigh et al. 2000; England et al. in press). Even though these dates are superceded by the 19.8 ka BP date adjacent to the Prince of Wales Icefield, they do suggest that mid-Wisconsinan shells were redeposited by Late Wisconsinan ice advance. Although a 40.1 ka BP shell fragment in glaciofluvial sediment on Amund Ringnes Island may be considered older than the mid-Wisconsinan, if this sediment was deposited during a pre-mid Wisconsinan glaciation, there is no evidence in the stratigraphic record of the Ringnes Islands for a glaciation of that age.

5.4 Deglaciation and Holocene ice dynamics

Apart from mid-Wisconsinan aged erratic shells, all of the chronologically constrained raised marine sediments and landforms surveyed on the Ringnes Islands and presented in this thesis record deglaciation and postglacial emergence during the early Holocene. Deglaciation of the northwest IIS commenced prior to 10 ka BP. However, between 10 and 9.4 ka BP, trunk ice in Hassel and Massey sounds had retreated to northeast Ellef Ringnes and northern Amund Ringnes islands, and ice had retreated from Prince Gustaf Adolf Sea onto western Ellef Ringnes Island (Figure 5.1). The distribution of chronologically constrained raised marine sediments and landforms dating the establishment of Holocene marine limit between eastern Ellef Ringnes and western Amund Ringnes islands records the sequential re-entry of the sea, associated with the southward retreat of trunk ice from Hassel Sound between 10 and 9.2 ka BP. Lamoureux and England (2000) demonstrated that deglaciation of Cornwall Island commenced 9 ka

BP, indicating that trunk ice had evacuated Massey and Hassel sounds within ~1000 ^{14}C years. A horizontal moraine along northeast Amund Ringnes Island provides further indication of the style of regional deglaciation. This moraine is interpreted to record deposition by a former ice-shelf occupying Massey Sound prior to 9 ka BP. This suggests that trunk ice decoupled from its bed during eustatic sea-level rise, concomitant with its separation from residual ice on Amund Ringnes Island.

Local ice caps persisted along the coastlines of both Amund and Ellef Ringnes islands for up to 1400 ^{14}C years after the initial evacuation of ice from Massey and Hassel sounds and southern Prince Gustaf Adolf Sea (Figure 5.1). The chronology of final deglaciation of residual ice caps on the Ringnes Islands remains unknown. Nevertheless, the distribution of ice-marginal landforms, particularly lateral meltwater channels, on a landscape otherwise appearing unaltered by glacial erosion suggests that these ice caps were cold-based (Dyke 1993), and became increasingly confined within upland valleys after the establishment of Holocene marine limit.

5.5 Postglacial emergence

5.5.1 Forms and response times of postglacial relative sea level curves

Postglacial relative sea level (RSL) curves from the Ringnes Islands record exponential crustal relaxation across the region due to early Holocene deglaciation, and indicate continuous, ongoing emergence of northern Amund Ringnes Island and east-central Ellef Ringnes Island. However, the current data indicate that west-central Ellef Ringnes Island has experienced a late Holocene transgression.

The half-lives of these three curves range from 1.8 ka adjacent to Massey Sound, to 1.25 ka at Deer Bay. Although this pattern is broadly consistent with the half-lives

presented by Dyke and Peltier (2000), the magnitude of emergence occurring within the first half-life of curves bordering Massey Sound decreases markedly from northern Amund Ringnes to northeast Ellef Ringnes islands. Because such differences reflect a northwestward reduction in ice thickness across the Ringnes Islands, these data suggest that the proportionality constant (which is related to mantle viscosity and ice sheet size) for both curves is uniform, since their half-lives do not reflect the apparent differences in the magnitude of the ice load. A fourth curve from the Ringnes Islands also records continuous, ongoing emergence of Malloch Dome, but its form and response time (2.9 ka) depart significantly from those of the other curves presented in this thesis, and may reflect non-glacioisostatic factors.

5.5.2 Pattern of postglacial isobases

Isobase maps and the pattern of shoreline delevelling demonstrate that both Amund and Ellef Ringnes islands occupied the northwest radius of the Innuitian uplift, lying at least 50 km inboard of its margin at the time of initial deglaciation (10 ka BP). There is no unequivocal evidence of a local glacioisostatic signature on Amund or Ellef Ringnes islands that can presently be separated from the progressive southeastward shrinkage of the Innuitian uplift throughout the Holocene. This pattern of shoreline delevelling supports earlier reconstructions that maximum Late Wisconsinan ice thickness in the central QEI occupied Norwegian Bay, which coincides with the position of an ice divide (cf. Dyke 1998, 1999; Lamoureux and England 2000; Atkinson 2003). The recent submergence of west-central Ellef Ringnes Island is attributed to the migration of the zero isobase ~150 km southeast since 10 ka BP.

Provisional isobases drawn across the Ringnes Islands record the diminishing thickness of the northwest IIS from Norwegian Bay to the Arctic Ocean. The continuity of the isobases across Amund and Ellef Ringnes islands is consistent with the glacial geologic evidence that suggests Massey and Hassel sounds were occupied by grounded ice during the last glaciation. Parallel isobases across Peary Channel suggest that this grounded ice extended beyond Massey Sound, although their northward deflection, parallel to the west coast of Axel Heiberg Island requires that ice thickness was greater on the eastern side of the channel (Figure 5.1). However, in the absence of other islands, there are no control points to confirm the actual isobase pattern over the channels themselves. The diminution of shoreline gradients and passage of the zero isobase across the Ringnes Islands record the shrinkage of the northwest radius of the Innuitian uplift, concomitant with the southeastward migration of the uplift centre.

5.6 Regional implications

Data presented in this thesis further clarify the chronology, extent and dynamics of the IIS. These data provide the opportunity to discuss some of the external forcing mechanisms and internal feedbacks that influenced its buildup and retreat, the possible linkages between the IIS and other circumarctic ice sheets, as well as its potential paleoenvironmental effects.

Firstly, the out-of-phase buildup of the LIS (24 to 20 ka BP) and IIS (post-19.8 ka BP) suggests that the history of these ice sheets was influenced by additional controls (cf. Dyke et al. 2002a; England et al. in press; Figure 5.2a). Glaciochemical analyses of the GISP2 ice-core that document air mass characteristics across the Summit region, central Greenland, suggest that two major circulation regimes prevailed during the last glacial-

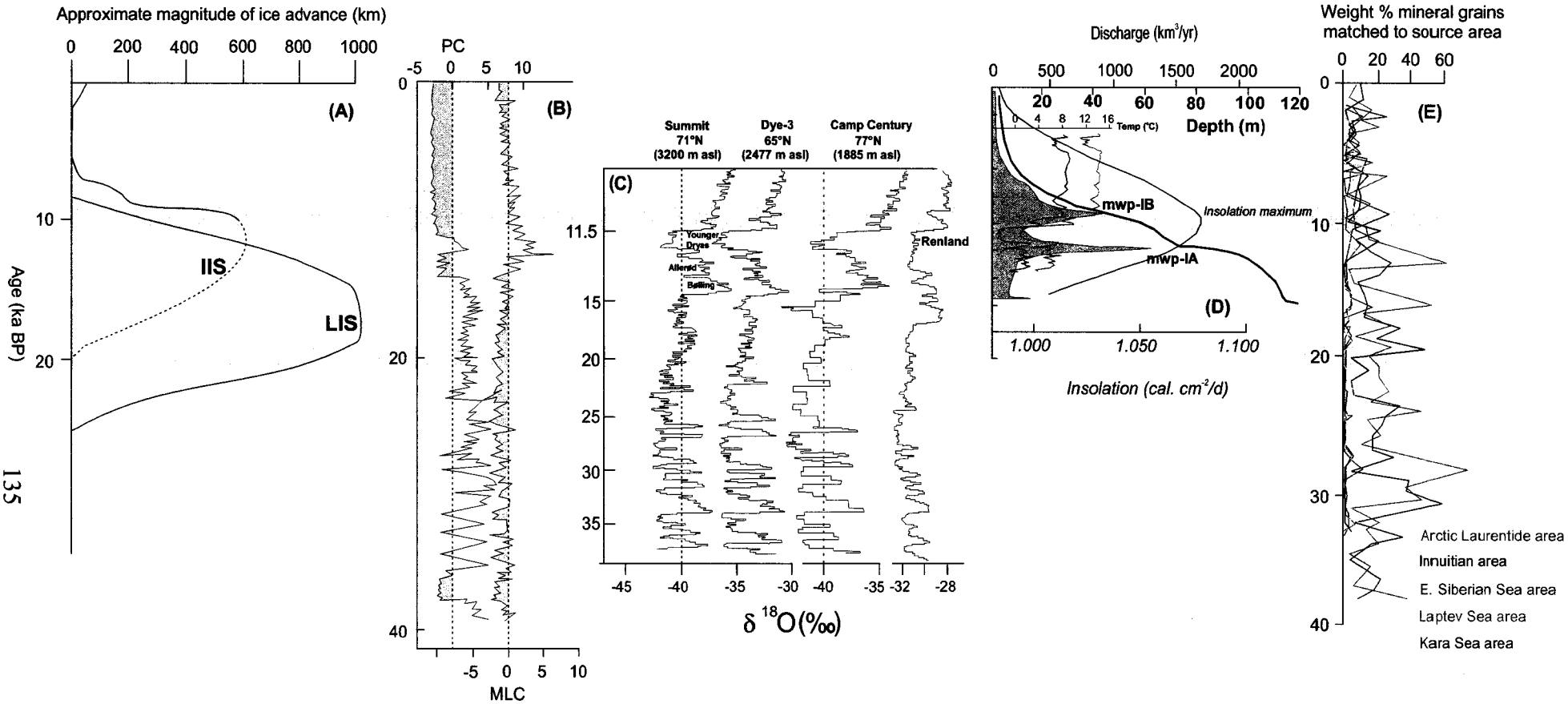

Figure 5.2. Schematic diagram showing relationship between; A) approximate age of buildup, retreat and extent of the IIS and LIS; B) variations in the two main principal components of the glaciochemistry of the GISP2 ice-core. Left line records changes in the relative importance of polar/high latitude circulation regimes, and the right line records mid-, low latitude circulation regimes (Mayewski et al.1997); C) oxygen isotope records from four sites on the Greenland Ie Sheet (Johnsen et al. 1992; see Figure 5.3 for locations); D) reconstruction of sea surface temperature (°C) in August (red line) and February (blue line) in the southwest Norwegian Sea (Koc Karpuz and Jansen 1992), estimated magnitude of glacial meltwater entering world's oceans (mwp-1A and mwp-1B are clearly seen) and palaeo sea-level, based on radiocarbon dated corals (Bard et al. 1990; Fairbanks 1990), and insolation at 60 oN (Berger 1988); E) IRD events in Fram Strait originating from circumarctic source areas (Darby et al. 2002). Age axis shown in cal. years BP. Grey bars denote approximate age for buildup (lower bar) and retreat (upper bar) of the IIS.

interglacial cycle (Mayewski et al. 1997; Figures 5.2b and 5.3). Shifts in circulation regimes coincide with abrupt changes in $\delta^{18}O$, indicating that during cold events (low $\delta^{18}O$), the region was dominated by a polar/high latitude circulation pattern, while during the Holocene, a mid- to low latitude circulation pattern prevailed (Mayewski et al. 1997; Figures 5.2b and c). Such variations in ice-core geochemistry on central Greenland may be of palaeoclimatic significance elsewhere in the circumarctic, including the QEI, due to the teleconnections that link atmospheric circulation patterns over long distances (cf. Stager and Mayewski 1997). For example, an atmospheric general circulation model (AGCM) simulation of glacial to interglacial variations of moisture sources for the Greenland Ice Sheet (GIS) suggests that northern Greenland received more precipitation from the North Pacific Ocean during the LGM, due to the northward displacement of storm tracks around the LIS (Charles et al. 1994). Due to the longer trajectory of the Pacific air masses, snow deposited on Greenland from such sources would be more strongly depleted in $\delta^{18}O$ than snow originating from North Atlantic moisture sources (Charles et al. 1994). This is reflected by the latitudinal influence on $\delta^{18}O$ depletion along the GIS, which increases from Dye 3 (65°N) to Summit (71°N) and Camp Century (77°N), despite the Dye 3 and Summit sites occurring at higher elevations (Figures 5.2c and 5.3). Perhaps significantly, the strongest depletion of $\delta^{18}O$ in the last 20 ka years occurs in the Camp Century ice-core, and coincides with an interval of ongoing IIS expansion. Hence, the strong depletion of $\delta^{18}O$ from precipitation reaching northern Greenland from Pacific moisture sources may have been augmented by the IIS, due to its adiabatic influence on air masses crossing the QEI, en route to Greenland. A fully coupled ocean-atmosphere GCM of the LGM climate confirms that strong westerly

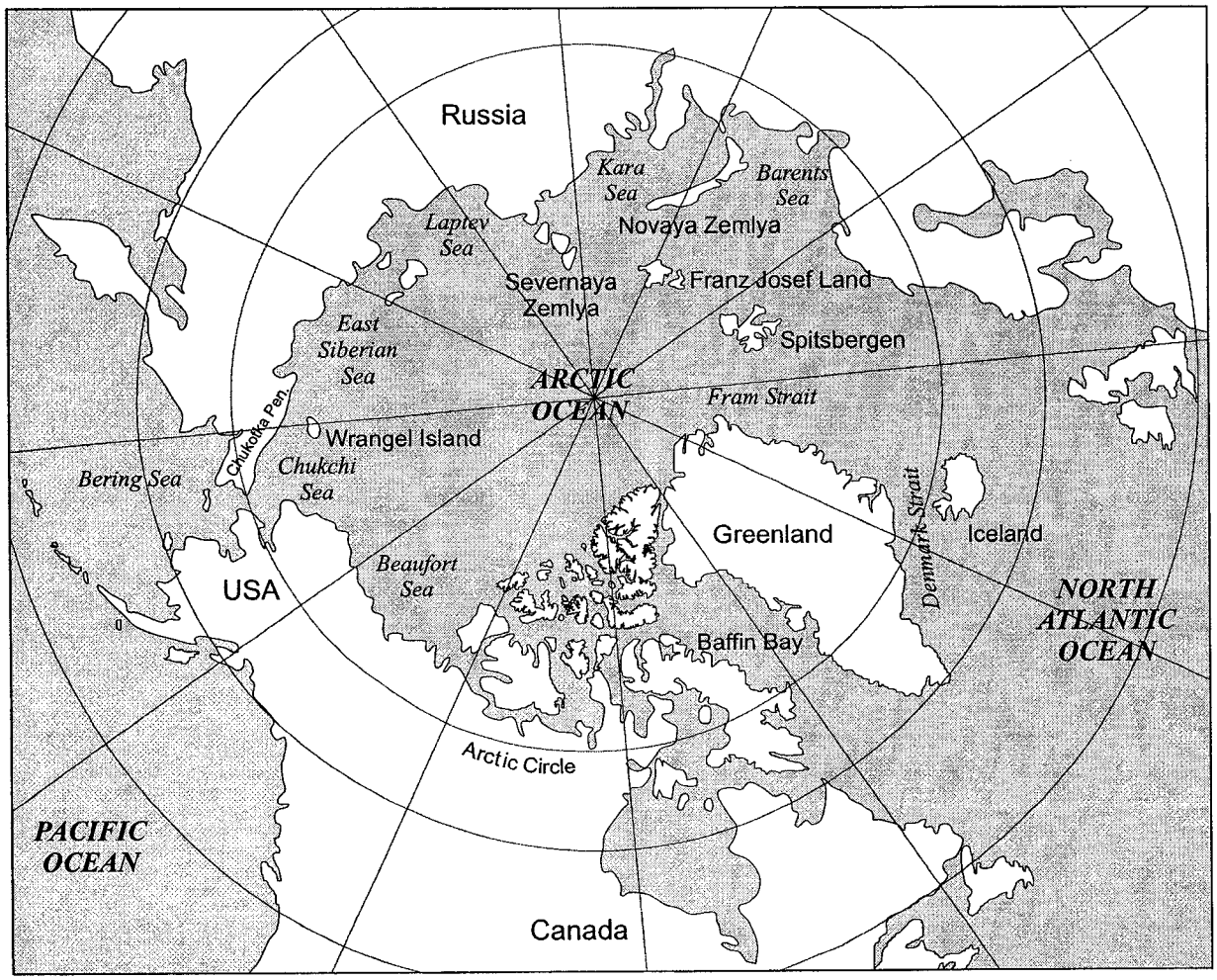

Figure 5.3. Location map of the circumarctic region, showing place names referred to in text.

winds over the Canadian Arctic arose from the northward deflection of the mid-latitude jet stream by the Laurentide and Cordilleran ice sheets, which resulted in increased surface relative humidity above ~60°N (Bush and Philander 1999). Hence the delayed buildup of the IIS likely reflects a positive feedback between the pre-LGM buildup of the LIS, which deflected the jet stream northwards, advecting more precipitation towards the QEI. Moreover, the earlier buildup of the LIS contributed to falling eustatic sea levels, which may have enabled the IIS to subsequently expand, particularly across the central and western QEI. England et al. (in press) proposed that expansion of the IIS was further augmented by the GIS, which impinged eastern Ellesmere Island, blocking the eastward outflow of Innuitian trunk glaciers into Nares Strait and causing the primary alpine divide to thicken, and strengthen westward ice-flow towards Norwegian Bay and ultimately the polar continental shelf (Figure 5.1).

Secondly, recent reconstructions of the extent of glaciation based on glacial geological evidence from Eastern Siberia and the Barents-Kara Sea favour a limited ice cover in these regions during the LGM, rather than a pervasive Eurasian Ice Sheet (cf. Grosswald 1988, 1998; Grosswald and Hughes 2002; Mangerud et al. 2002; Brigham-Grette et al. 2003; Gualtieri et al. 2003; Figure 5.3). These reconstructions suggest that the LGM of northeast Siberia was characterized by the growth of valley and alpine glaciers (Brigham-Grette et al. 2003), while the eastern Siberian and Chukchi seas remained ice-free (Gualtieri et al. 2003; Figure 5.3). Svendsen et al. (1999) and Mangerud et al. (2002) proposed that the Barents-Kara Ice Sheet did not extend beyond the nearshore, shallow marine environment north of the Russian mainland, with the Taymyr Peninsula and Laptev Sea remaining ice-free at the LGM. Collectively, these

studies suggested that the Eastern Siberian and Kara-Barents ice sheets reached their maximum extent ≤60 ka BP. Although the pre-LGM glacial history of the QEI remains unaddressed, there is currently no unequivocal evidence of a pre-Late Wisconsinan ice sheet that was ever more extensive than the IIS. Hence, the last Innuitian ice buildup, which may have reached its maximum extent during the Late Wisconsinan, coincides with an interval of restricted glaciation elsewhere in the circumarctic. Hence, the Quaternary glacial history of the QEI may also reflect feedbacks between the extent of glaciation in these regions during, and prior to the LGM, likely due to their influence on atmospheric circulation patterns and associated variations in moisture budget across the Innuitian region. This is supported by GCM simulations of LGM climate across the circumarctic, which indicate that the northward deflection of the mid-latitude jet stream by the LIS had the additional effect of reducing the strength of westerlies over the eastern North Pacific Ocean. This favoured anticyclonic air flow over eastern Siberia, which drew cold, dry Arctic air south to isolate the region climatically, and create an extreme polar desert east of the Barents-Kara Ice Sheet (Manabe and Broccoli 1985; Peltier 1994; Bush and Philander 1999; Marsiat and Valdes 2001; Siegert and Marsiat 2001).

Thirdly, the deglacial history of the IIS also appears to be influenced by additional controls, since its retreat from the polar continental shelf at ~10 ka BP postdates the initial rise of global eustatic sea level at 16.5 ka BP (cf. Yokoyama et al. 2000; Hanebuth et al. 2000) and the Last Termination (~14.5 ka BP; Figure 5.3d). Thus, any deglaciation of the IIS between 16.5 and ~10 ka BP likely occurring by thinning, rather than marginal recession (cf. Dyke et al. 2002a). Peaks of Innuitian ice-rafted debris (IRD) abundance in the Arctic Ocean at ~16 and ~12.8 ka BP are attributed to episodes of major iceberg

release from the IIS (Darby et al. 2002; Figure 5.3e). These may relate to periodic thinning of the IIS, possibly associated with increased ice-flux along Massey and Nansen sounds (cf. Bischof et al. 1996; Bischof and Darby 1999; O'Grady and Syvitski 2002). Darby et al. (2002) noted that the timing of these episodes preceded Heinrich events in the North Atlantic, and suggested that disintegration of the IIS may have triggered retreat of the LIS, as well the cold peaks of the Dansgaard-Oescher cycles. However, Darby et al. (2002) remarked that higher-resolution sediment cores are required to resolve these potential relationships. In contrast, the deglacial chronology presented in this thesis demonstrates that significant retreat of the IIS lags deglaciation of the LIS. Moreover, this retreat also postdates the Younger Dryas, which defines a return to full glacial temperatures between 11 to 10 ka BP (Mangerud et al. 1974; 1980; Dyke and Savelle 2000; Figure 5.2). Although the initial rate of ice retreat in the western Arctic is unknown, the absence of deglacial landforms on the Ringnes Islands prior to 10 ka BP suggests that the IIS remained on the polar continental shelf throughout the Last Termination, and persisted there until the end of the Younger Dryas. This persistence may reflect in part, a positive feedback between the mass balance of the IIS and climatic conditions in the Innuitian region, and cooling in the circum-subpolar North Atlantic resulting from large meltwater discharges which may have temporarily shut down North Atlantic Deep Water production, causing the North Atlantic polar front to shift south (Broecker et al. 1988).

However, after 10 ka BP, the northwest IIS evidently became more susceptible to breakup, likely due to the combined effects of ongoing global eustatic sea-level rise (Fairbanks 1989; Bard et al. 1990), changes in mass balance in response to the early

Holocene insolation maximum (Berger 1988; Koerner and Fisher 1990; Van der Veen 1996), reorganization of circumpolar circulation patterns (Mayewski et al. 1997) and warmer sea surface temperatures in the North Atlantic, Baffin Bay and the Beaufort Sea (Koç Karpuz, and Jansen 1992; Dyke et al. 1996; Briffa et al. 2001; Figure 5.3). The southeast migration of the Innuitian uplift centre from Norwegian Bay to Devon Island is attributed to the vulnerability of the northwest IIS to earlier and more rapid break-up along its marine-based margins, and the proximity of the southeast IIS to Baffin Bay, which favoured higher snow accumulation and greater ice thickness (cf. Dyke 1998; Figure 5.1). In contrast, the persistence of local ice caps on Amund and Ellef Ringnes islands throughout an interval of continued Holocene warming (Bradley 1990; Koerner and Fisher 1990) may reflect a delayed response of these island-based ice caps to Younger Dryas cooling, or possibly Preboreal cooling triggered by the diversion of Lake Agassiz outflow from the North Atlantic to the Arctic Ocean (Fisher et al. 2002). Dyke et al. (2002b) noted that Preboreal cooling was particularly strong in the Beaufort Sea region, and may have resulted in readvances of the LIS between 9.8 and 9.6 ka BP.

A final implication of the data presented in this thesis concerns the origin of streamlined grooves on the Lomonosov Ridge (~1000 m deep) in central Arctic Ocean Basin, at least during the Late Wisconsinan (cf. Polyak et al. 2001). The extent and thickness of the IIS inferred from the isobase pattern across the northwest QEI suggest that it was an unlikely source for these enigmatic bedforms. This is supported by the abundance of Innuitian IRD in the Arctic Ocean Basin, which suggests icebergs were drifting freely from the QEI to Fram Strait throughout the last glaciation (Bischof et al. 1996; Figure 5.2).

5.7 Future Research

Three areas of future research are identified following the recognition that ice flowing from Innuitian divides that spanned the eastern and central Queen Elizabeth Islands, subsumed parts of the Ringnes Islands and likely extended on to the polar continental shelf.

Firstly, evidence that the IIS extended across the northwest QEI provides the impetus to address the extent and dynamics of Late Wisconsinan glaciation in the westernmost QEI. The age and origin of northwest-oriented flutings reported on Lougheed Island (Hodgson 1981) are currently unknown. They may record flow from an Innuitian ice divide that spanned the *entire* central QEI, from Belcher Channel to Desbarats Strait (Figure 5.1). Alternatively, these flutings may relate to the northward flow of the LIS from the Canadian mainland prior to the last glaciation (cf. Vincent et al. 1984; Hodgson 1989). Future emphasis should also be placed on Quaternary geologic studies of Prince Patrick, Mackenzie King and Borden islands (Figure 5.1), to determine whether the polar margin of the western QEI remained ice-free during the Late Wisconsinan, or if it was overridden by ice from regional divides, or supported local, island-based ice caps. This research constitutes part of J. England's NSERC Northern Chair and will be initiated during the 2004 field season.

Secondly, an outstanding issue concerning the glacial history of the western QEI is the origin of glacially transported granite erratics reported on Lougheed and Prince Patrick islands (Figure 5.1). Hodgson (1990) concluded that these erratics had been transported up to 1000 km to Prince Patrick Island from unknown sources to the south or east, within a 150° arc of the island. Results of the statistical analyses comparing the

geochemistry of granite erratics distributed across Ellesmere, Amund and Meighen suggest that they form a single dispersal train extending from the Precambrian Shield of southeast Ellesmere Island. Although this technique does not identify specific source areas for this dispersal train, preliminary results suggest that it does not contain erratics originating from specific outcrops on Somerset Island. Hence, this technique may be useful in linking large numbers of granite erratics of presently unknown origin on Lougheed and Prince Patrick islands to Laurentide or Innuitian source areas. Individual samples from these groups can then be used to establish source provenance more reliably by geochronological analyses.

Thirdly, the latest International Bathymetric Chart of the Arctic Ocean (IBCAO, Jakobsson et al. 2000) shows trough mouth fans (TMF's) in front of channels that extend across the continental shelf of the QEI, from Nansen and Viscount Melville sounds, Peary Channel and Prince Gustaf Adolf Sea (Figure 5.4). Elsewhere in the Arctic, as well as in the polar North Atlantic and Antarctic, these indicate that ice streams within Quaternary ice sheets advanced across the shelf during sea-level lowstands, depositing large amounts of ice-rafted debris (IRD) into the marine environment (O'Grady and Syvitski 2002; Ó Cofaigh et al. 2003). Glacial geological evidence recording Late Wisconsinan ice-flow along Massey and Nansen sounds is attributed to ice streams discharging the from northwest IIS (Atkinson 2003, chapters 2 and 3, this volume; cf. Bednarski 1998). However, the glacial history of the western QEI, which borders Prince Gustaf Adolf Sea TMF, remains largely uninvestigated, although northwest-oriented ice-flow features of unknown age are reported on Lougheed Island (Hodgson 1981). Clearly, any potential relationship between these TMF's and the distribution of Late Wisconsinan

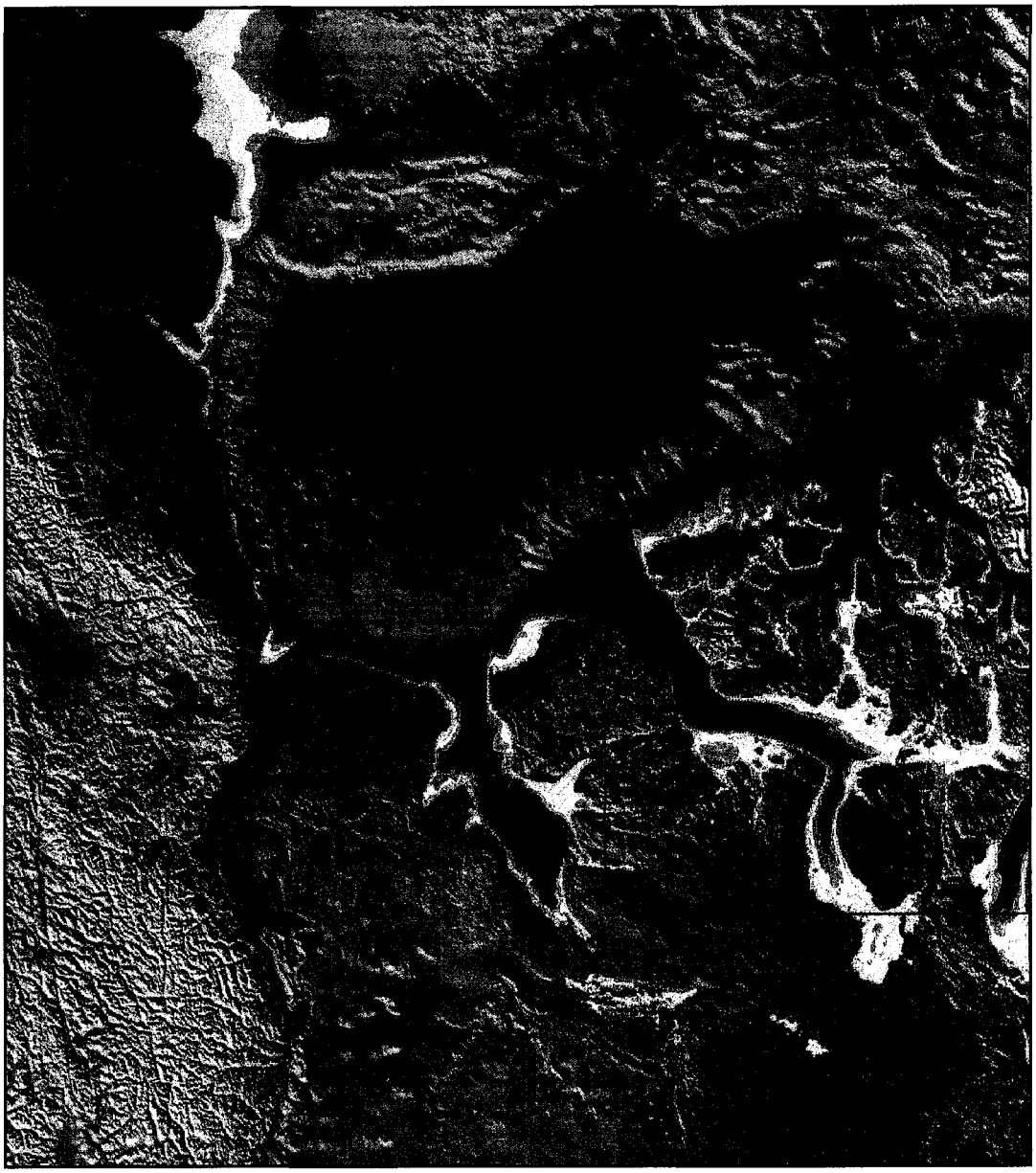

Figure 5.4. International Bathymetric Chart of the Arctic Ocean digital bathymetric model (Jakobsson et al. 2000). TMF, trough mouth fan; ST, shelf trough. Adapted from O'Grady and Syvitski 2002. Place names as in Figure 5.1.

ice streams would have important implications for the stability of the IIS (cf. Ó Cofaigh et al. 2003). However, the evolution and significance of the large-scale morphology of the continental shelf of the QEI, vis-a-vis the configuration, dynamics and sedimentary history of the Innuitian or pre-Late Wisconsinan ice sheets, are unknown.

Therefore, although logistically demanding, investigations of the Quaternary record of the continental shelf could provide new details on the extent, dynamics and deglacial chronology of former ice sheet(s) across the QEI. Important components of this research would include geophysical investigations, as well as the stratigraphy and chronology of sediment cores. Moreover, if granite dispersal trains do contain geochemically distinctive signatures, it may be possible to correlate sediment sources in the TMF's and deep-sea sediment cores to specific Innuitian or Laurentide ice streams (cf. Scourse et al. 2000; Hemming et al. 2002; Darby et al. 2002). Characterizing the sediment sources of IRD layers in deep-sea sediment cores has the potential to unravel the sequence of events spanning the last glaciation.

5.8 References

Atkinson, N. 2003. Late Wisconsinan glaciation of Amund and Ellef Ringnes islands, Nunavut: evidence for the configuration, dynamics and deglacial chronology of the northwest sector of the Innuitian Ice Sheet. Canadian Journal of Earth Sciences, **40**: 351-363.

Bard, E., Fairbanks, R.G., and Zindler, A. 1990. Comparison between radiocarbon and uranium series ages on glacial age Barbados corals. Nature, **345**: 405-409.

Bednarski, J.M. 1998. Quaternary history of Axel Heiberg Island, bordering Nansen Sound, Northwest Territories, emphasizing the last glacial maximum. Canadian Journal of Earth Sciences, **35**: 520-533.

Berger, A. 1988. Milankovitch theory and climate. Reviews of Geophysics, **26**: 624-657.

Bischof, J.F., and Darby, D.A. 1999. Quaternary ice transport in the Canadian Arctic and extent of Late Wisconsinan glaciation in the Queen Elizabeth Islands. Canadian Journal of Earth Sciences, **36**: 2007-2022.

Bischof, J.F., Clark, D.L., and Vincent, J.S. 1996. Pleistocene paleoceanography of the central Arctic Ocean: The sources of ice rafted debris and the compressed sedimentary record. Paleoceanography, **11**: 743-756.

Blake, W., Jr. 1987. Geological Survey of Canada Radiocarbon Dates XXVI. Geological Survey of Canada, Paper **86-7**.

Blake, W., Jr. 1992. Holocene emergence at Cape Herschel, east-central Ellesmere Island, Arctic Canada: implications for ice sheet configuration. Canadian Journal of Earth Sciences, **29**: 1958-1980.

Bradley, R.S. 1990. Holocene paleoclimatology of the Queen Elizabeth Islands, Canadian High Arctic. Quaternary Science Reviews, **9**: 365-384.

Briffa, K., Korhola A., Snowball I, Koç N., and Nesje A. 2001. Holocene Climate Dynamics in High Latitude Europe and the North Atlantic. PAGES-PEPIII Past Climate Variability Through Europe and Africa: An International Conference, Program with Abstracts, Centre des Congrès, Aix-en-Provence, France.

Brigham-Grette, J., Gualtieri, L.M., Glushkova, O.Y., Hamilton, T.D., Mostoller, D., and Kotov, A. 2003. Chlorine-36 and ^{14}C chronology support a limited last glacial maximum across central Chukotka, northeastern Siberia, and no Beringian ice sheet. Quaternary Research, **59**: 386-398.

Broecker, W.S., Andree, M., Wolfli, W., Oeschger, H., Bonani, G., Kennett, J., and Peteet, D. 1988. The chronology of the last deglaciation: Implications to the cause of the Younger Dryas event. Paleoceanography, **3**: 1-19.

Bush, A.B.G., and Philander, S.G.H. 1999. The climate of the Last Glacial Maximum: Results from a coupled atmosphere-ocean general circulation model. Journal of Geophysical Research, **104**, No. D20: 24,509-24,525.

Charles, C.D., Rind, D., Jouzel, J., Koster, R.D., and Fairbanks, R.G. 1994. Glacial-interglacial changes in moisture sources for Greenland: influences on the ice core record of climate. Science, **263**: 508-511.

Clark, P.U., and Mix, A.C. 2002. Ice sheets and sea level of the Last Glacial Maximum. Quaternary Science Reviews, **21**: 1-7.

Darby, D.A., Bischof. J.F., Spielhagen, R.F., Marshall, S.A., and Herman, S.W. 2002. Arctic ice export events and their potential impact on global climate during the late Pleistocene. Paleoceanography, **17**: 1-17.

Dyke, A.S. 1993. Landscapes of cold-centred late Wisconsinan ice caps, Arctic Canada. Progress in Physical Geography, **71**: 223-247.

Dyke, A.S. 1998. Holocene delevelling of Devon Island, Arctic Canada: implications for ice sheet geometry and crustal response. Canadian Journal of Earth Sciences, **35**: 885-904.

Dyke, A.S. 1999. The last glacial maximum and the deglaciation of Devon Island: support for an Innuitian Ice Sheet. Quaternary Science Reviews, **18**: 393-420.

Dyke, A.S., and Peltier, W.R. 2000. Forms, response times and variability of relative sea-level curves, glaciated North America. Geomorphology, **32**: 315-333.

Dyke, A.S., and Savelle, J.M. 2000. Major end moraines of Younger Dryas age on Wollaston Peninsula, Victoria Island, Canadian Arctic: implications for paleoclimate and for formation of hummocky moraine. Canadian Journal of Earth Sciences, **37**: 601-619.

Dyke, A.S., Dale, J.E., and McNeely, R. N. 1996. Marine molluscs as indicators of environmental change in glaciated North America and Greenland during the last 18 000 years. Géographie physique et Quaternaire, **50**: 125-184.

Dyke, A.S., Andrews, J.T., Clark, P.U., England, J.H., Miller, G.H., Shaw, J., and Veillette, J.J. 2002a. The Laurentide and Innuitian ice sheets during the Last Glacial Maximum. Quaternary Science Reviews, **21**: 9-31.

Dyke, A.S., St-Onge, D.A., and Savelle, J.M. 2002b. Younger Dryas and Preboreal end moraines, readvances, and recession rates, western Canadian Arctic. Quaternary Sciences from Land to Sea II: In honor of John T. Andrews. Geological Society of America Annual Meeting, Denver, Colorado, Paper **180-6**.

England, J. 1998. Support for the Innuitian Ice Sheet in the Canadian High Arctic during the Last Glacial Maximum. Journal of Quaternary Science, **13**: 275-280.

England, J., Atkinson, N., Dyke, A.S., Evans, D.J.A., and Zreda, M. in press. Late Wisconsinan buildup and wastage of the Innuitian Ice Sheet across southern Ellesmere Island, Nunavut: dominance of the Greenland Ice Sheet. Canadian Journal of Earth Sciences.

Fairbanks, R.G. 1989. A 17,000 year glacio-eustatic sea-level record: influence of glacial melting rate on the Younger Dryas event and deep ocean circulation. Nature, **342**: 637-642.

Fisher, T.G., Smith, D.G., and Andrews, J.T. 2002. Preboreal oscillation: North Atlantic cooling caused indirectly by a glacial Lake Agassiz flood, 11,300 years ago. Quaternary Science Reviews, **21**: 873-878.

Grosswald, M.G. 1988. An Antarctic-style ice sheet in the Northern Hemisphere: towards a new global glacial theory. Polar Geography and Geology, **12**: 239-267.

Grosswald, M.G. 1998. Late-Weichselian Ice Sheets in Arctic and Pacific Siberia. Quaternary International, **45/46**: 3-18.

Grosswald, M.G., and Hughes, T.J. 2002. The Russian component of an Arctic Ice Sheet during the Last Glacial Maximum. Quaternary Science Reviews, **21**: 121-146.

Gualtieri, L., Vartanyan, S., Brigham-Grette, J., and Anderson, P.M. 2003. Pleistocene raised marine deposits on Wrangel Island, northeast Siberia and implications for the presence of an East Siberian ice sheet. Quaternary Research, **59**: 399-410.

Hanebuth, T., Stattegger, K., and Grootes, P.M. 2000. Rapid flooding of the Sunda Shelf: a late-glacial sea-level record. Science, **288**: 1033-1035.

Hemming, S.R., Vorren, T.O., and Kleman, J. 2002. Provinciality of ice rafting in the North Atlantic: application of $^{40}Ar/^{39}Ar$ dating of individual ice rafted hornblende grains. Quaternary International, **95**: 75-85.

Hodgson, D.A. 1981. Surficial geology, Lougheed Island, Northwest Arctic Archipelago. Geological Survey of Canada, Paper **81-1C**.

Hodgson, D.A. 1985. The last glaciation of west-central Ellesmere Island, Arctic Archipelago, Canada. Canadian Journal of Earth Sciences, **22**: 347-368.

Hodgson, D.A. 1989. Quaternary stratigraphy and chronology (Queen Elizabeth Islands). *In* Quaternary Geology of Canada and Greenland, Fulton, R.J. (ed), Geological Survey of Canada, Geology of Canada, No 1, pp. 452-459.

Hodgson, D.A. 1990. Were erratics moved by glaciers or icebergs to Prince Patrick Island, western Arctic Archipelago, Northwest Territories? Geological Survey of Canada, Paper **90-1D**, pp. 67-70.

Jakobsson, M., Cherkis, N., Woodward, J., MacNab, R, and Coakley, B. 2000. New grid of Arctic bathymetry aids scientists and mapmakers. *EOS*, Transactions of the American Geophysical Union, **81**: 89, 93, 96.

Johnsen, S.J., Clausen, H.B., Dansgaard, W., Fuhrer, K., Gundestrup, N., Hammer, C.U., Iverson, P., Jouzel, J., Stauffer, B., and Steffensen, J.P. 1992. Irregular glacial interstadials recorded in a new Greenland ice core. Nature, **359**: 311-313.

Koç Karpuz, N., and Jansen, E. 1992. A high resolution diatom record of the last deglaciation from the S.E. Norwegian Sea: documentation of rapid climate changes. Paleoceanography, 7: 499-520.

Koerner, R.M., and Fisher, D.A. 1990. A record of Holocene summer climate from a Canadian high-Arctic ice core. Nature, **343**: 630-631.

Lamoureux, S.F., and England, J. 2000. Late Wisconsinan of the central sector of the Canadian High Arctic. Quaternary Research, **54**: 182-188.

Manabe, S., and Broccoli, A.J. 1985. The influence of continental ice sheets on the climate of an Ice Age. Journal of Geophysical Research, **90D**: 2167-2190.

Mangerud, J. 1980. Ice-front variations of different parts of the Scandinavian Ice Sheet, 13,000-10,000 years BP. *In* Studies in the Lateglacial of North-west Europe. *Edited by* J.J. Lowe, J.M. Gray, and J.E. Robinson. Pergamon Press, Oxford, pp. 23-30.

Mangerud, J., Anderson, S.T., Berglund, B.E., and Donner, J.J. 1974. Quaternary Stratigraphy of Norden, a proposal for terminology and classification. Boreas, **3**: 109-126.

Mangerud, J., Astakhov, V., and Svendsen, J-I. 2002. The extent of the Barents-Kara ice sheet during the Last Glacial Maximum. Quaternary Science Reviews, **21**: 111-119.

Marsiat, I., and Valdes, P.J., 2001. Sensitivity of the Northern Hemisphere climate of the Last Glacial Maximum to sea surface temperatures. Climate Dynamics, **17**: 233-248.

Mayewski, P.A., Meeker, L.D., Twickler, M.S., Whitlow, S., Yang, Q., Berry Lyons, W., and Prentice, M. 1997. Major features and forcing of high-latitude northern hemispheric circulation using a 110,000-year-long glaciochemical series. Journal of Geophysical Research, **102**, No. C12: 26,345-26,366.

Ó Cofaigh, C., England, J., and Zreda, M. 2000. Late Wisconsinan glaciation of southern Eureka Sound: evidence for extensive Innuitian ice in the Canadian High Arctic during the Last Glacial Maximum. Quaternary Science Reviews, **19**: 1319-1341.

Ó Cofaigh, C., Taylor, J., Dowdeswell, J. A., and Pudsey, C. J. 2003. Palaeo-ice streams, trough mouth fans and high-latitude continental slope sedimentation. Boreas, **32**: 37–55.

O'Grady, D.P., and Syvitski, J.P.M. 2002. Large-scale morphology of Arctic slopes. *In* Glacier-influenced sedimentation on high-latitude continental margins. *Edited by* J.A. Dowdeswell, and C. Ó Cofaigh. Geological Society of London, Special Publications, **203**: 11-31.

Peltier, W. R. 1994. Ice Age Paleotopography. Science, **265**: 195-201

Polyak, L., Edwards, M.H., Coakley, B.J., and Jokobsson, M. 2001. Ice shelves in the Pleistocene Arctic Ocean inferred from glaciogenic deep-sea bedforms. Nature, **401**: 453-457.

Scourse, J.D., Hall, I.R., McCave, I.N., Young, J.R., and Sugden, C. 2000. The origin of Heinrich layers: evidence from H2 for European precursor events. Earth and Planetary Science Letters, **182**: 187-195.

Siegert, M.J., and Marsiat, I. (2001) Numerical reconstructions of LGM climate across the Eurasian Arctic. Quaternary Science Reviews, **20**: 1595-1605.

Stager, J.C., and Mayewski, P.A. (1997) Abrupt early to mid-Holocene climatic transition registered at the Equator and the Poles. Science, **276**: 1834-1836.

Van der Veen, C.J. 1996. Tidewater calving. Journal of Glaciology, **42**: 375-385.

Vincent, J-S., Morris, W.A., and Occhietti, S. 1984. Glacial and nonglacial sediments of Matuyama paleomagnetic age on Banks Island, Canadian Arctic Archipelago. Geology, **12**: 139-142.

Yokoyama, Y., Lambeck, K., De Deckker, P., and Fifield, L.K. 2000. Timing of the Last Glacial constrained by lowest sea-level observations. Nature, **406**: 713-716.